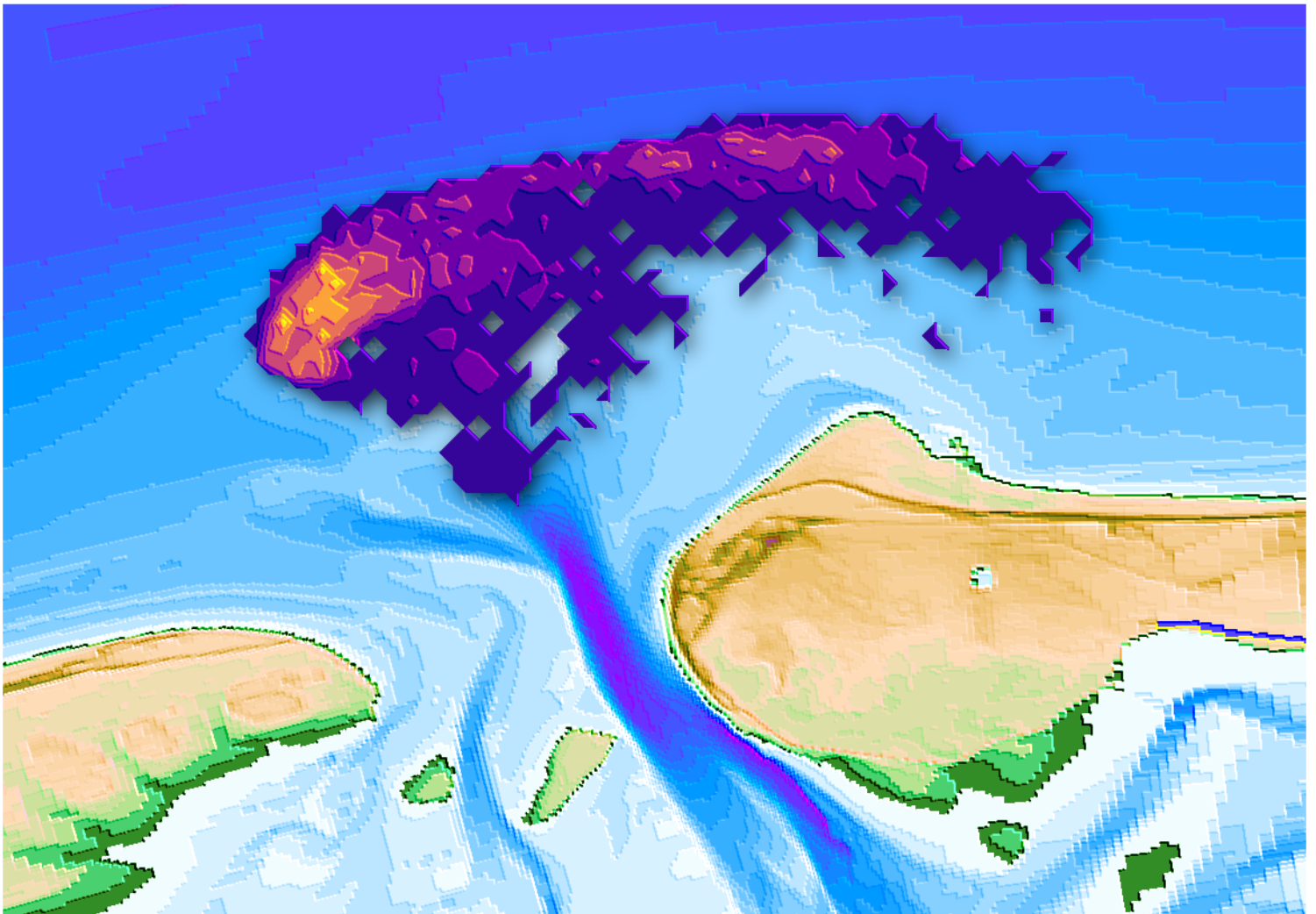


Analysing dispersal of sand nourishments using SedTRAILS

Evaluating the application of the SedTRAILS model on the Ameland ebb-tidal delta nourishment



Analysing dispersal of sand nourishments using SedTRAILS

Evaluating the application of the SedTRAILS model on the Ameland ebb-tidal delta nourishment

by

M. Meijer

to obtain the degree of Master of Science
at the Delft University of Technology,
to be defended publicly on 18 July, 2024 at 14:30.

Student number:	4706161
Project duration:	February 12, 2024 – 18 July, 2024
Thesis committee:	Dr. ir. S. G. Pearson, TU Delft, graduation chair
	Dr. ir. E. P. L. Elias, Deltares
	Dr. K. B. J. Dunne, TU Delft
	Dr. L. Brakenhoff, Rijkswaterstaat
	Dr. N. PannoZZo, TU Delft
	Ir. T. de Wilde, Deltares

Cover: Stylized figure showing a SedTRAILS result of nourishment dispersal.

An electronic version of this thesis is available at <http://repository.tudelft.nl/>.

Preface

With this report, I am concluding my MSc degree in Civil Engineering at Delft University of Technology. Over the past five months, I have written this thesis at Deltares in Delft as a graduation internship. It has been a privilege to work among the team at the department of Applied Morphology and with my fellow interns there. I have learned a great deal during my time there, and I hope I can put that to good use in future endeavors.

I would like to thank the members of my thesis committee. Stuart's constant excitement and enthusiasm were the best motivator a student could ask for. Edwin's feedback and suggestions were always insightful, helping me to stay on track and always keep the end goal in mind. I was always impressed with how much knowledge he has in this field and this setting, and his comments always got to the core of what I needed to work on. Natascia and Tim were both fantastic to work with, always helpful when I had questions, with insightful suggestions when I got stuck. Kieran and Laura, while not as directly involved, also always provided valuable feedback throughout the entire thesis. They have all helped me tremendously throughout this process.

I also want to thank my family and my friends for listening to both my excited explanations and my worries and stress. Further thanks go to two friends in particular: Lucas and Anais. You have been a welcome constant in my time at Civil Engineering in Delft, and I am incredibly grateful for all your support and encouragement throughout my time at TU Delft and during my thesis.

*Martin Meijer
Delft, July 2024*

Summary

In 2019, a 5 million m³ sand nourishment was placed at the Ameland ebb-tidal delta. This pilot nourishment aimed to investigate the feasibility and effectiveness of ebb-tidal delta nourishments and to understand the dynamics in this system. To assess how this nourishment has dispersed through the ebb-tidal delta system, SedTRAILS was used. SedTRAILS is a particle-based sediment transport model currently in development. A new process for interaction with the bed and burial of sediment was recently added to the model. The impact of this process on dispersal and sediment pathways needed to be analysed, as not much is known about the effects of its inclusion on transport and dispersal.

Several schematisations of wave- and tidal forcing were tested. The wave forcing selection had little effect on the overall model results. Storm conditions included in the more detailed schematisation were underrepresented in the model results. The implementation of wave-driven bed velocity had little influence on result as well due to small magnitudes that were calculated for this. A significant difference was found between using a morphological tide and an artificial spring-neap tidal cycle however, requiring further investigation.

Investigation of the burial formulation gave insight into the response of the model to changes in the different parameters. Direct dependence of erosion probability on deposition probability presents a major limitation in the current implementation of burial. Additionally, deposition probability in its current form is positively dependent on the maximum bed shear stress. Inclusion of burial does provide significant room for calibration of results.

Through modelling these various configurations of SedTRAILS, results consistently showed a recirculation of sediment from the nourishment on the ebb-tidal delta together with bypassing around the edge of the ebb-tidal delta, as seen in Figure 1. However, the degree to which bypassing occurs depends heavily on the chosen burial configuration. The bypassing is largely a result of flow around the periphery of the ebb-tidal delta and differs from known bar migration and shoal attachment pathways. Transport into the Wadden Sea basin was not found, likely due to the underestimation of influence of storm conditions.

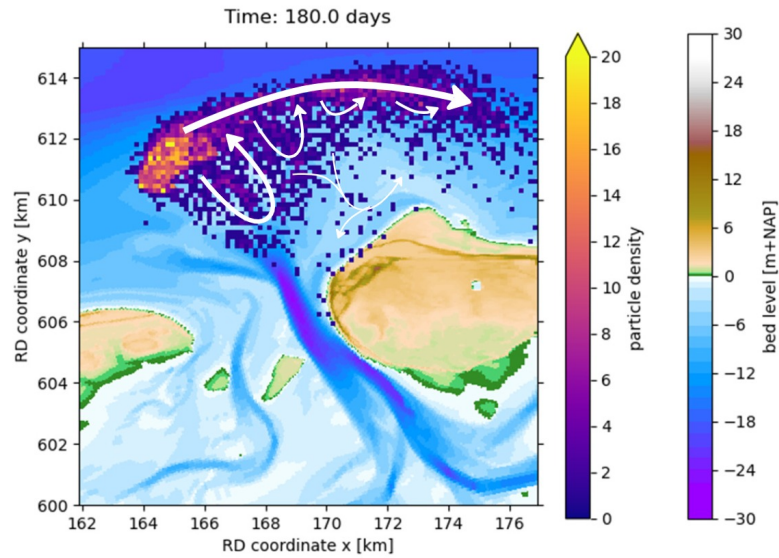


Figure 1 Result of 180 days of simulation of the Ameland pilot nourishment with SedTRAILS, using six wave conditions, a spring-neap tidal cycle and burial parameters $b_e = 1.7 \cdot 10^{-5}$, $\theta_s = 0.1$, $\gamma_e = 0.0055$. The arrows indicate the main transport pathways over the ebb-tidal delta throughout the simulation.

To improve dispersal modelling with SedTRAILS, the impact of storm conditions needs to be more accurately included in the model. An under-representation of energetic wave conditions leads to a consistent underestimation of wave-related transport. Additionally, more investigation into the effects of the spring-neap tidal cycle is required. The significant difference presented here is an early indication that this is an important factor for SedTRAILS. Validation of dispersal modelled with SedTRAILS can be achieved through quantification of transport, assigning a volume of sediment per particle.

Contents

Preface		1
Summary		2
1	Introduction	6
1.1	Context	6
1.2	Research objectives	8
1.3	Report structure	8
2	Literature review	9
2.1	Tidal inlets in barrier island coasts	9
2.2	Ameland inlet and pilot nourishment	10
2.3	Delft3D-FM	16
2.4	SedTRAILS	17
2.4.1	Transport formulation	18
2.4.2	Bed interaction and burial	20
2.4.3	Wave-driven bed velocity	20
2.4.4	Past applications	21
3	Methods	25
3.1	Conceptual application of model	25
3.2	Model set-up	26
3.2.1	Delft3D-FM	27
3.2.2	Wave condition schematization	28
3.2.3	Offshore boundary	29
3.2.4	SedTRAILS	31
4	Results	34
4.1	Sensitivity to changes in forcing	34
4.1.1	Number of wave conditions	34
4.1.2	Wave-driven bed velocity	40
4.1.3	Water level boundary	43
4.2	General sensitivity of burial parameters	44
4.2.1	b_e - Maximum free-to-trapped transition probability	45
4.2.2	θ_s - Scale value determining the distribution of residence times	46
4.2.3	γ_e - Long-term equilibrium proportion of free particles	47
4.2.4	Summary of sensitivity	48
4.3	Effects of erosion and deposition probabilities	49
4.3.1	Run 1 - Original burial parameters	49
4.3.2	Runs 2, 3 and 4 - scaling deposition probability	50
4.3.3	Run 5 - changing the scale parameter	54
4.3.4	Runs 6 and 7 - scaling deposition and erosion	55
4.4	Summary of findings	56
5	Discussion	57
5.1	Forcing conditions	57
5.1.1	Number of wave conditions	57
5.1.2	Wave-driven bed velocity	58
5.1.3	Offshore boundary	58
5.2	Burial formulation	59
5.3	Modelling the Ameland pilot nourishment	60
5.4	Nourishment modelling with SedTRAILS	63

6	Conclusions	65
7	Recommendations	69
7.1	Recommendations for model set-up	69
7.1.1	Forcing conditions	69
7.1.2	SedTRAILS settings	70
7.2	SedTRAILS calibration and validation	70
7.2.1	Quantification	71
7.2.2	Validation data	71
	References	73
A	Processing methods and scripts	78
A.1	Pre-processing scripts	78
A.1.1	Partition merging (Python)	78
A.1.2	Source set-up (Python)	78
A.1.3	Combining wave conditions (MATLAB)	79
A.2	Post-processing scripts	80
A.2.1	Loading SedTRAILS output in Python	80
A.2.2	Unstructured grid plotting (Python)	81
A.2.3	Particle density plotting - two ways (Python)	82
A.2.4	Alternative wave combination method (Python)	83
B	Sensitivity runs	85
B.1	b_e : Maximum free-to-trapped transition probability	85
B.2	θ_s : Transition scale value	88
B.3	γ_e : Long-term equilibrium proportion of free particles	91
C	Other modelled nourishments at Ameland	94
C.1	Alternate pilot nourishment location	94
C.2	2019 beach nourishment	95
D	Preliminary quantification	97
D.1	Particle counting	97
D.2	Bed level changes	97

1 Introduction

1.1 Context

As the climate changes and sea level rises, coasts are increasingly susceptible to erosion. This problem is particularly important to address in the Netherlands (Gornitz 1991). For decades, the Dutch government has worked on erosion prevention through the governmental body Rijkswaterstaat. They have been tasked with maintaining the coastline of the year 1990, the Basiskustlijn (BKL) (Rijkswaterstaat 1990). Maintaining this coastline is primarily done through "dynamic coastal management", as opposed to the construction of static structures such as dikes or groynes. Dynamic coastal management typically takes the form of nourishing the coast with sand. Nourishments have historically been in the form of beach or shoreface nourishments ((a) and (b) in Figure 1.1), which are relatively small in scale (Brand et al. 2022).

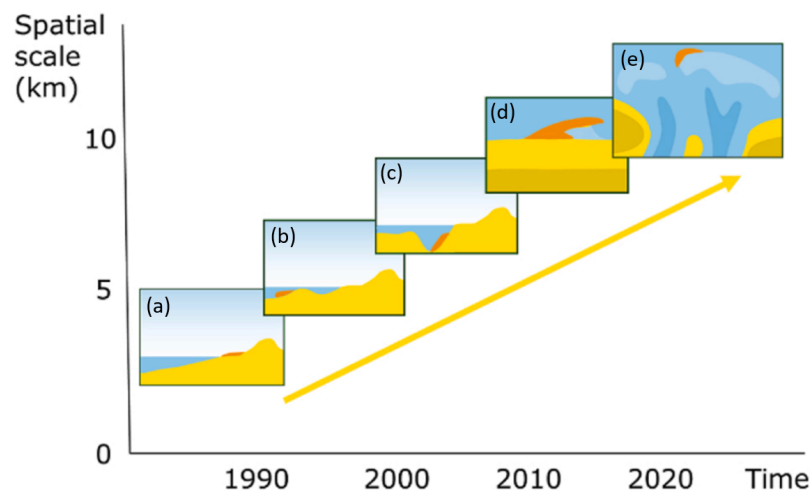


Figure 1.1 Overview of different types of nourishments and their typical spatial scales over time. From bottom left to top right: (a) beach nourishment, (b) foreshore nourishment, (c) channel wall nourishment, (d) the Sand Engine and (e) the Ameland ebb-tidal delta nourishment (Brand et al. 2022).

The use of beach and foreshore nourishments to maintain the BKL means that frequent application is required to maintain the coastline. Typically, these nourishments do not last more than 8 years. To increase the resilience of the coasts of the Netherlands, Rijkswaterstaat has started looking for longer-term solutions and larger scale interventions (Brand et al. 2022).

The Sand Engine at Hoek van Holland ((d) in Figure 1.1) was the first of its kind. This "mega"- or system nourishment consisted of approximately 21.5 million m³ of sand. It was designed to utilise the naturally present waves and currents along the coast of North- and South-Holland to distribute the sediment over a large area (Stive et al. 2013). Nourishing at this large scale has both proven effective for maintaining the Dutch coast and provided additional benefits for ecological development and recreation (Huisman et al. 2021).

One major advantage the Sand Engine has over smaller-scale nourishments is its impact on ecology. With less frequent nourishing of the coast, local ecosystems have more time to recover from burial. Additionally, it has provided new space for dune

growth and pioneer plant species. The additional dune growth also serves to strengthen the natural coastal defences at the dutch coast (Huisman et al. 2021).

With the success of the Sand Engine, another system nourishment was planned, this time at the Ameland tidal inlet ((e) in 1.1). This nourishment had more research-oriented goals, mainly being placed to study the dynamics of the inlet, with coastal management as a secondary goal (Ebbens 2019).

Due to the advantages in long-term coastal management and ecological benefit that system nourishments bring with them, their design is becoming increasingly important as well. Predicting the evolution of a large-scale nourishment before placement is difficult. Currently available hydrodynamic models can already provide a lot of information on the impact of nourishments on systems, but give limited information on sediment pathways. A different (Lagrangian) model approach can provide this insight, complementing the traditional Eulerian approach.

Harlequin (2021) investigated the effect of the nourishment through Eulerian morphodynamic modelling in Delft3D-4. While the modelling done here provided valuable information on the morphodynamic impact of the nourishment, it gave only limited information on where sediment from the nourishment has gone since its placement. Additionally, such a model study is difficult to build, making future evaluations more difficult.

Compare two studies of the Ameland tidal inlet with similar goals but different methodologies. Pearson et al. (2020) utilised a Eulerian modelling framework to investigate the sediment connectivity between different zones in the tidal inlet system. This required many different lengthy model runs. In Pearson et al. (2021), on the other hand, connectivity could be studied much more easily and rapidly by estimating sediment pathways using a Lagrangian approach. To simulate these sediment pathways, the Lagrangian model SedTRAILS was used.

SedTRAILS is a model that simulates transport of particles and is in active development at the TU Delft and Deltares (Elias and Pearson 2020, Pearson et al. 2021, Pearson et al. 2023). SedTRAILS gives insight into flow patterns over time and the pathways sediment takes through a system (Pearson et al. 2021). This insight is valuable for system nourishment design. Knowing where the sediment goes and which parts of the system it can reach within a certain timescale are important in assessing effectiveness. SedTRAILS has already been used to model the Ameland nourishment for that reason (Lambregts 2021). Early on, these pathways were a visualisation of the sediment transport field generated by a Eulerian model. This gave insight on the pathways of sediment in a system, but no information on transported volumes or timescales (Pearson et al. 2021).

To remedy this, the approach of Soulsby et al. (2011) is now used to model sediment particle velocities. Grain velocities are calculated by the model itself based on modelled hydrodynamics. An especially new aspect of the model is burial of sediment. This process allows for more interaction with the bed by the particles simulated in SedTRAILS. The particles can get stuck, simulating how sediment grains can get covered by other sediment. Not much is known about how the inclusion of burial affects the movement of particles and what impact this has when modelling dispersal of a nourishment.

1.2 Research objectives

There are two main objectives in this report: firstly, to test and assess the impact and sensitivity of the burial formulation within SedTRAILS; secondly, an increased understanding of the dispersal of the Ameland pilot nourishment through the Ameland tidal inlet system. These two objectives coincide with each other, as the Ameland pilot nourishment functions as a case study for testing and assessing the burial formulation.

Several schematisations for wave and tidal forcing will be assessed. An existing Delft3D-FM model set-up for the Ameland tidal inlet is used as the basis for these analyses. Sensitivity to changes in parameters within the bed interaction (burial) formulation will be assessed to increase understanding of its inclusion in the transport formulation and the effects it has on modelling dispersal. These extensive tests of the burial formulation will provide a basis for assessing the dispersal of the Ameland pilot nourishment.

The main research question that will be answered is: *"How can SedTRAILS be used to analyse dispersal of sand nourishments in hydrodynamically complex environments?"* The following sub-questions are used to answer the main research question:

- 1 How does dispersal of sediment change under a different schematisation in wave- and tidal forcing?
- 2 How is dispersal of sediment particles affected by changes in sediment burial probabilities?
- 3 What dispersal of the Ameland pilot nourishment is modelled when burial is included in the transport formulation?

1.3 Report structure

Chapter 2 provides an overview of literature relevant to the Ameland tidal inlet, the pilot nourishment and the SedTRAILS model. A model description of SedTRAILS is provided here as well. In chapter 3, the implementation of the transport formulation and an explanation of how SedTRAILS is used is given, as well as the basic set-up and settings used in modelling the nourishment. After this, chapter 4 gives results of varying forcing conditions and several model parameters. In chapter 5, limitations and uncertainties of the methods and results are discussed based on the methodology and to what extent the results reflect previous research into the Ameland pilot nourishment and ebb-tidal delta dynamics. In chapter 6, the research questions are answered and the objectives are addressed, after which recommendations for follow-up research are given in chapter 7.

2 Literature review

To understand the system in which the Ameland pilot nourishment was placed and the processes relevant to modelling it, some background information must first be given. A short overview of tidal inlets in barrier island coasts is provided along with a description of the Ameland tidal inlet. The pilot nourishment is also described in this section. This chapter also includes relevant information on the numerical models that will be used to model the nourishment: Delft3D-FM and SedTRAILS. In particular, the transport formulation used in SedTRAILS is described in detail.

2.1 Tidal inlets in barrier island coasts

Tidal inlets function as parts of a barrier island system, the inlets functioning as the gateway for water to fill into and drain out of the tidal basins behind the barrier islands (Swart and Zimmerman 2009). Figure 2.1 shows a general overview of a tidal inlet system, including the dominant sediment pathways for along-shore transport. Of particular relevance is the ebb-tidal delta that forms on the seaward side around the main channel in the inlet. Ebb-tidal deltas form an important link in sediment bypassing processes in barrier island systems. In unbroken, wave-dominant coasts, large volumes of sediment are transported alongshore in the littoral drift. A tidal inlet breaks up the alongshore transport. However, ebb-tidal deltas provide ways for sediment to bypass the inlet (FitzGerald 1988, Swart and Zimmerman 2009).

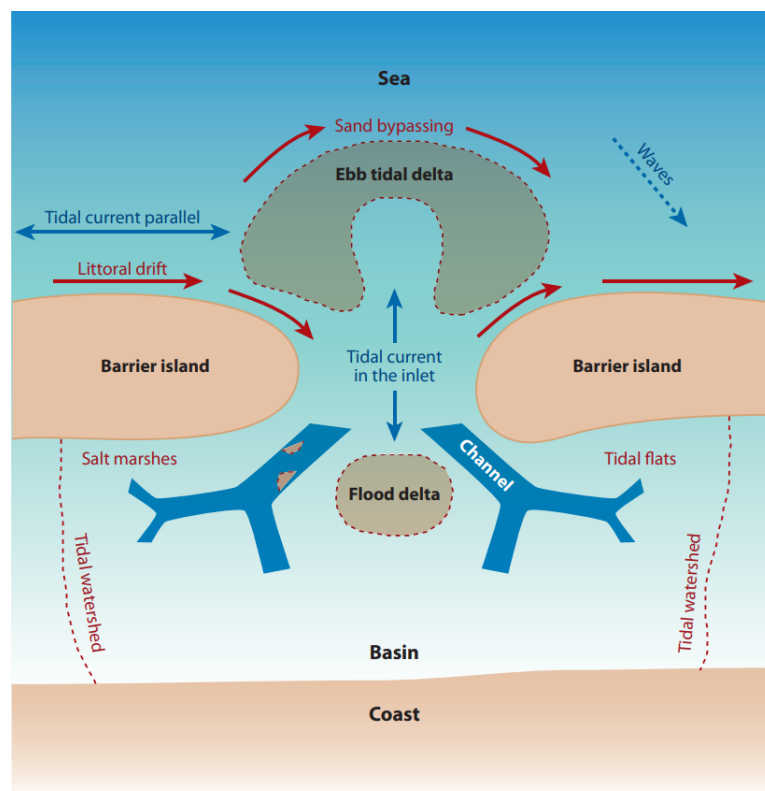


Figure 2.1 Schematized tidal inlet with main morphological features and processes labelled (Swart and Zimmerman 2009).

Bypassing at a stable tidal inlet system primarily occurs through migration of bars along the periphery of the ebb-tidal delta. These bars are the result of strong along-shore currents created by tidal currents and wave forcing along the edge of the delta (FitzGerald

1988, Herrling and Winter 2018). Often, bar complexes form on the downdrift side of the ebb-tidal delta (relative to the dominant sediment transport direction) (FitzGerald 1988). However, sediment bypassing more akin to littoral drift on a wave-dominated coast can occur at more wave-dominated tidal inlets (Fitzgerald et al. 2000). For very fine sand grains ($125 \mu\text{m}$), wave-driven suspended sediment transport along the periphery dominates independent of bar migration (Herrling and Winter 2018).

2.2 Ameland inlet and pilot nourishment

The Ameland tidal inlet is located in the north of the Netherlands and forms part of the Wadden Sea. The inlet is bordered by the barrier islands Terschelling to the West and Ameland to the East. The main morphological features as described in Elias et al. (2019) are shown in Figure 2.2.

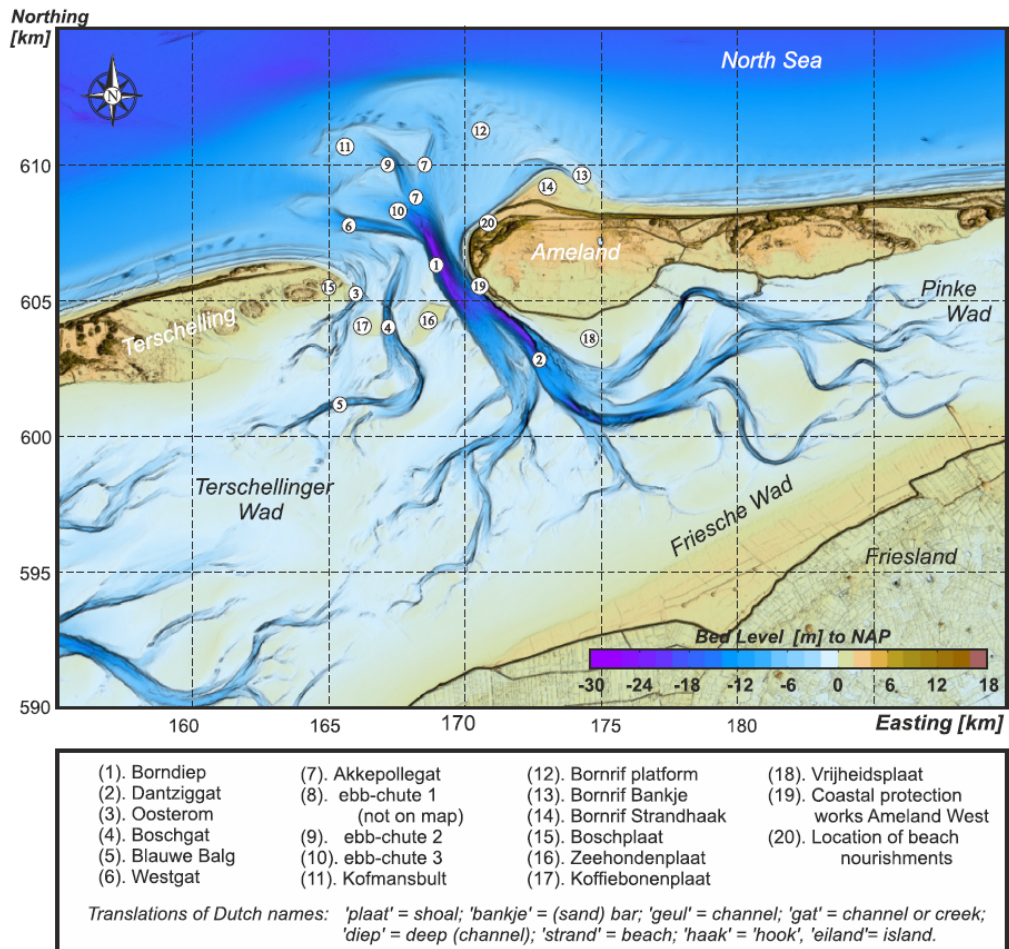


Figure 2.2 Main structures of the Ameland tidal inlet identified from a combination of 2017 and 2018 bathymetry (Elias et al. 2019).

The inlet has Borndiep as its main channel to the east, the Boschgat working as a secondary channel. To the west, Westgat forms a flood channel and Akkepollegat function as an ebb chute. The Kofmansbult and Bornrif are the major ebb shoals on the ebb-tidal delta. The Koffiebonenplaat separates the two channels in the inlet and forms a significant barrier for transport on the west side of Borndiep. The distribution of channels and shoals on the ebb-tidal delta only reflects the situation as it was in 2018, as the system is highly dynamic.

Elias et al. (2019) conclude that the eastward movement of the Borndiep channel had a large impact on the system. While Borndiep was previously located in the western part of the inlet, the channel moved eastward starting in 1854. This movement started to affect the west coast of Ameland around 1926 and is the reason for 'hard' interventions in this region, marked in Figure 2.2 as number 19.

Another major change within the system is structural erosion of the Boschplaat, the section of coast along the northeast of Terschelling. This started in the 1970s and has continued into the present day.

Sediment characteristics

On the natural bed, sediment with a D_{50} between 170 and 230 μm can be found, with fining taking place rotationally around the inlet in eastward direction. Coarser sediment was generally found in deeper channels (Elias et al. 2022).

Tidal conditions

The mean tidal amplitude around Ameland is approximately 2 m, with a neap tidal amplitude of 1.5 m and spring tidal amplitude of 3 m. Storm-related water set-up of more than 1.5 m has been observed as well (Elias et al. 2022).

Wave climate

For most of the wave record between 2007 and 2017, the observed significant wave height did not exceed 2 m. However, a small chance of more intense storms exists. Wave periods under normal conditions typically vary between 3 s and 6 s. For regular storm waves, with significant wave heights between 2 m and 3 m, this period is around 6.0 s, increasing to 7.6 s for harsher conditions (Elias et al. 2022).

Even though prevailing winds come mainly from a southwestern direction, the orientation of the islands causes most waves to come from a northnorthwesterly direction. A wind and wave rose of conditions at Schiermonnikoog, which are representative for those at Ameland (Elias et al. 2022), are shown in Figure 2.3.

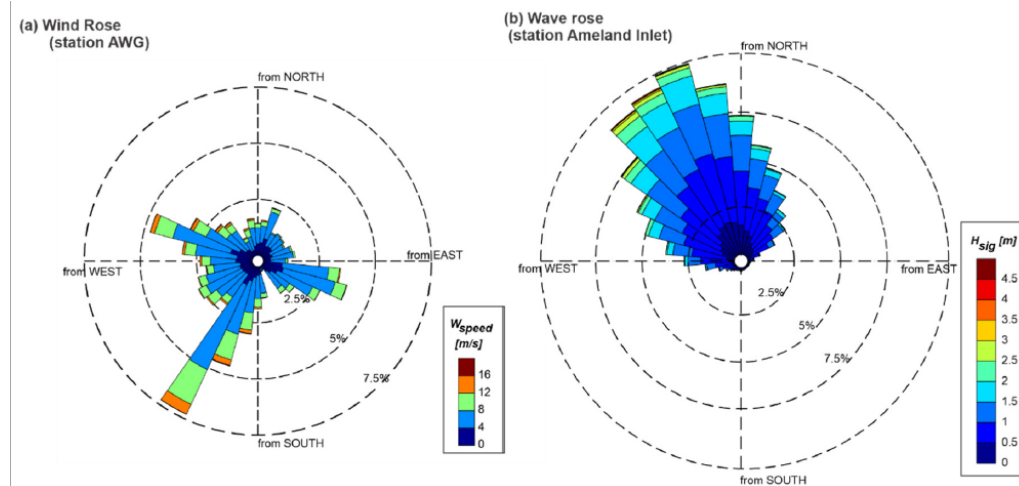


Figure 2.3 Wind and wave conditions at the Ameland tidal inlet (Elias et al. 2022).

Classification of coastlines, and thus ebb-tidal deltas, is often based on the relative magnitude of wave height and tidal range. This gives an indication as to which mechanisms are dominant for shaping the system and transporting sediment (Davis and Hayes 1984). Waves and tides have different levels of influence in different zones of the ebb-tidal delta. The Ameland tidal inlet is considered a mixed-energy system (Elias 2021), with tides and waves having varying levels of influence on different parts of the

ebb-tidal delta. Figure 2.4 shows how waves and tides affect different parts of the ebb-tidal delta. The outer western edge is predominantly shaped by waves, with the central ebb-tidal delta being more tide-dominated. The shallow area to the east on the ebb-tidal delta is again more wave-dominated (Elias 2021).

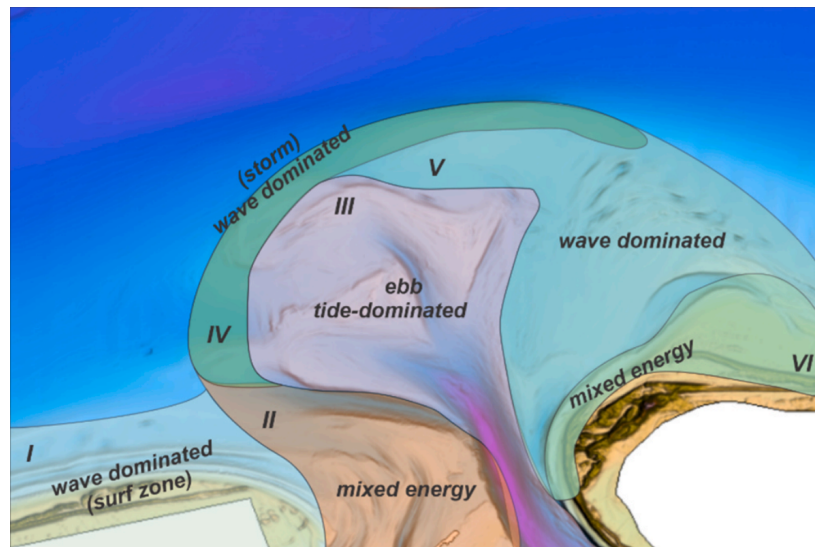


Figure 2.4 Dominant sources of energy in different zones of the Ameland ebb-tidal delta (Elias 2021).

As mentioned in the previous section, sediment bypassing at tidal inlets at barrier coastlines occurs mainly through the formation of bars on the downdrift side of the tidal inlet (relative to the dominant sediment transport direction). Formation of these bars has been observed at Ameland as well, as the Bornrif platform evolved from bars to a shoal to eventually attach at the northwestern coast of Ameland (Elias et al. 2019). Sawtooth bar migration has also been observed further east of the ebb-tidal delta (Brakenhoff et al. 2019). However, this does not always lead to a net transport of sediment. With a wave direction predominantly travelling in an eastern direction, the dominant sediment bypassing direction along the ebb-tidal delta is eastward as well. There is also a residual tidal current in eastward direction along the periphery of the ebb-tidal delta, assisting in flow bypassing (Elias 2021).

As part of the Kustgenese 2.0 project, a pilot nourishment was placed on the ebb-tidal delta of the Ameland inlet. This nourishment was put in place between March 2018 and February 2019 and consisted of approximately 5 million m³ of sand placed on the outer edge of the delta (see Figure 2.5). The nourishment was placed mainly to study the dynamics at play in tidal inlet systems, but it also served to offer a soft solution to the problem of the shrinking ebb-tidal delta. The North Sea coasts of the Wadden islands is subjected to harsh wind and wave conditions relative to the Wadden Sea coasts. These outer coasts get their sediment supply mainly from ebb-tidal deltas. When the ebb-tidal deltas shrink, so does the sediment bypassing capacity. This decrease in sediment supply to the downstream coasts could then lead to significant erosion (Swart and Zimmerman 2009).

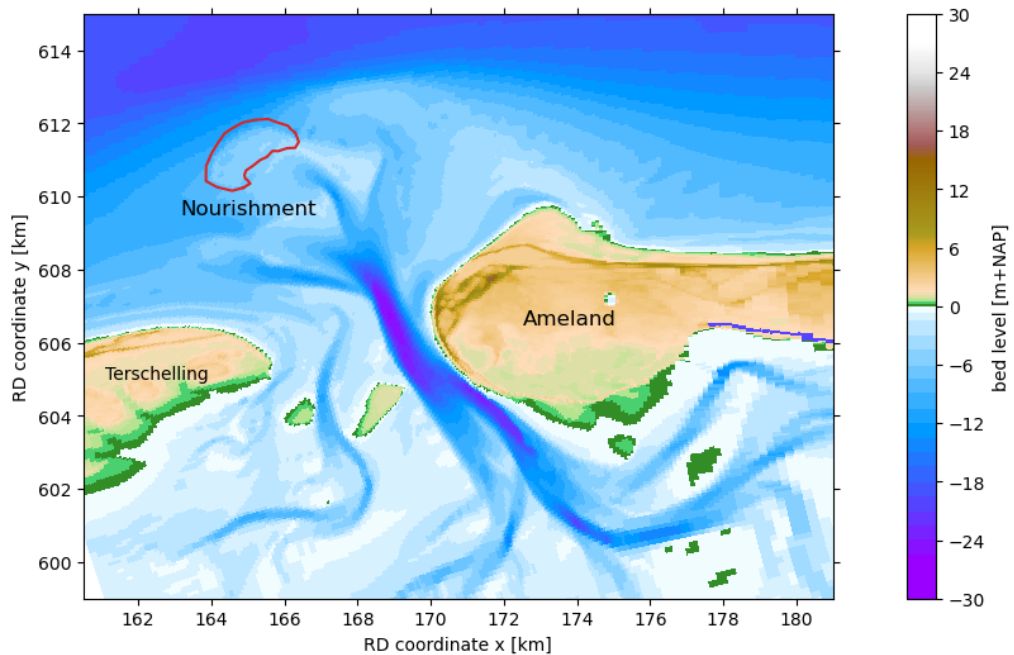


Figure 2.5 Bathymetry of Ameland inlet in spring 2018 with nourishment added and its location marked with a red outline.

Sediment used for the nourishment was dredged from an area with a D_{50} between 170 and 200 μm (Ebbens 2019).

Through SedTRAILS modelling done by Lambregts (2021), it was found that this nourishment did not significantly impact the sediment pathways within the system. The main pathways from the nourishment identified by Lambregts were a mainly wave-driven path along the outer edge of the ebb-shield just east of the nourishment and a mainly tide-driven path that went further south. These pathways coincide with the nourishment's aim of supplying the northern coasts of the Wadden Sea with more sediment.

It was noted in Elias (2021) that the ebb-shield the nourishment was placed nearby stopped outbuilding in 2016, after which it rotated and moved eastward slightly. Had this outbuilding continued, tide-driven transport of the nourishment would have been much more significant. As this did not happen, transport of the nourishment from its original location is mainly wave-driven. This wave-driven transport was also noted by Van Rhijn (2021) and Lambregts (2021).

Since its placement, the nourishment has shown steady erosion over time. Harlequin (2021) summarized volume changes together with model results of the erosion of the nourishment (Figure 2.6). This shows a gradual decrease in volume, interrupted by large drops during storm events in winters. For instance, there is a large decrease between October 2019 and April 2020.

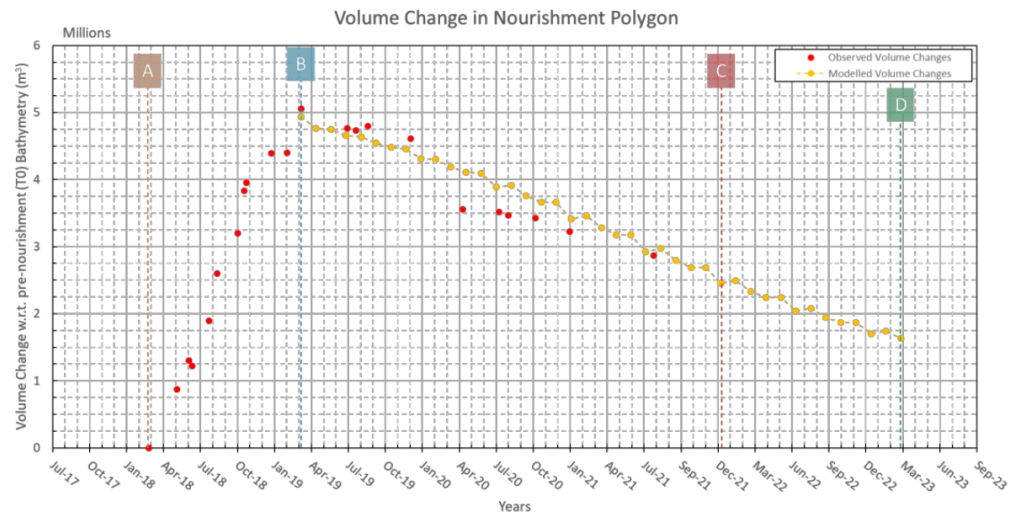


Figure 2.6 Volume changes within the nourishment polygon (red outline in 2.5) over time. Both observed (red dots) and modelled (orange dots and line) volume changes are included. Placement of the nourishment took place between markers A and B (Harlequin 2021).

The nourishment's decrease in volume can be seen in the bathymetry as well. Figure 2.7 shows strongest erosion from the outer edge of the nourishment, especially shortly after placement (C). The initial response concerns deposits along the outer edge of the ebb-shield just East of the nourishment (C), with more sediment depositing on the western edge of ebb-chute 2 afterwards (D and E).

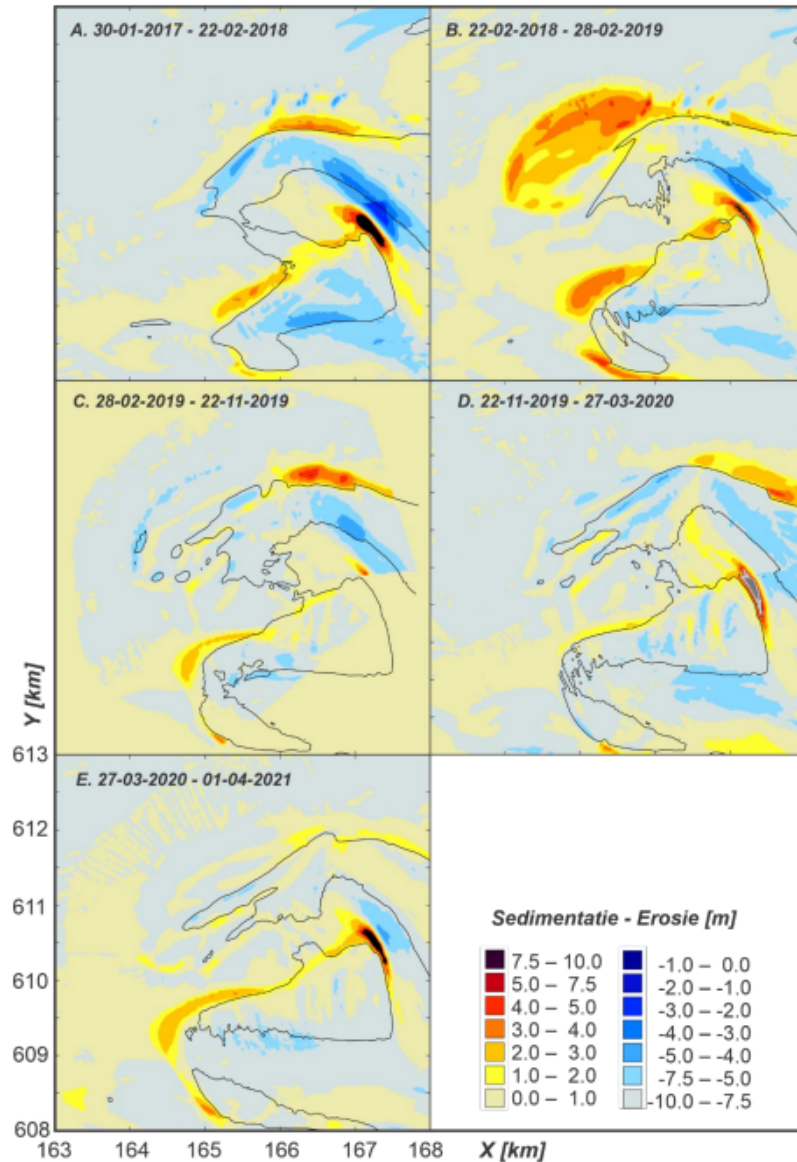


Figure 2.7 Erosion-sedimentation map at the nourishment location between January 2017 and April 2021 (Elias 2021). The nourishment was placed in the period shown in B.

Morphodynamic modelling of the specific impact of the nourishment was performed by Harlequin (2021). Figure 2.8 shows the difference in modelled bed level changes when comparing a simulation with and without the pilot nourishment present. One major impact is accumulation just Southeast of the nourishment. This difference is likely caused by increased wave dissipation from the nourishment. There is also significant outbuilding of the ebb-shield just east of the nourishment, which can also be observed in the measurements (Figure 2.7).

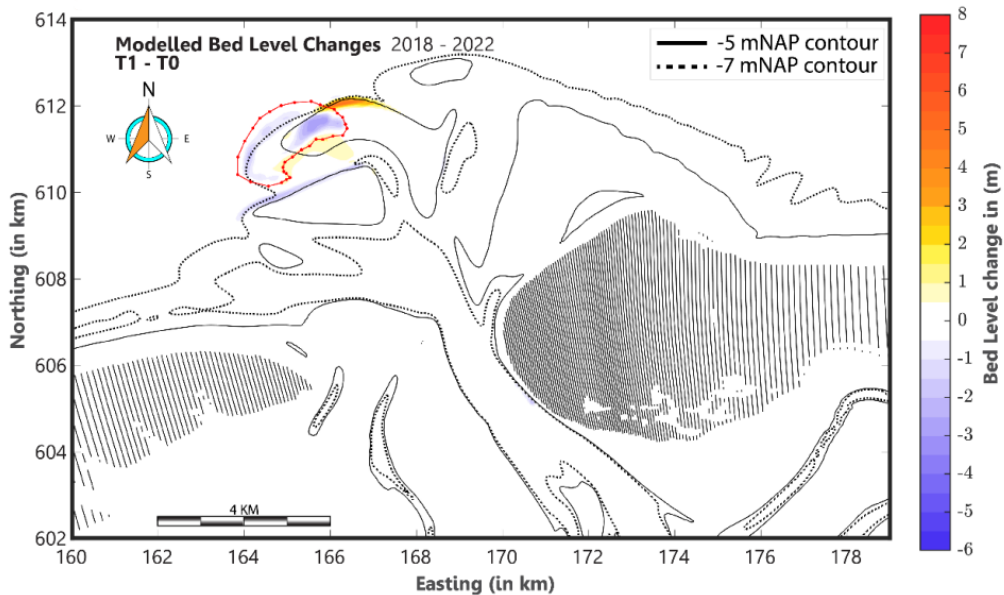


Figure 2.8 Difference in bed level changes of a morphodynamic Delft3D run with and without the nourishment added to the bathymetry. Changes are representative for a period between 2018 and 2022 (Harlequin 2021).

2.3 Delft3D-FM

To use SedTRAILS, an underlying velocity field must first be generated. For this report, that was done with Delft3D-FM. Delft3D Flexible Mesh (FM) is a process-based hydrodynamic modelling suite. While it can be used to model morphodynamics and sediment transport, it will be used here in morphostatic mode, meaning the bed level does not change. Delft3D-FM gets its name from its functionality to use so-called "unstructured" grids, where grid cells are not restricted to continuous grid lines. This allows for more efficient increases in resolution in areas where more detail is required.

Waves in the Delft3D-FM simulation are calculated using the D-Wave module, which uses SWAN (Booij et al. 1999). SWAN is a spectral wave model, which returns wave statistic information such as the significant wave height and peak period at each grid cell for each time step.

For running the SedTRAILS model, several variables need to be calculated by Delft3D. Firstly, the depth-averaged velocity. Delft3D-FM can be run in 3D as the name implies, but is often used for 2DH (two-dimensional in horizontal direction) simulations. For flow velocities, a logarithmic velocity profile is assumed over the depth. This velocity profile is then integrated over the depth. A reason to model in 3D would be to include, for instance, stratification over the water column that cause density-driven flows. As there is very little freshwater outflow, density-driven flows are not significant at the Ameland tidal inlet (Elias et al. 2019).

Both the mean and maximum bed shear stresses are required for SedTRAILS. Bed shear stresses are often the result of both waves and currents. A mean and maximum bed shear stress based on the combined action of currents and waves can then be defined, as is shown in Figure 2.9. This allows for both calculation of threshold of motion from the maximum shear stress from waves as and transport from tide- and wave-induced currents.

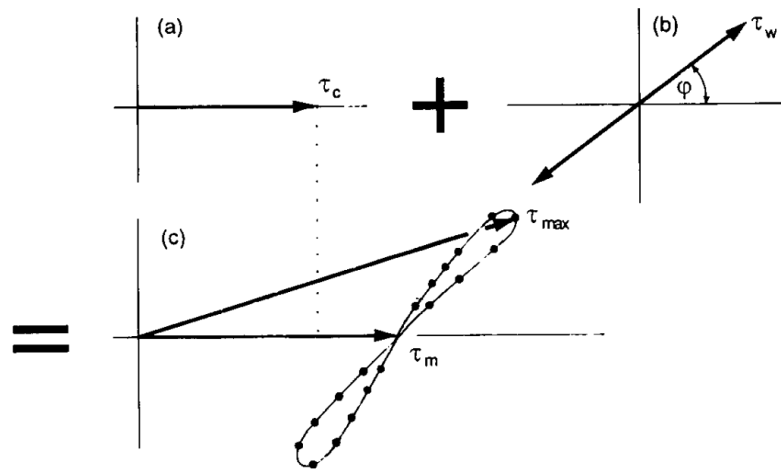


Figure 2.9 Method for determining mean and maximum bed shear stresses from combined action of waves and currents (Soulsby et al. 1993).

Additionally, the non-linear wave velocity components are of interest. This is elaborated on in subsection 2.4.2, as it is directly relevant to the workings of SedTRAILS.

For a more in-depth description of Delft3D-FM and its use, reference is made to the Delft3D-FM user manual (Deltares 2023). More information on its configuration in this report will be provided in Chapter 3.

2.4 SedTRAILS

Many different sediment transport models exist, so-called Eulerian models (e.g., Delft3D (Lesser et al. 2004), XBeach (Roelvink et al. 2009)) and particle-based or Lagrangian models (early examples are PTM (MacDonald and Davies 2006) and SandTrack (Soulsby et al. 2011), more recently TRACMASS (Aldama-Campino et al. 2020), NEMO (Madec et al. n.d.), OpenDrift (Dagestad et al. 2018)). A particle-based model currently in development is Sediment TRANsport visualization & Lagrangian Simulator, or SedTRAILS for short (Elias and Pearson 2020). This is a new Lagrangian numerical model that aims to look at individual sediment particles as they are transported through a velocity field, usually generated by Delft3D (Lesser et al. 2004).

SedTRAILS was first developed under the Research Program B&O (Beheer en Onderhoud kust) (Rijkswaterstaat n.d.) at TU Delft and Deltares, and later also within the research program TRAILS (TRacking Ameland Inlet Living Lab Sediment) at WUR (Wageningen University n.d.). SedTRAILS was first proposed in Elias and Pearson (2020), based on code developed for simulating coral larvae dispersal (Storlazzi et al. 2017). While the recent Lagrangian models mentioned previously tend to focus on water masses and tracer properties, SedTRAILS is focussed fully on the transport of sand particles.

There is a fundamental difference in approach when comparing Eulerian and Lagrangian models. Figure 2.10 illustrates this difference. In a Eulerian model such as Delft3D-FM, changes to a fixed part of the model are modelled. A Lagrangian model instead focusses on the motion itself, "following the motion of the fluid element" (Shadloo et al. 2016). Eulerian and Lagrangian approaches are often combined, using Eulerian velocity fields to estimate trajectories (van Sebille et al. 2018).

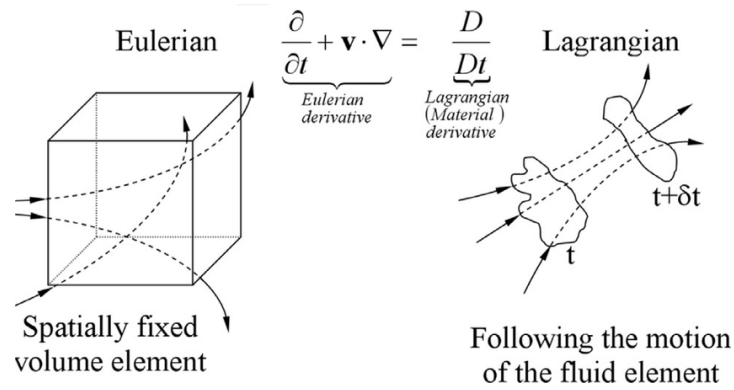


Figure 2.10 The difference between Eulerian and Lagrangian models in the context of hydrodynamics (Shadloo et al. 2016).

The Lagrangian approach has already been widely used in ocean analysis, using fluid particles as tracers for volume transport, salinity, or biochemical components (van Sebille et al. 2018). These tracers can be used to calculate (gross) transport through a system. SedTRAILS, a Lagrangian model, simulates particles representing sediment. Introducing a particle to the simulation is done by defining a particle source. This is the starting location of a particle at a specified time step. This specified time step is usually the start of the simulation.

It should be noted that SedTRAILS is in still development. While used in some publications (see section 2.4.4), it has not been nearly as broadly used or verified as the more established (particle tracking) models named in this introduction. This holds especially true for the transport formulation with burial included. While previous versions used the sediment transport field provided by Delft3D-FM, the latest version of SedTRAILS calculates its own sediment velocity vectors.

2.4.1 Transport formulation

The main method for calculating transport that SedTRAILS utilizes is outlined in Soulsby et al. (2011). The velocity of each grain at each time step can be calculated based on the flow velocity from a Eulerian hydrodynamic simulation. This is done with the following formula:

$$\vec{u}_{gr} = F \cdot P \cdot R \cdot [\vec{U}_c + \vec{\Delta}] \quad (2.1)$$

Where:

- F : Freedom factor, 0 if particle is trapped, 1 if particle is free to move. This is elaborated on in the following section.
- P : Probability of motion based on shear stress (between 0 and 1)
- R : Velocity reduction factor based on mode of transport, since particles move faster in suspended load than bed load
- U_c : Flow velocity at given point
- Δ : Horizontal diffusivity component [m/s], calculated using $D = \Delta^2/2\Delta t$, where D is the horizontal diffusivity (typical value of $D = 0.2m^2/s$) and Δt is the simulation time step.

Particles are then moved using this formulation:

$$\frac{d}{dt}\vec{x}(t) = \vec{u}_{gr}(\vec{x}(t), t) \quad (2.2)$$

Where:

- $\vec{x}(t)$: Time-dependent position vector [m]
- \vec{u}_{gr} : Grain velocity vector [m/s]

How this works in practice is shown in Figure 2.11. Particles get moved in the direction of the current. Factor P ensures that particles only move when the bed shear stress is high enough. Factor R is different depending on the mode of transport and can reduce grain velocity significantly. Factor F is only either 1 or 0, depending on whether a particle can be considered "buried" or not.

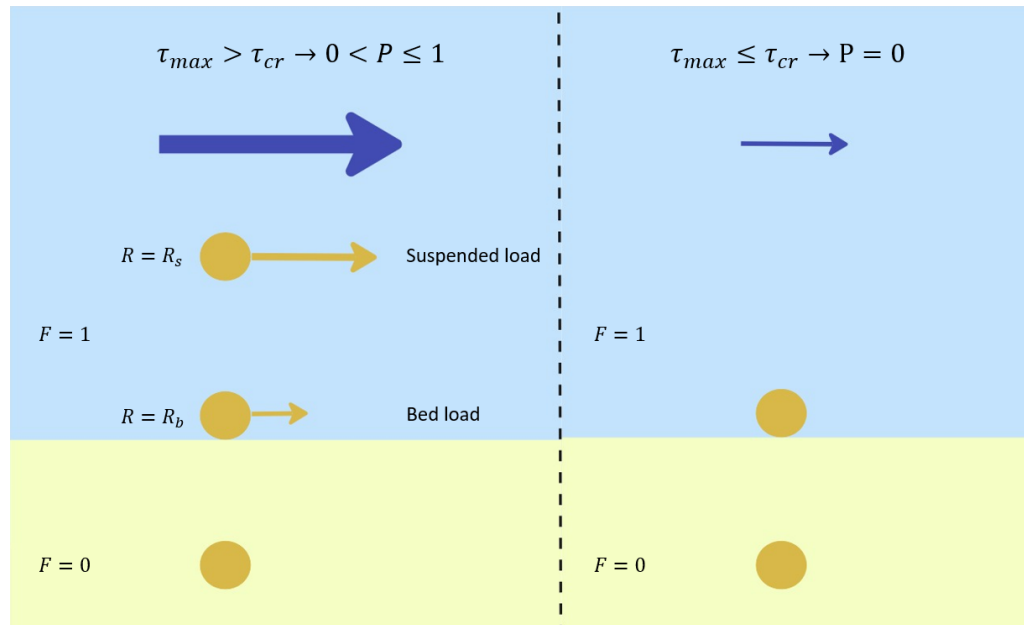


Figure 2.11 Depiction of SedTRAILS grain velocity calculation depending on parameters F (burial), P (probability of motion) and R (mode of transport). The arrow at the top represents the flow velocity \vec{U}_c . The orange circle represents a particle, with the orange arrow representing the grain velocity.

Importantly, this formulation does not directly include forcing through waves. While the maximum bed shear stress as a result of waves is used in calculating the value for several factors and the flow velocity includes wave-induced currents, there is no direct dependence on wave-related processes. Because there is no direct inclusion of wave forcing, the direction in which sediment moves is only influenced by the direction the current is moving in.

2.4.2 Bed interaction and burial

Of particular interest to this report is the factor F . This factor models interaction with the bed. The method is based on the concept that a particle is either buried and unable to move ($F = 0$) or free ($F = 1$). Whether a particle goes from being unable to move to being able to is based on transition probabilities. These are the probability that a particle goes from trapped to free and the probability that a particle goes from free to trapped, in the paper named a and b respectively. a and b are calculated with the following formulation:

$$b = 0, \quad \text{if } \theta_{max,a} \leq \theta_{cr,a} \quad (2.3)$$

$$b = b_e \{1 - \exp[-(\theta_{max,a} - \theta_{cr,a})/\theta_s]\} \quad \text{if } \theta_{max,a} > \theta_{cr,a} \quad (2.4)$$

$$a = \frac{\gamma_e b}{1 - \gamma_e} \quad (2.5)$$

These then depend on three tuneable parameters:

- b_e : Maximum free-to-trapped transition probability [1/s]
- θ_s : Scale value that determines the distribution of residence times [-]
- γ_e : Long-term equilibrium proportion of particles that are free [-]

In this formulation, $\theta_{max,a}$ and $\theta_{cr,a}$ are directly calculated using the bed shear stress and sediment properties. $\theta_{max,a}$ is based on the maximum bed shear stress, with $\theta_{cr,a}$ being the critical Shields parameter at which sediment starts moving. The likelihood that a particle deposits thus depends on the difference between the critical bed shear stress for erosion and the maximum bed shear stress that occurs.

2.4.3 Wave-driven bed velocity

As mentioned in section 2.3, Delft3D-FM is often run with a depth-averaged velocity. When waves propagate through a system, but especially when they break, the return current or undertow can become the dominant direction for this flow (see Figure 2.12). When waves propagate through water, however, there is a small residual near-bed velocity, shown at the bottom of Figure 2.12. While undertow (offshore-directed) is a significant factor in hydrodynamics, as it especially transports suspended sediment offshore, the velocity near the bed can be in the opposite direction (onshore-directed). Since near-bed velocity is more significant to sediment transport, it can be used to more accurately model the influence from waves on transport patterns and pathways.

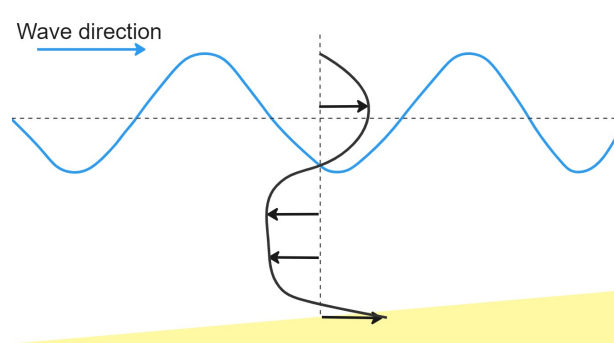


Figure 2.12 Residual velocity profile under breaking waves, including Stokes' drift near the surface, undertow for most of the water column, and a small near-bed orbital velocity. Adapted from Bosboom and Stive (2022).

A method to calculate the wave-driven bed velocity, outlined in Ruessink et al. (2012), uses the Ursell number to estimate wave skewness and asymmetry, which are then used to calculate the near-bed orbital velocity. This non-linear wave velocity component is calculated within Delft3D-FM.

The current implementation is a simple addition of the non-linear component to the overall flow velocity, and changes equation 2.1 into the following:

$$\vec{u}_{gr} = F \cdot P \cdot R \cdot \left(\vec{U}_c + \vec{U}_{w,nonlinear} + \vec{\Delta} \right) \quad (2.6)$$

This wave-driven bed streaming or non-linear wave velocity component is sometimes referred to as Ruessink bed streaming in the remainder of this report, as it reflects the naming convention within SedTRAILS and offers a shorthand for referring to this specific model aspect.

2.4.4 Past applications

At first, SedTRAILS was developed as a tool for visualisation (hence the visualisation part of the name). The particles it simulated did not represent the actual movement of sand particles, but were rather visualisations of the net sediment transport field. Instead of calculating a grain velocity vector field using the Soulsby et al. (2011) transport formulation, particles were transported using the sediment transport vector field generated in Delft3D (Figure 2.13). This gave quick and easy insights into net sediment pathways without requiring extensive extra calculations. Note that the main difference between the method seen in Figure 2.13 and the method described above is a replacement of the Eulerian Sediment Transport Fields section with the grain velocity calculations using the Soulsby et al. (2011) formulation.

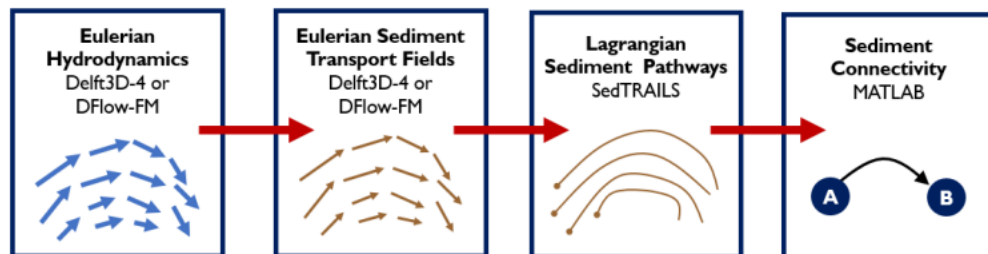


Figure 2.13 Original concept for calculating sediment pathways in SedTRAILS Pearson et al. (2021).

One of the first applications of SedTRAILS at the Ameland inlet was a connectivity study described in Pearson et al. (2021). Here, different areas in the system were mapped out to analyse more broadly which pathways sediment takes through the system. The model area was first divided into subsections using k-means clustering of the bathymetry. This resulted in the network seen in Figure 2.14a.

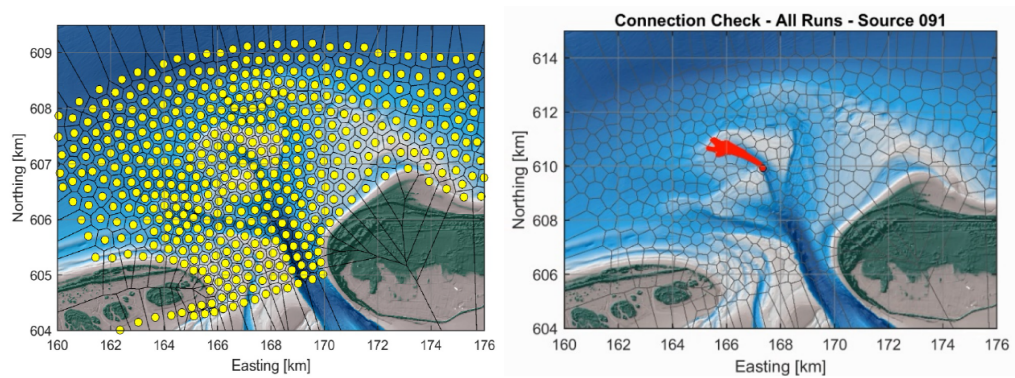


Figure 2.14 Connectivity network from Pearson et al. (2021) (left) and an example of Sed-TRAILS results from the same study (right). This result is only from one section of the connectivity network that was set up for the analysis.

Connectivity was studied by finding for each cell the degree (amount of other cells it connected to) and strength (amount of particles from other cells entering).

General pathways were also modelled, with each cell in the connectivity network (Figure 2.14, left) acting as a particle source. These pathways (Figure 2.15) show some recirculation on the eastern section of the ebb-tidal delta, with some significant pathways leading from the central ebb-tidal delta and along the edge of the delta eastward.

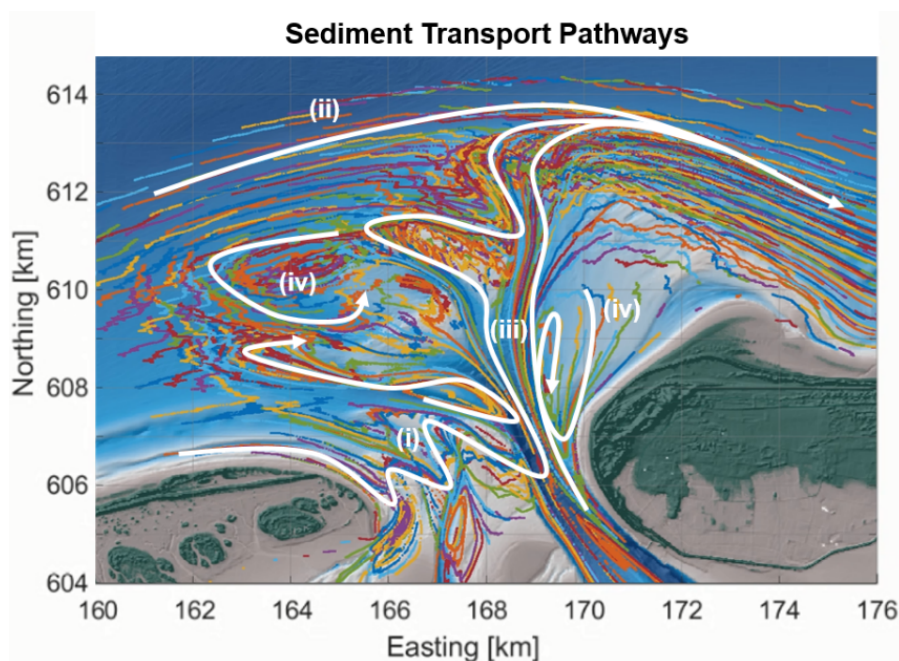


Figure 2.15 Sediment pathways at the Ameland tidal inlet. The pathways were modelled with SedTRAILS using a sediment transport vector field created using Delft3D. The pathways as shown are: (i) inlet bypassing, (ii) transport along outer delta, (iii) transport through main ebb channel, (iv) recirculation (Pearson et al. 2021).

With this version of SedTRAILS, more work was also done analysing sediment pathways in the Ameland tidal inlet by Lambregts (2021). This thesis used SedTRAILS to analyse both the sediment pathways present in the system as well as the effect the nourishment had on the flows and sediment transport patterns in the system, resulting in Figure 2.16.

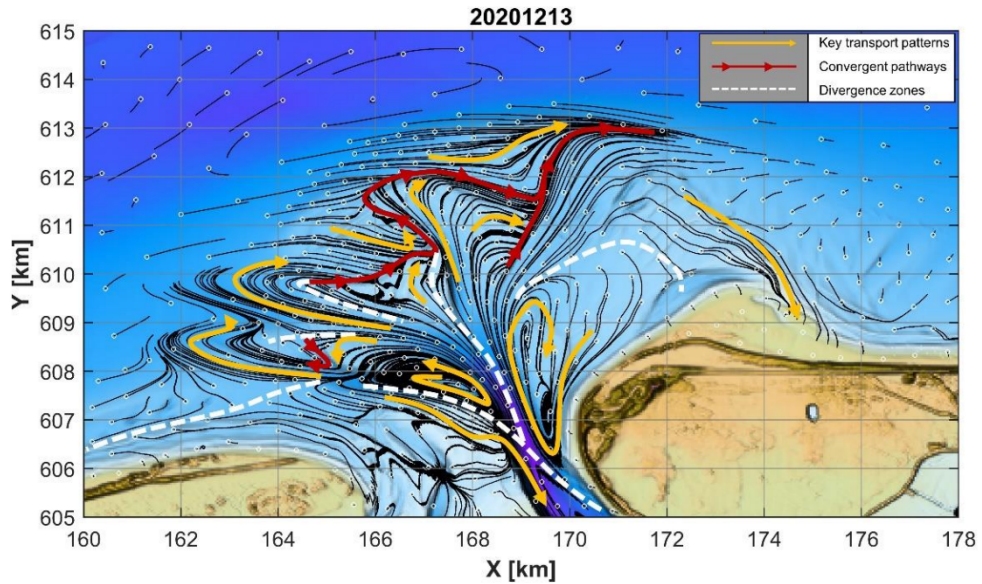


Figure 2.16 Sediment pathways as concluded from SedTRAILS results by Lambregts (2021). The white circles indicate particle sources, with their trajectories marked in black lines.

This report also analysed pathways of sediment from the nourishment using SedTRAILS, although not in great detail. Pathways under the influence of only tides and a combination of tides and waves were generated, an example of which is shown in Figure 2.17. Since these pathways remained largely unchanged in simulations with and without the nourishment present, the nourishment was deemed to be system-following (Lambregts 2021).

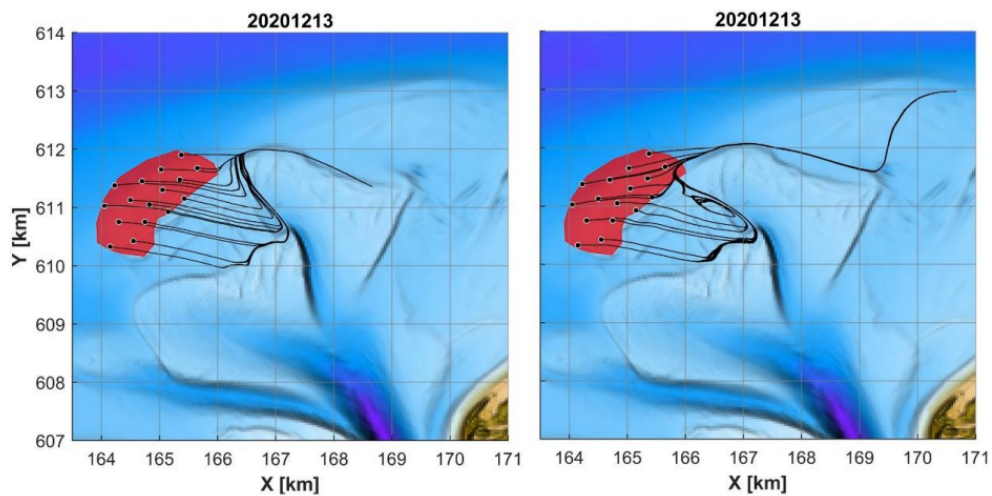


Figure 2.17 SedTRAILS sediment pathways away from the nourishment (Lambregts 2021). The left figure shows a tide-only simulation, while the right figure included waves in the forcing.

Other systems have been modelled using SedTRAILS as well, e.g., sediment pathways in Burrard Inlet in Canada (Meijers 2021) and the Western Scheldt (Elias et al. 2021), and both sediment and mangrove propagule pathways at the coast of Demak in Indonesia (Thillaigovindarasu 2023 and Bisschop 2023).

The first publication using SedTRAILS that used the [Soulsby et al. \(2011\)](#) transport formulation instead of a Delft3D transport field is [Pearson et al. \(2023\)](#). In this paper, an idealised inlet was modelled. Importantly, the freedom factor was not used. The main goal was to generate Lagrangian Coherent Structures, a way to visualise places within a system that particles tend to move towards or away from.

While insightful, these applications have not used SedTRAILS for the modelling of nourishment dispersal, nor have they used the full [Soulsby et al. \(2011\)](#) transport formulation with burial included. To focus on modelling the nourishment and to assess the forcing conditions and burial factor, a new methodology must be developed.

3 Methods

This chapter provides the methodology to answer the research questions outlined in chapter 1. First, the approach is conceptually described, after which the general model set-up of Delft3D-FM and SedTRAILS are provided. The wave conditions and water level boundaries are then provided, along with the burial sensitivity that will be tested.

3.1 Conceptual application of model

To assess dispersal of the nourishment, a slightly different approach to previous uses of SedTRAILS (e.g., Lambregts (2021), Pearson et al. (2021)) has to be taken. The main difference is in both the particle source set-up and how the generated pathways are processed. The methodology, schematised in Figure 3.1, begins with Delft3D-FM simulations to generate a velocity and bed shear stress field. This is then processed by SedTRAILS and, using equation 2.1, turned into a grain velocity field. Importantly, the second step calculates factors P and R from 2.1, but not the burial factor, F . Instead, erosion and deposition probabilities a and b are calculated for this velocity field. The freedom factor is determined again for each time step in the SedTRAILS simulation. The value for this factor is quite extreme, being either 1 or 0. If F is not redetermined for each time step in the SedTRAILS simulation, the stochastic nature of the burial factor is lost, as a particle would always move or always be buried at specific locations and time steps. Implementation of the freedom factor is then done by generating a random number between 0 and 1 for each particle at each time step and comparing it to the relevant transition probability a or b .

After grain velocity calculations are complete, the particles are released and their pathways through the system are tracked. Finally, these results are aggregated at the end using python code (see Appendix A) to find the particle density throughout the simulation. This results in graphs with shaded squares as on the right in Figure 3.1.

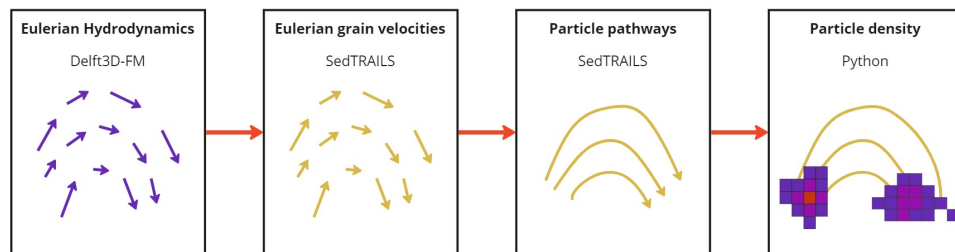


Figure 3.1 Steps performed to achieve results as outlined in the remainder of this report.

This method for calculation in this specific case study conceptually works as shown in Figure 3.2.

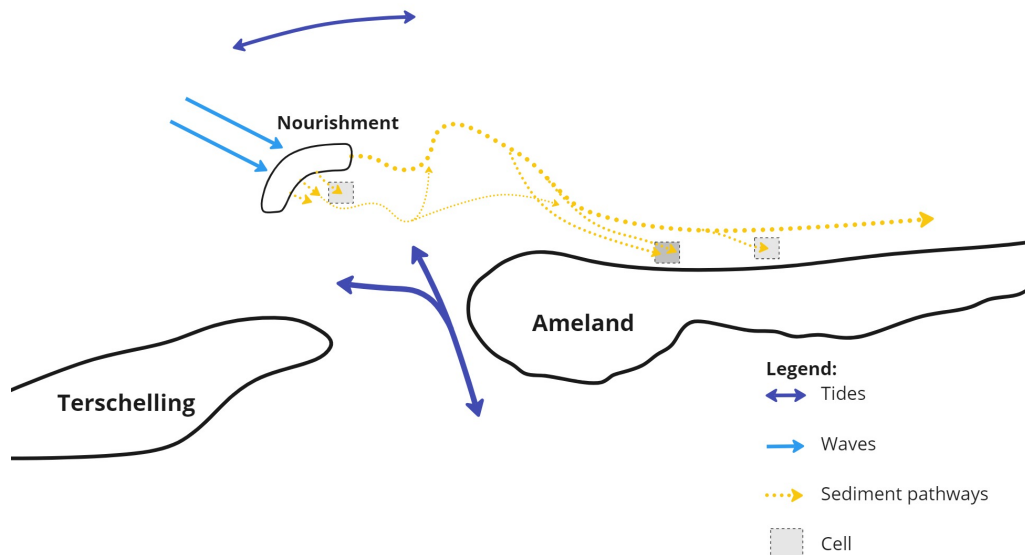


Figure 3.2 Conceptual model for particle simulations at the Ameland tidal inlet. Particles are released at the nourishment location and through wave and tidal forcing transported through the system. The particles are then aggregated into cells and counted to assess how many particles end up in specific locations.

The model can be run for much longer than the provided velocity field. Once the end of the velocity field is reached, SedTRAILS loops back to the beginning. For this reason, it is important to choose the bounds of this velocity field such that the difference between the two ends is minimal. As SedTRAILS utilizes a threshold of motion within its transport calculation (factor P), choosing a moment where flow velocities are low for this cut-off point reduces the effect of differences in velocity on the calculation significantly (see Figure 3.3).

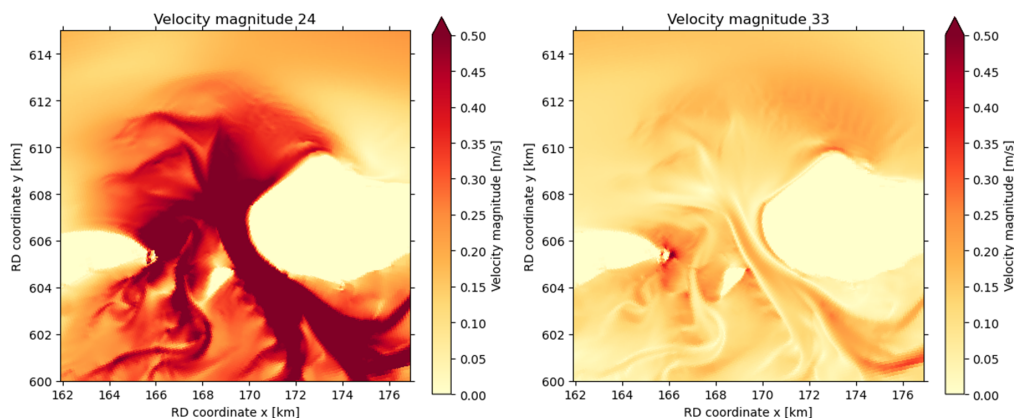


Figure 3.3 Example of two moments in flow-only Delft3D-FM simulation. The left figure shows a moment during rising tide. The right figure shows the moment around flow reversal, where velocities are briefly very small in the entire system.

3.2 Model set-up

The basic set-up of both the Delft3D-FM model and SedTRAILS are described in this section. For Delft3D-FM, the grid and bathymetry for the flow and wave models is given, along with the wave and water level boundary conditions. For SedTRAILS, the particle source setup and a default set of parameters is given.

3.2.1 Delft3D-FM

The basic set-up of Delft3D-FM lines up with the Delft3D-4 configuration that was used in Harlequin (2021), using the 2018 T1 bathymetry from that report as the bathymetry here (Figure 3.4). The unstructured grid used here is a direct conversion from the curvilinear grid used in Harlequin (2021), retaining all nodes, edges and faces. The grid has a variable resolution of between 30x40m at the inlet and 300x350m near the boundaries, giving cell area sizes of between 0.0012 km² and 0.127 km² (Harlequin 2021). The 2018 T1 bathymetry is based on measurements from 2018 but has the pilot nourishment inserted.

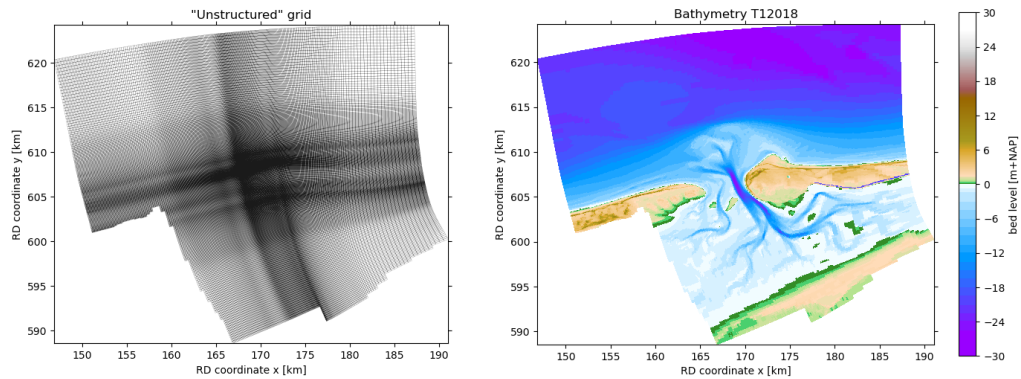


Figure 3.4 Grid and bathymetry of Delft3D-FM flow simulation

The wave forcing is calculated on a separate grid and bathymetry that broadly match those of flow (Figure 3.5). The wave grid is coarser than the flow grid, with a grid resolution of 50x80m (0.0049 km²) at the inlet and 750x650m (0.505 km²) near the boundaries. The wave grid is also extended east and west to account for proper wave propagation through those boundaries.

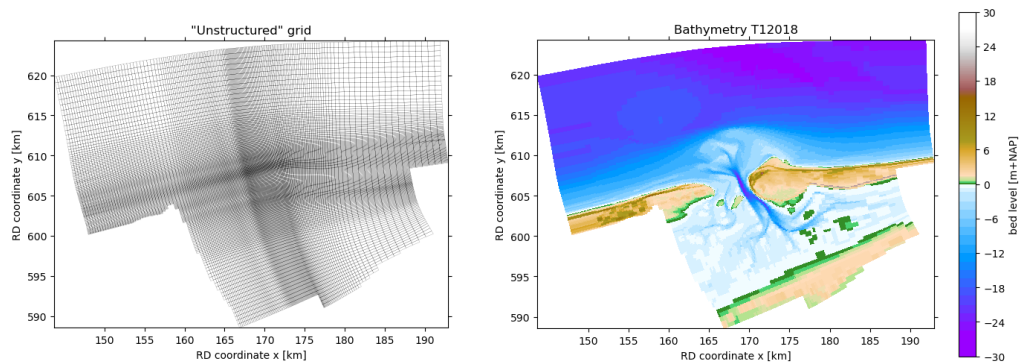


Figure 3.5 Grid and bathymetry of Delft3D-FM wave simulation

The lower resolution for the wave grid lowers computational time for the wave component of the simulation. This does introduce uncertainty when results from the wave grid are placed onto the flow grid. In this context, it was deemed an acceptable loss in resolution, as the spatial scale for the most relevant morphological features (the nourishment, major ebb-chutes, Borndiep inlet channel) is larger than the resolution of the wave grid. Since the simulation does not update the bed level, smaller-scale features that can sometimes develop into larger scales (as noted by Elias et al. (2019)) are not as relevant. However, care must be taken with this lower resolution. The lower resolution grid causes wave-related hydrodynamics to be interpolated onto the flow grid at

the wrong location. This results in a loss of detail and changes in location of breaking waves and wave propagation over the ebb-tidal delta. This is important to particle pathways. It is likely that this will need to be corrected in future model studies of this system.

Boundary conditions are applied on the open boundaries to the east, west and north. For the D-Flow-FM model, a water level boundary is used on the northern boundary, with a water level gradient (Neumann) boundary enforced at the East and West boundaries. This is to prevent instabilities in the model that occur when using three water level boundaries. In the D-Wave model, a parametric JONSWAP spectrum is assigned at each boundary through the significant wave height, peak period and the wave direction.

3.2.2 Wave condition schematization

When schematizing the wave climate at the Ameland tidal inlet (see Figure 2.3), [Harlequin \(2021\)](#) identified two sets of wave conditions. These conditions are shown in tables 3.1 and 3.2. The wave conditions were manually selected from dividing the existing wave climate into different directional and wave height bins.

Wave condition	Wave height [m]	Wave period [s]	Wave direction [deg]	Probability of occurrence [%]	Wind speed [m/s]	Wind direction [deg]
1	0.80	4.27	293.10	27.41	6.71	293.10
2	0.75	4.70	352.56	23.97	6.57	352.56
3	0.75	3.79	56.32	11.93	6.57	56.32
4	1.87	5.29	298.08	21.34	9.77	298.08
5	1.83	5.49	346.96	11.83	9.66	346.96
6	1.66	4.72	51.86	3.52	9.17	51.86

Table 3.1 Six wave conditions for velocity field generation at the Ameland tidal inlet ([Harlequin 2021](#))

Wave condition	Wave height [m]	Wave period [s]	Wave direction [deg]	Probability of occurrence [%]	Wind speed [m/s]	Wind direction [deg]
1	0.83	3.96	276.59	13.06	6.80	276.59
2	0.77	4.62	312.20	13.57	6.63	312.20
3	0.75	4.70	352.56	23.29	6.57	352.56
4	0.75	3.79	56.32	11.59	6.57	56.32
5	1.55	4.62	278.04	7.31	8.86	278.04
6	1.57	5.16	312.01	7.46	8.91	312.01
7	1.55	5.19	348.83	8.55	8.86	348.83
8	1.52	4.50	54.07	2.90	8.77	54.07
9	2.38	5.34	281.34	2.44	11.23	281.34
10	2.43	5.81	312.57	3.53	11.37	312.57
11	2.40	5.76	345.15	2.95	11.29	345.15
12	2.27	5.18	47.30	0.51	10.92	47.30
13	3.53	6.26	285.70	0.49	14.52	285.70
14	3.63	6.80	312.29	1.57	14.81	312.29
15	3.54	6.79	341.88	0.76	14.55	341.88
16	3.21	5.88	41.34	0.01	13.60	41.34

Table 3.2 Sixteen wave conditions for velocity field generation at the Ameland tidal inlet (Harlequin 2021)

Both these sets of wave conditions are simulated one wave condition per simulation, resulting in a set of six and sixteen Delft3D results. The increased number of wave conditions is used to assess the effect of including more energetic conditions, such as conditions 13-16 in Table 3.2, on SedTRAILS.

To assess broadly how waves impact the dispersal of the nourishment, a SedTRAILS simulation without wave forcing is also performed.

3.2.3 Offshore boundary

For the Ameland tidal inlet, a morphological tide was determined. This tidal window is 24 hours and 50 minutes long. It is referred to as a morphological tide as it was calibrated to match the mean residual transport through the Borndiep inlet channel when using a spring-neap tidal cycle (Jiao 2014). This tidal window was used to model the system in this report as well and can be found in Figure 3.6.

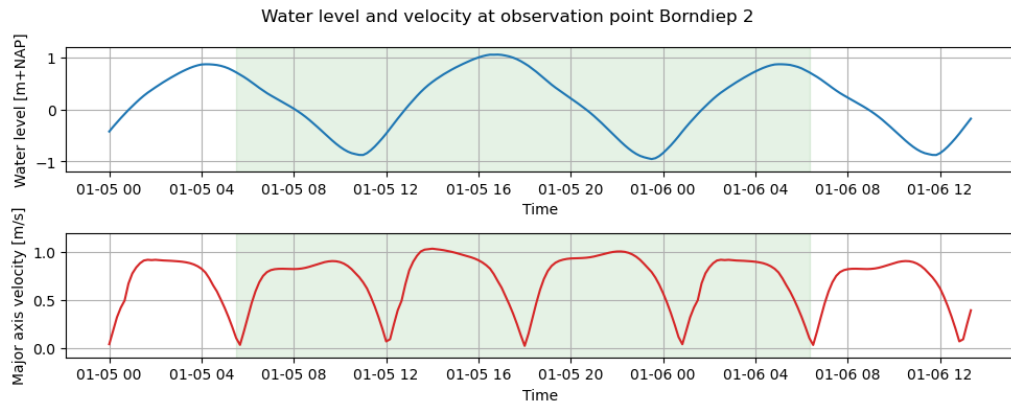


Figure 3.6 Morphological tidal window that will be simulated. Both water level and velocity are the result of a flow-only simulation. The green field indicates the field that is simulated in Delft3D-FM, and thus the section that will be used as the velocity field for SedTRAILS. The red line shows the major axis velocity magnitude along the tidal ellipse.

In reality, however, the system is better characterized by a spring-neap tidal cycle, as mentioned in section 2.2. Figure 3.7 shows a clear variation in water levels over a month long period, with periods of neap- and spring-tide. The variation in tidal amplitude brings with it changes in currents and dynamics. This is especially important in areas with strong tidal influence (Schrijvershof et al. 2023).

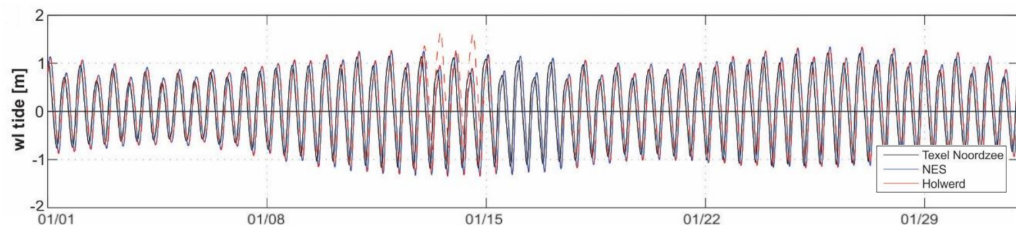


Figure 3.7 Water level from three measuring stations near the Ameland tidal inlet (Elias 2017).

To assess the significance of a changing tidal amplitude for SedTRAILS simulations, a morphological (Figure 3.6) and a spring-neap tide (Figure 3.8) will be compared.

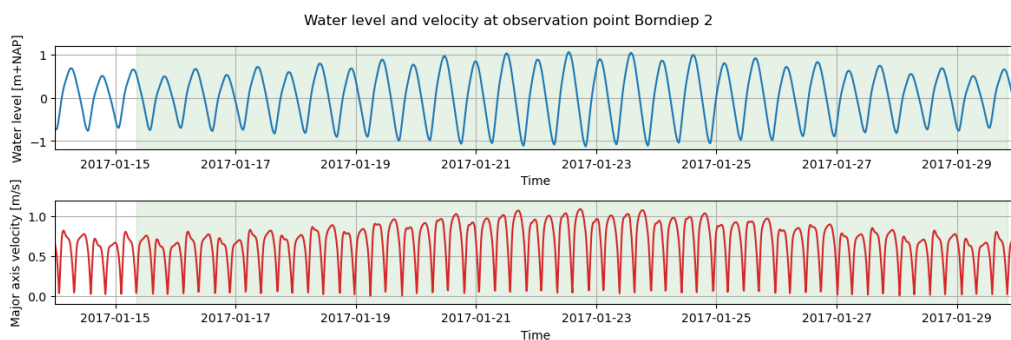


Figure 3.8 Spring-neap tidal window that will be simulated. Both water level and velocity are the result of a flow-only simulation. The green field indicates the field that is simulated in Delft3D-FM, and thus the section that will be used as the velocity field for SedTRAILS. The red line shows the major axis velocity along the tidal ellipse.

The spring-neap tidal cycle in

Figure 3.8 was created using the method as described in Schrijvershof et al. (2023). In this case, a full Wadden Sea model was run to create water level data at the Ameland model boundaries. This water level data could in turn be converted to a representative spring-neap tidal cycle. This is the tidal cycle used to test the tidal schematisation.

As the spring-neap tidal cycle requires a much longer simulation time than the morphological tide, the spring-neap tidal cycle is only simulated with six wave conditions. As such, results of the morphological tide with six wave conditions are compared to results of the spring-neap tidal cycle with six wave conditions.

3.2.4 SedTRAILS

In the previous section, two sets of several wave conditions were defined to all run separately. However, SedTRAILS needs just one Eulerian velocity field. To combine these wave conditions together, a weighted average based on the probability of occurrence of each wave condition is made, schematized in Figure 3.9. After being combined, the Eulerian hydrodynamics can be turned into a grain velocity field using equation 2.1.

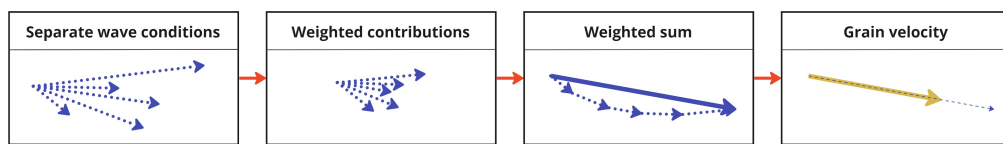


Figure 3.9 Process of averaging vectors from several Delft3D-FM hydrodynamic models before being processed into grain velocities. The dotted arrows indicate vectors (e.g., currents, bed shear stresses) in separate Delft3D-FM results. The solid blue line is the weighted average of these separate vectors. The last diagram shows this same vector as a thin dashed arrow, with the grain velocity as a solid yellow arrow.

An alternative method would be to take the weighted average of particle positions afterwards, as shown in Figure 3.10. This method will be tested as well.

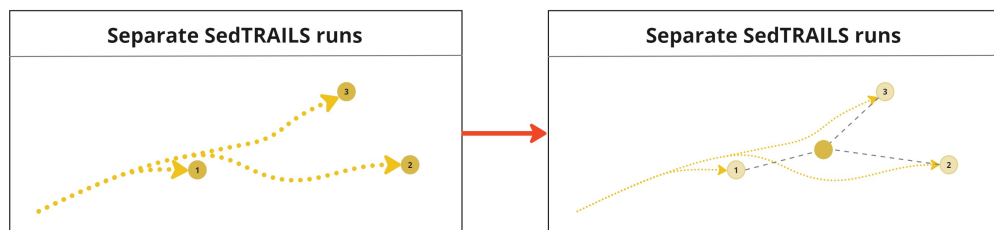


Figure 3.10 Method for averaging particle positions of multiple separate SedTRAILS runs.

For modelling of the nourishment, particle sources within SedTRAILS are defined only on the nourishment. 5000 points were uniformly randomly generated within the nourishment boundary polygon (red outline in Figure 2.5). This method results in a mostly uniform distribution of starting points for the particles in the simulation, shown in Figure 3.11. Details of this method can be found in Appendix A.

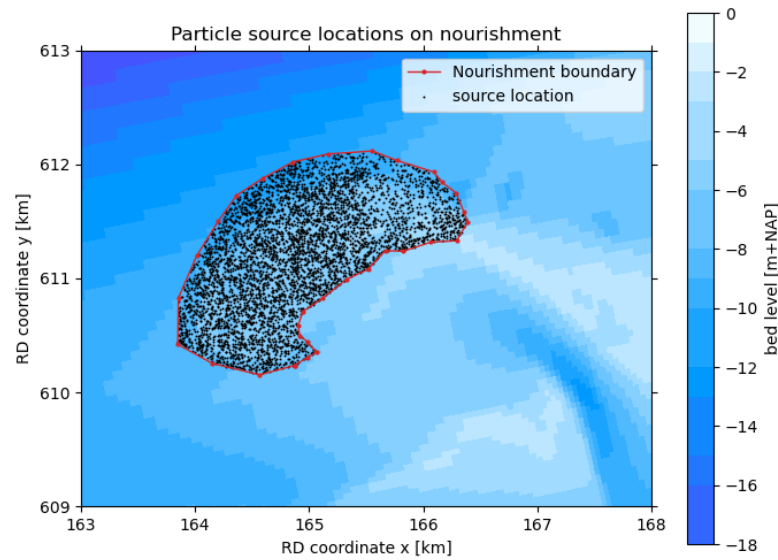


Figure 3.11 Locations of particle sources (and thus starting locations of particles) for SedTRAILS model runs.

One particle is released from each source at the start of the simulation, meaning 5000 particles start being forced by the grain velocity field at the starting time step. While not perfect, using this approach over a more continuous release of particles better represents the initial large availability of sediment from the nourishment.

Within SedTRAILS are some parameters that can be set. The following is an overview of all parameters that are considered the default settings for this report. The time step and diffusion coefficient were kept to default parameters in SedTRAILS. The median grain diameter corresponds to the grain size of sediment used for the Ameland pilot nourishment (Ebbens 2019). The burial parameters are not the standard values as defined in Soulsby et al. (2011). Instead, these were chosen as a starting point for sensitivity analysis, as this burial configuration showcases differences between runs in the given timespan adequately. Any deviation from these values will be indicated as necessary.

General model set-up

Time step of SedTRAILS simulation	Δt	=	30	s
Diffusion coefficient	D	=	0.1	m^2s^{-1}
Median grain diameter	D_{50}	=	200	μm

Burial parameters

Maximum free-to-trapped transition probability	b_e	=	$1.7 \cdot 10^{-3}$	s^{-1}
Scale value for residence time distribution	θ_s	=	1.2	
Long-term equilibrium proportion of free particles	γ_e	=	0.01	

Table 3.3 Default parameters for SedTRAILS modelling.

Sensitivity of the three burial parameters is tested by adjusting the values of each parameter individually. The values that will be tested can be found in Table 3.4. When not indicated, values are set to that of the grey column in the same table. The values for θ_s and γ_e correspond to the default values as defined in Soulsby et al. (2011). The value for b_e was scaled up as the original proposed value was very low.

b_e	θ_s	γ_e
$1.1 \cdot 10^{-7}$	0.01	0.01
$1.3 \cdot 10^{-7}$	0.05	0.05
$1.7 \cdot 10^{-7}$	0.10	0.10
$2.0 \cdot 10^{-7}$	0.15	0.15
$2.3 \cdot 10^{-7}$	0.20	0.20
	0.50	
	0.80	

Table 3.4 Values for burial sensitivity analysis. The values for each parameter are changed independently of the other parameters. When the value is not indicated, parameters take the value marked in grey.

After the general sensitivity, additional simulations are performed. These are to assess burial at another burial probability scale and to work towards finding a more definitive set of burial parameters for modelling the Ameland pilot nourishment. The values that will be tested are shown in Table 3.5.

Run	1	2	3	4	5	6	7
b_e	$1.7 \cdot 10^{-7}$	$1.7 \cdot 10^{-5}$	$3.4 \cdot 10^{-5}$	$7.2 \cdot 10^{-5}$	$1.7 \cdot 10^{-5}$	$3.4 \cdot 10^{-5}$	$7.2 \cdot 10^{-5}$
θ_s	0.1	0.1	0.1	0.1	1.2	0.1	0.1
γ_e	0.1	0.0055	0.0026	0.0013	0.0055	0.0055	0.0055

Table 3.5 Burial parameters for consideration of modelling the Ameland pilot nourishment. They are grouped into broad categories based on the way in which the values for the burial parameters are varied.

The first run uses the default values for the burial parameters as outlined in Soulsby et al. (2011). Run 2 scales up deposition probability by a factor 100 and erosion probability by a factor 5 compared to run 1. These were chosen somewhat arbitrarily as a means of exploring the effects of the burial formulation on particle movement. Due to direct dependence of erosion probability and deposition probability (see equation 2.3), parameter γ_e often has to be scaled down to account for changes in the deposition probability. This is due to b_e scaling up b by a set factor. This then directly influences a . The scaling down of γ_e was thus done by factoring the scale of b_e on the value of a .

Runs 3 and 4 raise the deposition probability without changing the erosion probability (with γ_e scaled appropriately to achieve this). Run 5 tests the influence of θ_s at this new order of magnitude. Runs 6 and 7 are similar to runs 3 and 4, except that no changes to γ_e are made. These runs provide a broad overview of options for the burial configuration when modelling nourishments.

4 Results

This chapter gives the results of simulations done within SedTRAILS. Section 4.1 shows the sensitivity of the SedTRAILS model to changes in wave forcing and the water level forcing of the boundary. In section 4.2, a general sensitivity analysis of the sediment burial formulation from 2.4.2 is shown. Section 4.3 shows the results from the burial configurations outlined in Table 3.5.

4.1 Sensitivity to changes in forcing

The results in this section were all modelled using the standard parameter set as defined in Table 3.3. This was to ensure the particles were still present in the case study area after 30 days. More information on these parameters is provided in the burial sensitivity analysis, Section 4.2. All simulations in this section lasted 30 days.

4.1.1 Number of wave conditions

Figures 4.1 and 4.2 shows the result of using six and sixteen wave conditions respectively. For the tidal boundary, the morphological tide as shown in Figure 3.6 was used. Under six wave conditions, particles move further along the outer edge of the ebb-tidal delta. In both simulations, particles tend to stay away from the ebb-shield between ebb-chutes 2 and 3. This is a result of low bed shear stress in this region. In the current burial formulation, low enough bed shear stress causes the deposition probability to go to zero. This leads to very few particles being in this area on average.

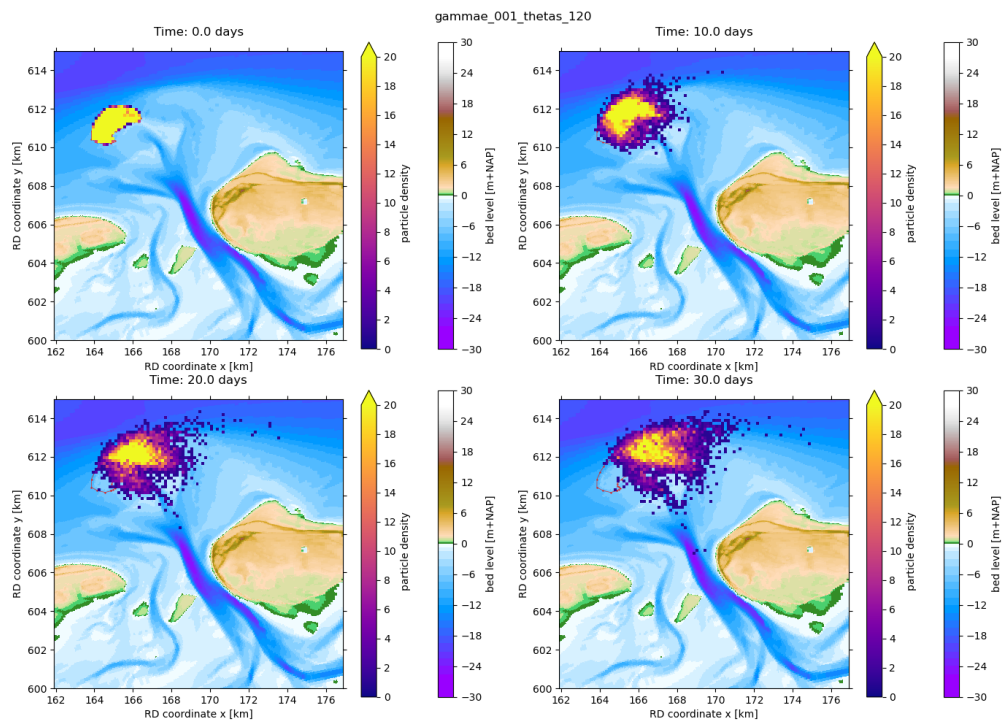


Figure 4.1 Result of releasing 5000 particles from nourishment location, forced by weighted average of six wave conditions and morphological tide. The four panels show the evolution of particle positions over time.

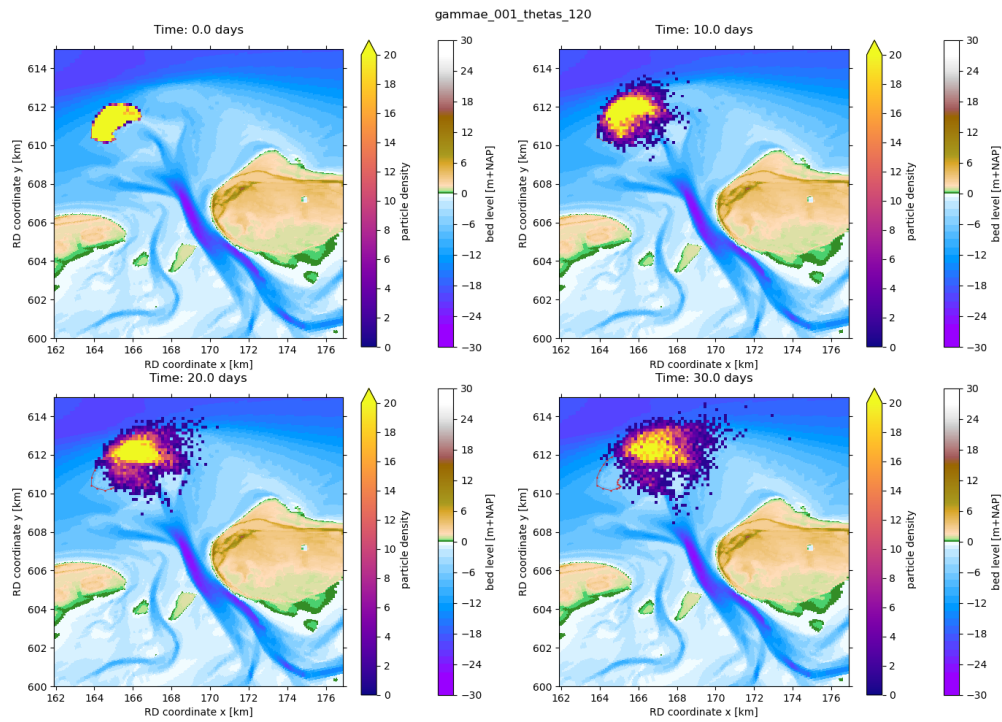


Figure 4.2 Result of releasing 5000 particles from nourishment location, forced by weighted average of sixteen wave conditions and morphological tide.

As these results are difficult to compare directly, circle plots are made. Here the mean position of the particles is the center and the radius is the standard deviation of particle positions. To illustrate this effect, Figure 4.3 shows both the particle density and the resulting circle. The start location is at $x : 164.880, y : 611.190$ (km in RD-new coordinate system), with a radius of 677 meters.

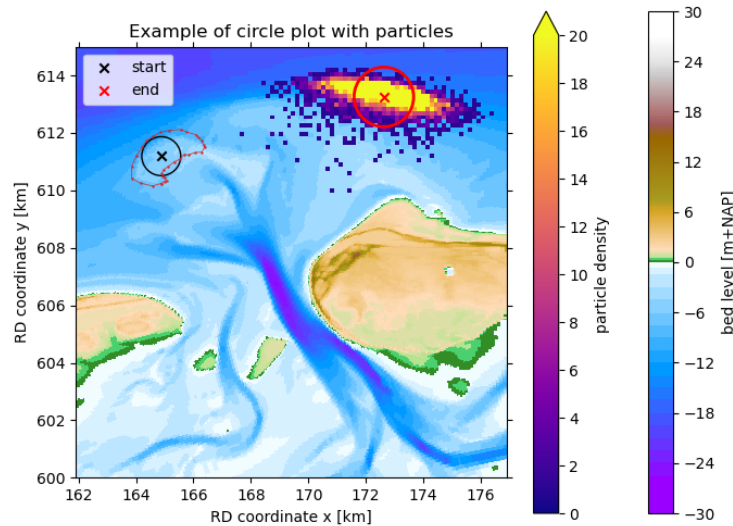


Figure 4.3 Example of how circle size and position are determined from model result. Result is a simulation after 10 days using a morphological tide, 6 wave conditions and burial configuration $b_e = 1.7 \cdot 10^{-3}, \theta_s = 0.1, \gamma_e = 0.1$.

Figure 4.4 shows that the difference between using six and sixteen wave conditions is very minimal. From the particle density plots (Figures 4.1 and 4.2), it was already clear that the main difference between the two sets of wave conditions was the number of particles that had moved further east along the edge of the ebb-tidal delta. However, as the burial method is based on probabilities, even simulations with the exact same parameters will have differences between them. It is entirely possible to simulate different amounts of these stray particles even with the exact same settings.

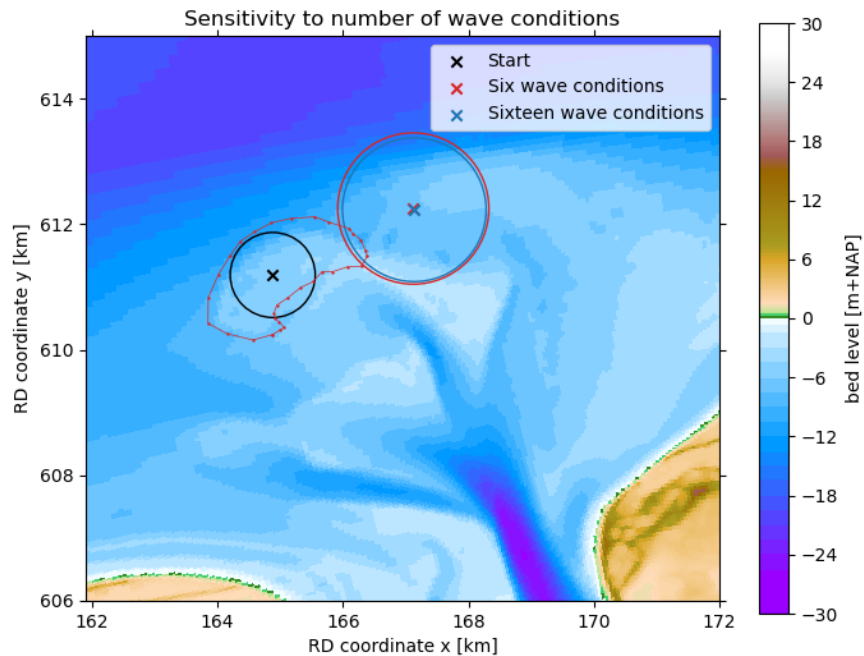


Figure 4.4 Comparison of runs with six and sixteen wave conditions. The center of the circle is the mean position of all particles, with the radius being the standard deviation of their positions. The position of the six and sixteen wave conditions circles are determined based on the position after 30 days of simulation time.

To assess whether this similarity is due to the method of averaging, an alternative method was also performed. Here, SedTRAILS was run six separate times under just one wave condition (see Figure 3.10). Then, particle positions were combined afterwards. Figure 4.5 shows that this method yields a very different result. However, it is not useful. As the freedom factor F uses a probability of erosion and deposition, particles that start in the same place may move shorter or longer distances between different runs. Averaging the position of these particles thus removes a significant amount of motion from the simulation. For that reason, it is not recommended to use this method of combining wave conditions with SedTRAILS.

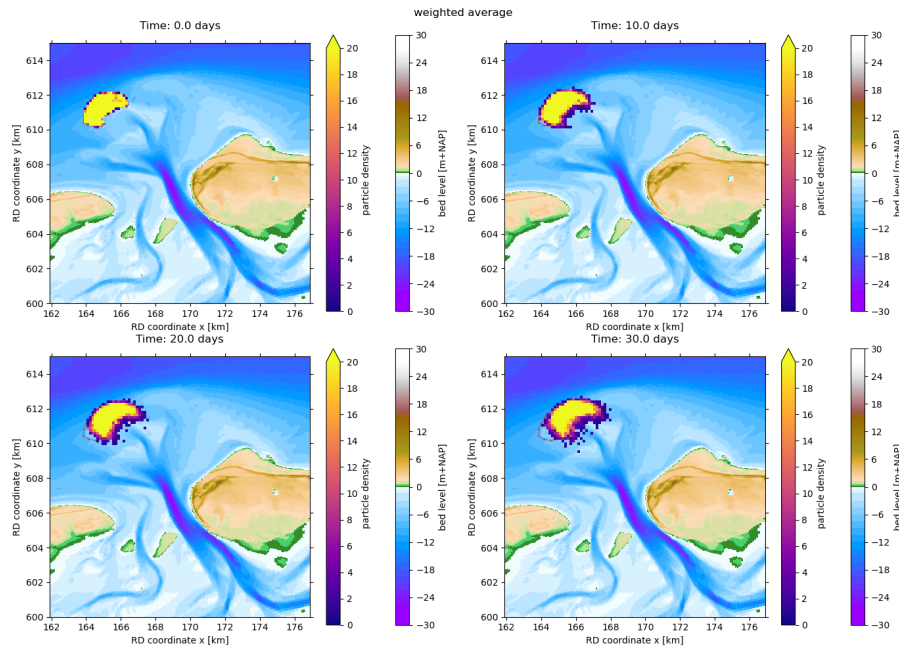


Figure 4.5 Model results when averaging the output of SedTRAILS instead of the input. These simulations were run with six wave conditions and a spring-neap tidal cycle.

At first, it seemed like the burial configuration used in comparing the wave condition sets was the cause of the similarity between runs. The low chance of erosion and high chance of deposition was theorized to cause a diffusion of results. However, with the much lower deposition probability as used in section 4.3, there was still minimal difference. Figure 4.6 shows that the results of six wave conditions (left) and sixteen wave conditions (right) are again very similar, even after a simulation time of 180 days. From this, it is evident that a significant change in burial does not impact the effects of wave forcing.

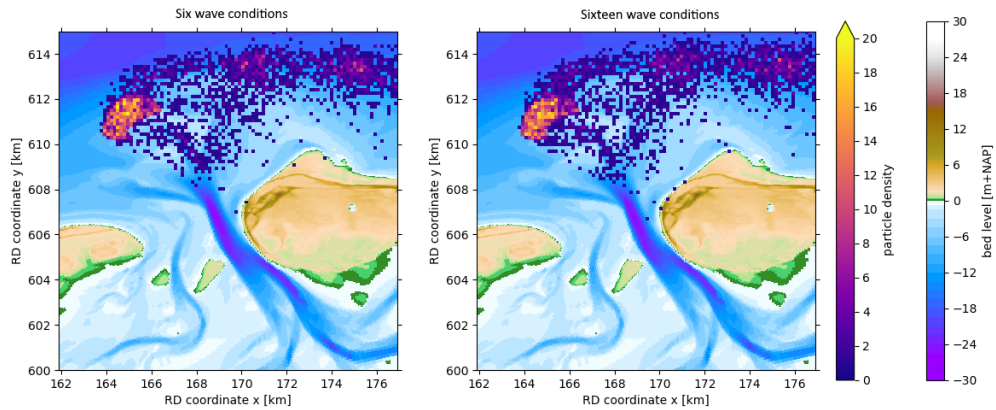


Figure 4.6 Result of SedTRAILS simulation under morphological tide of six (left) and sixteen (right) wave conditions after 180 days. Burial parameters used are: $b_e = 1.7 \cdot 10^{-5} s^{-1}$, $\theta_s = 0.1$, $\gamma_e = 0.0055$

In Chapter 3, it was explained that the different wave conditions are combined based on a weighted average. Since both sets of wave conditions represent the same system, it is likely that averaging leads to two very similar grain velocity fields. Indeed, when comparing the velocity fields directly (Figure 4.7), there is no significant difference between using six and sixteen wave conditions. With storm conditions being highly unlikely, the higher-probability low-energy conditions dominate in the velocity field.

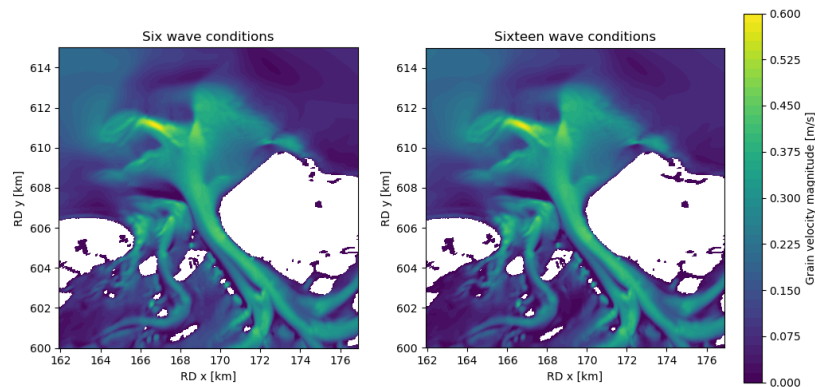


Figure 4.7 Comparison of grain velocity fields from weighted average of six (left) and sixteen (right) wave conditions. Both runs used a morphological tide with burial parameters $b_e = 1.7 \cdot 10^{-5}$, $\theta_s = 0.1$, $\gamma_e = 0.0055$, showing time step 100 to illustrate the similarity.

To assess how big this impact is, a highly energetic wave condition was run separately. Figure 4.8 shows the result of only using the 15th wave condition from Table 3.2 as the input velocity field. The burial configuration is identical to the configuration used for Figure 4.6. The transport is much more spread out compared to using an averaged velocity field (e.g., Figure 4.6), with more interaction with the inlet as well as the coast of Ameland.

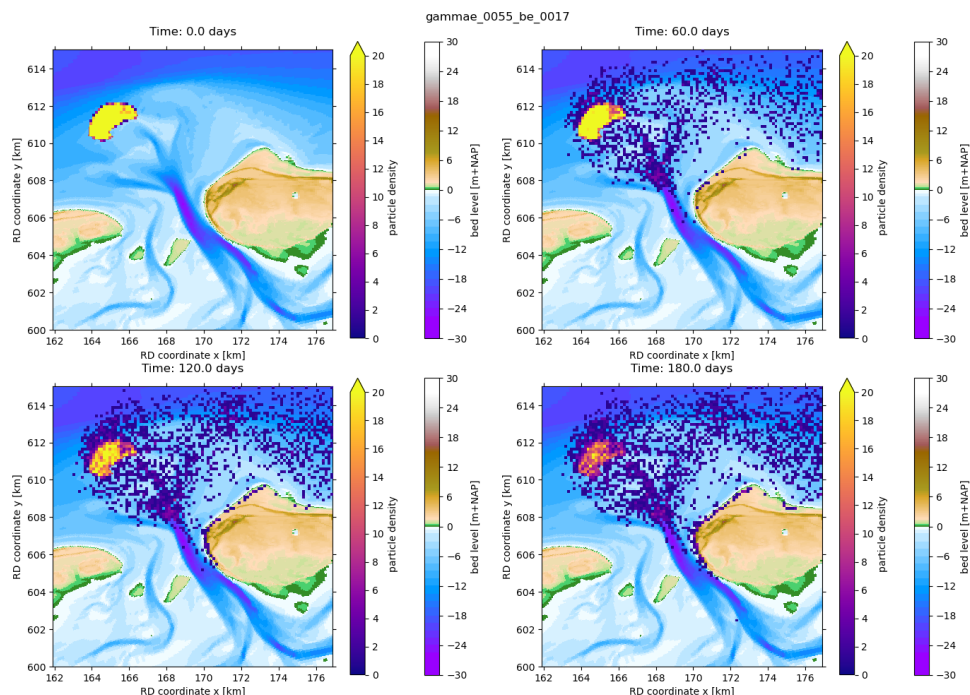


Figure 4.8 Result of simulating 5000 particles under a morphological tide with only wave condition 15 ($H_s = 3.54m$, probability of occurrence 0.76%. See Table 3.2).

To assess if waves play a significant role in transport from the nourishment, the model's response to only tidal forcing was investigated as well. Figure 4.9 shows that without wave forcing, there is very little movement of sediment. Wave-induced currents and bed shear stresses clearly play a significant role in dispersal of the nourishment. Only a small amount of particles are able to move, as for most of the tidal cycle, the bed shear stress at the nourishment is not strong enough to initiate motion. This aligns with previous assessments of wave-driven transport being dominant at the nourishment location (Elias 2021 and Lambregts 2021).

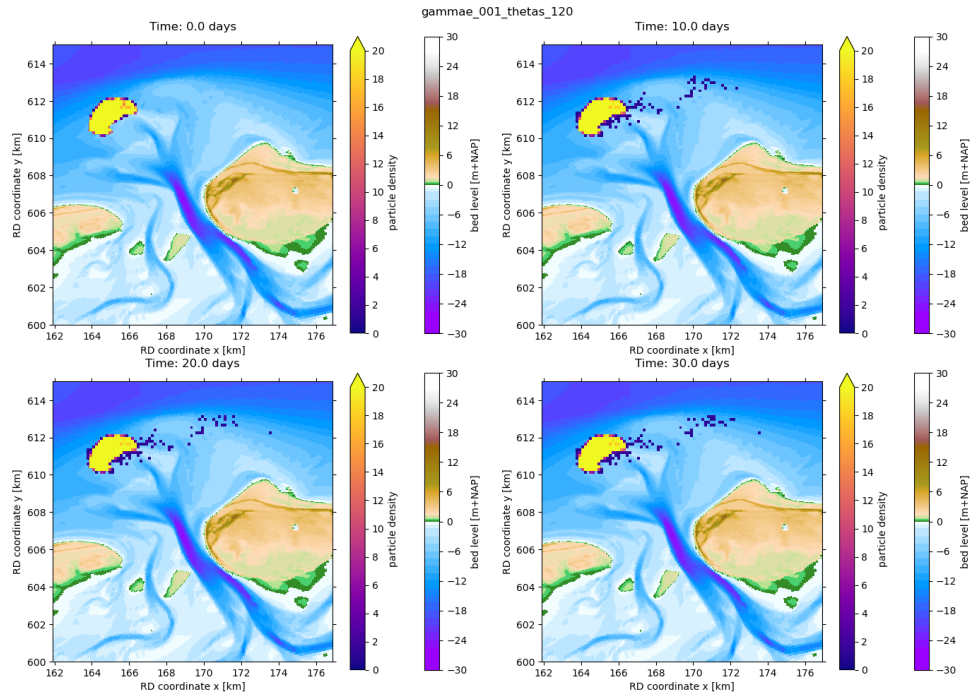


Figure 4.9 Result of releasing 5000 particles from nourishment location with a morphological tide and no waves.

The major pathways in Figure 4.9 coincide broadly with those found in Lambregts (2021) (Figure 4.10). However, due to the inclusion of burial, the pathways are not quite as smooth in this new simulation.

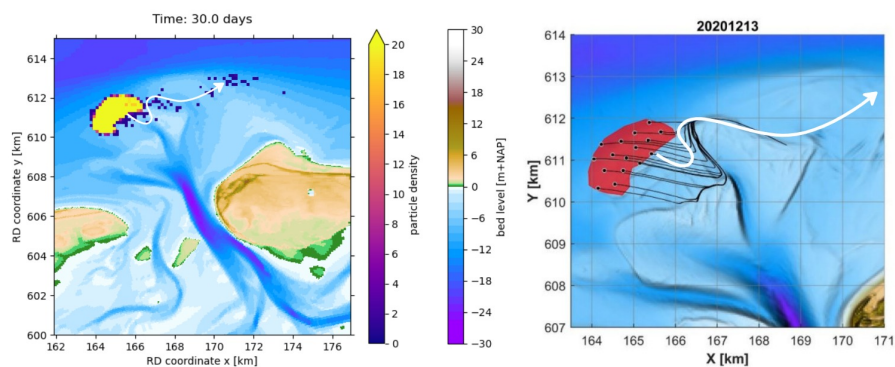


Figure 4.10 Comparison of tide-only SedTRAILS simulation including burial (left) with tide-only SedTRAILS simulation results from Lambregts (2021) (right). The white arrow represents the general path of sediment in the left figure, which has been overlaid on the right figure to illustrate their similarity.

4.1.2 Wave-driven bed velocity

Enabling the addition of the wave-driven bed velocity as described in section 2.4.3 introduces some minimal changes, both for six and sixteen wave conditions. Figures 4.11 and 4.12 show the results of enabling the wave-driven bed velocity with both six and sixteen wave conditions. The run with sixteen wave conditions, now with wave-driven bed velocity enabled, has more particles travelling along the sediment bypassing route of the ebb-tidal delta. The two sets of wave conditions have more similar results with wave-driven bed velocity enabled than without.

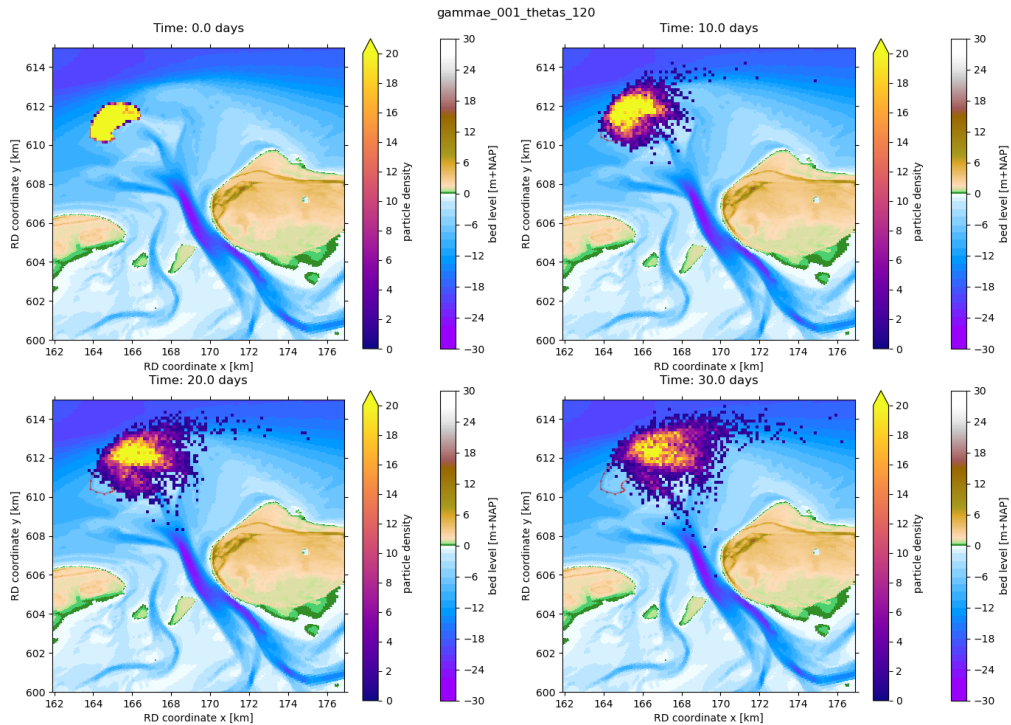


Figure 4.11 Result of releasing 5000 particles from the nourishment location, forced by weighted average of six wave conditions and morphological tide, with wave-driven bed velocity enabled.

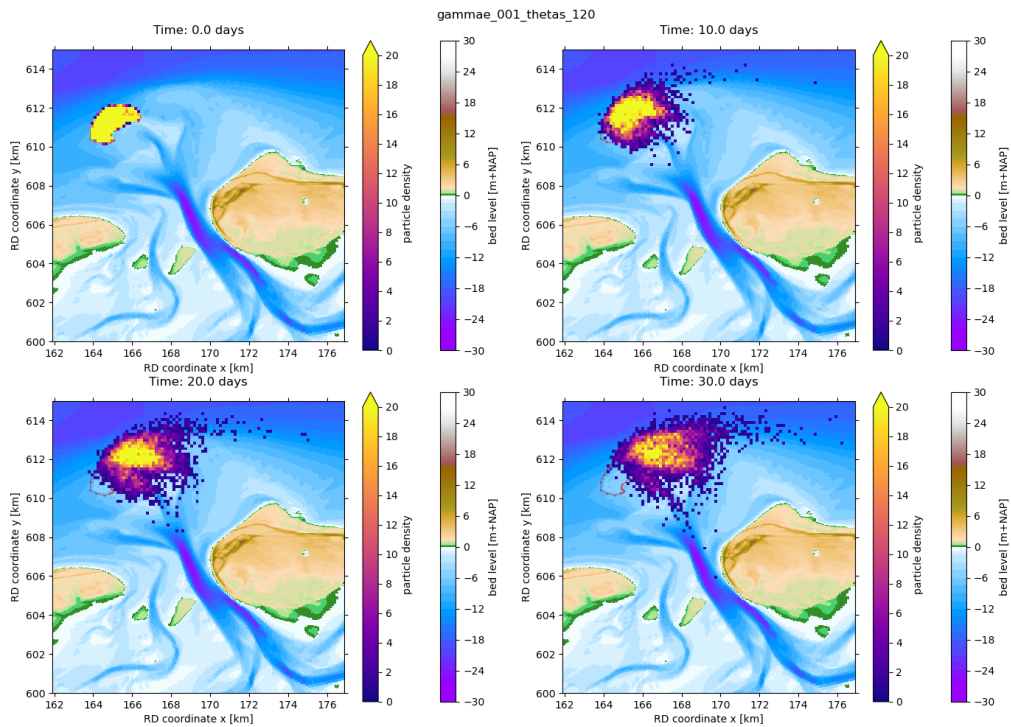


Figure 4.12 Result of releasing 5000 particles from the nourishment location, forced by weighted average of sixteen wave conditions and morphological tide, with wave-driven bed velocity enabled.

As it is once again difficult to see the difference, a circle plot is included in Figure 4.13. The positions and radii of the circles are also given in Table 4.1.

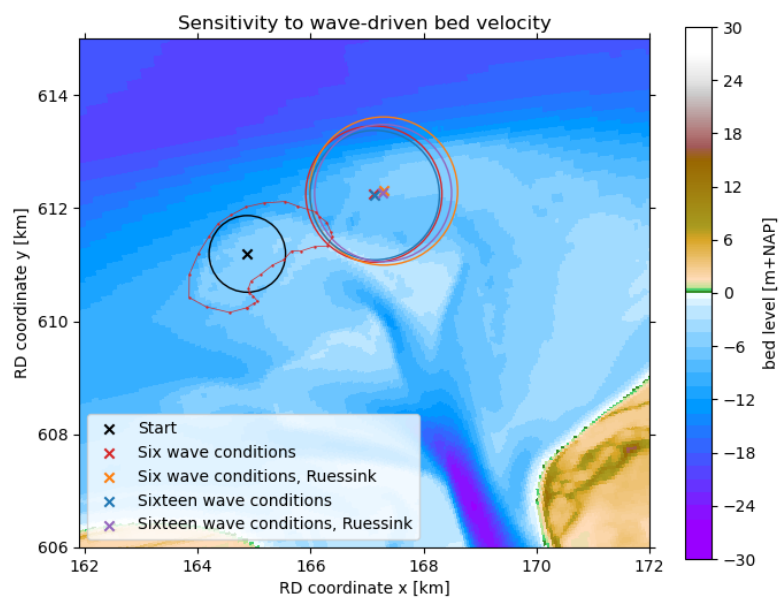


Figure 4.13 Comparison of runs with six and sixteen wave conditions, with wave-driven bed velocity both disabled and enabled (indicated in the legend with "Ruessink").

Amount of wave conditions	Ruessink	x center [km]	y center [km]	radius [m]
6	No	167.121	612.250	1205
6	Yes	167.295	612.302	1310
16	No	167.137	612.230	1145
16	Yes	167.284	612.267	1213

Table 4.1 Circle centers and radii for sets of wave conditions, with and without the wave-driven bed velocity (Ruessink). The coordinates for the centers are given in the RD-new coordinate system.

The main effect the wave-driven bed velocity has here is a slight increase in spread (increase in standard deviation of between 68 m and 95 m) and a slightly further transport (average position approximately 150 m further east) within the 30 days runtime of SedTRAILS. This effect is more pronounced with six wave conditions than sixteen, likely due to the low probability of occurrence that the wave conditions have in the set of sixteen. The increased spread is partly caused by more particles travelling further east along the sediment bypassing route, but partly by a general increase in spread along the central ebb-tidal delta (see for example Figure 4.20). The further transport is a direct result of the addition of the wave-driven bed velocity. The sediment bypassing route is caused primarily by waves along the edge of the ebb-tidal delta (FitzGerald 1988). The addition of wave-driven bed velocity introduces further velocities in this direction, causing slightly further transport along the sediment bypassing route. There is also more significant transport in the immediate vicinity of the pilot nourishment (see Figure 4.14), causing sediment to be transported faster.

In general, the wave-driven bed velocity is quite small, of an order of magnitude of 4 cm/s at the coast. Magnitudes on the ebb-tidal delta itself range between 0 and 3 cm/s (Figure 4.14).

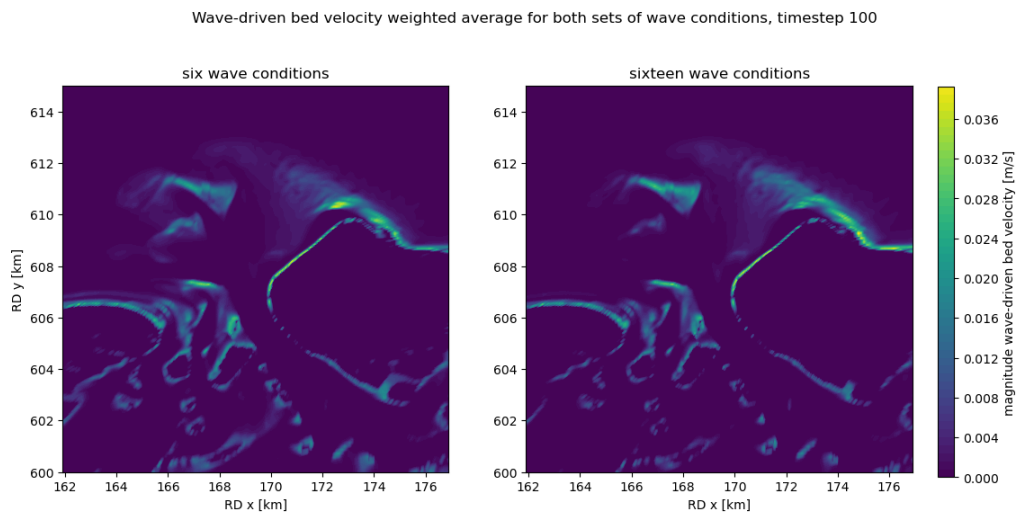


Figure 4.14 Magnitude of the wave-driven bed velocity when using a weighted average of six (left) and sixteen (right) wave conditions. Moment is at time step 100 of the morphological tide simulation, early during rising tide when water levels are low, for illustration.

While the inclusion of wave-driven bed velocity has a larger impact on transport than an increase in the number of wave conditions modelled, its effects are too small to be considered significant. This is surprising, as the addition of velocity where waves break should affect the result when using sixteen wave conditions more. This is illustrated in Figure 4.15. The higher energy wave conditions included in the set of sixteen (as seen on the right of the figure) have higher contributions than the lower energy conditions (left). This contribution also affects more areas within the system. However, the probability of occurrence is so low (<1%) that this contribution does not have a significant impact on the eventual grain velocity field.

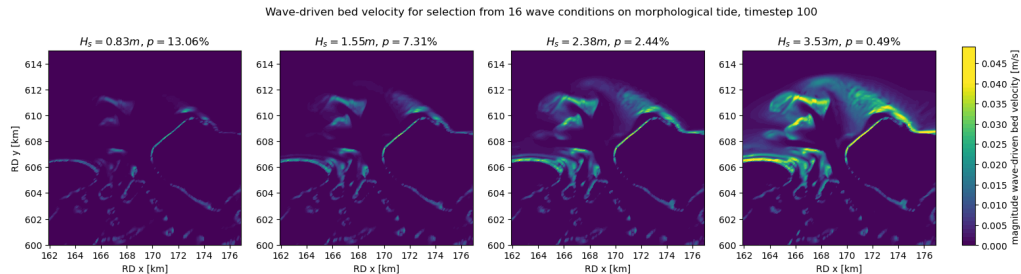


Figure 4.15 Magnitude of the wave-driven bed velocity that occurs for four of the sixteen wave conditions. The wave condition's corresponding significant wave height is noted as well. The probability of occurrence for these four wave conditions is also given.

The inclusion of more energetic conditions is the main reason there is a small difference between the two sets of wave conditions. When using sixteen wave conditions, the wave-driven bed velocity along the bar bypassing route is more significant. The magnitude on the western ebb-tidal delta is also generally higher for this set. However, since the magnitude overall is small compared to the flow velocity, these differences have no observable effect on results.

4.1.3 Water level boundary

To assess the use of the morphological tide as outlined in Jiao (2014), a spring-neap tidal cycle was used as a boundary condition for the velocity field. The two runs that are compared here both used six wave conditions (Table 3.1) and the parameters in Table 3.3. Both runs simulated a period of 30 days to ensure that two entire spring-neap tidal cycles took place by the end of the simulation period. The simulation with a morphological tide is shown in Figure 4.1. The simulation with a spring-neap tidal cycle is shown in Figure 4.16.

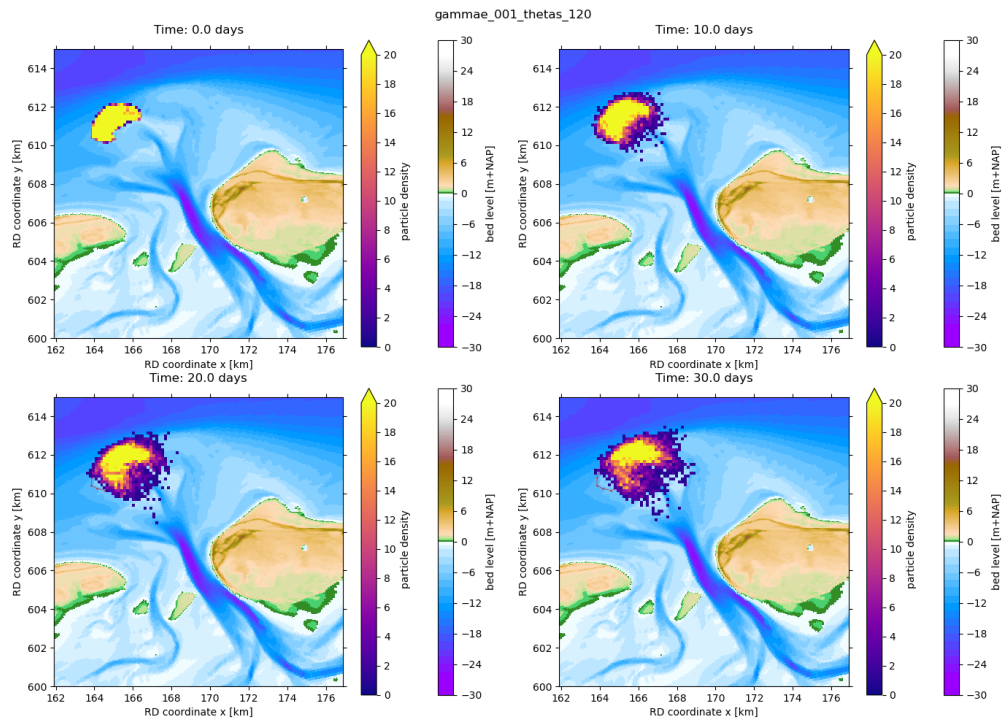


Figure 4.16 Result of releasing 5000 particles from nourishment location, forced by weighted average of six wave conditions and a spring-neap tidal cycle.

The result of using a spring-neap tidal cycle shows a significant change from the morphological tide. Overall, the mass of particles moves through the system much more slowly. Movement is far less significant during neap tide than spring-tide. A section of particles spread out over the ebb-shield the nourishment was placed against, while the rest somewhat uniformly move along the outer edge of the delta.

This run does not have the outliers that were present under morphological tide. This indicates that the strength of the sediment bypassing route is partly caused by the use of a morphological tide. The number of particles just south of the nourishment location is also much more significant here.

Important to note is that calibration of this spring-neap tidal cycle was outside the scope of this thesis. As such, the large difference shown here is an indication that more investigation is required.

4.2 General sensitivity of burial parameters

This section shows the impact changes in the three tuneable burial parameters have on overall model results. As a reference, the parameters in Table 3.3 are seen as the default run. Only deviations from the values shown in that table are mentioned. All runs are 10 days, as this timespan is short enough to allow for many different simulations while showing adequate differences for the different parameters. The simulations in this section were all made with a morphological tide and six wave conditions.

This section will not show the full density plots, as this would take up too much space and it would be difficult to compare them. Instead, the full model results can be found in Appendix B. Circle plots, with the average particle location as the center and the standard deviation as the radius, are used to directly compare results of changes in the three different parameters.

4.2.1 b_e - Maximum free-to-trapped transition probability

Figure 4.17 shows five runs with different values for b_e . With an increase in b_e , the spread of particles becomes slightly smaller, while the distance travelled overall becomes slightly greater. At this scale, the model is not particularly sensitive to changes in b_e . However, it should be noted that the "default" value of $1.7 \cdot 10^{-3}$ is a factor 10^4 larger than the value considered default by Soulsby et al. (2011). This is explored more in section 4.3.

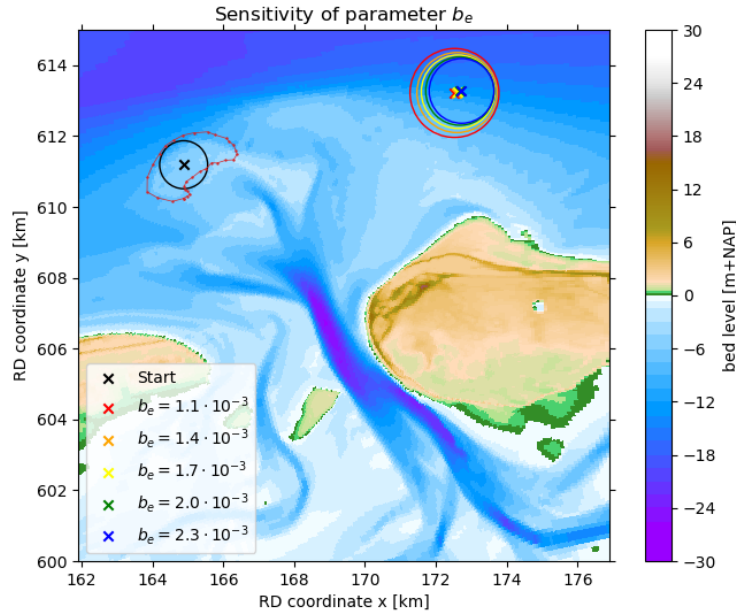


Figure 4.17 Circle plot comparing simulations of 10 days with varying value for b_e .

The coordinates of the centers and the radii of the circles is also provided in Table 4.2. These show a gradual decrease in radius for increasing values of b_e , with a difference of more than 300 m between the lowest and highest value tested. The position changes on a magnitude of approximately 200 m.

b_e	x center [km]	y center [km]	Radius [m]
$1.1 \cdot 10^{-3}$	172.526	613.217	1255
$1.3 \cdot 10^{-3}$	172.597	613.228	1130
$1.7 \cdot 10^{-3}$	172.627	613.252	1037
$2.0 \cdot 10^{-3}$	172.679	613.269	965
$2.3 \cdot 10^{-3}$	172.727	613.275	914

Table 4.2 Centers and radii of circles in Figure 4.17. Coordinates of center are given in the RD-new coordinate system.

4.2.2 θ_s - Scale value determining the distribution of residence times

Figure 4.18 shows the effect of changes in θ_s on model results. From this, it becomes clear that a higher value for θ_s results in a larger spread of particles. Unlike changes in b_e , this parameter does not affect the overall speed at which particles move through the system. Instead, it only scales the bed shear stress required to make deposition and erosion probability go from 0 to the maximum value (b_e).

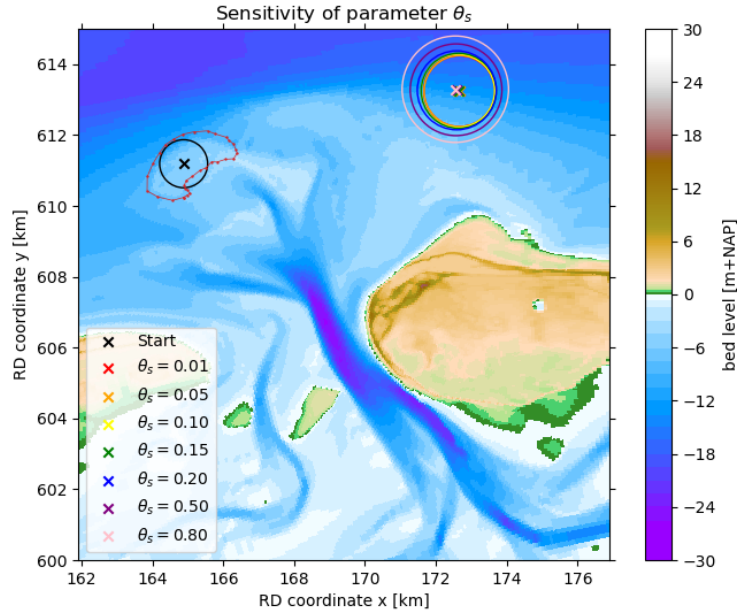


Figure 4.18 Circle plot comparing simulations of 10 days with varying values for θ_s

The coordinates of the centers and the radii are provided in Table 4.3. The radius increase becomes more significant with higher values of θ_s and there are only minor differences in the position of the center.

θ_s	x center [km]	y center [km]	Radius [m]
0.01	172.665	613.240	1002
0.05	172.672	613.242	1005
0.10	172.627	613.252	1037
0.15	172.646	613.250	1060
0.20	172.592	613.263	1115
0.50	172.572	613.279	1295
0.80	172.551	613.294	1502

Table 4.3 Centers and radii of circles in Figure 4.18. Coordinates of center are given in the RD-new coordinate system.

θ_s specifically affects the difference between $\theta_{max,a}$ and $\theta_{cr,a}$. This scale is central to the way burial is implemented. Figure 4.19 shows a damping of the effects of maximum bed shear stress (expressed in the Shields parameter) as θ_s increases. In practice, changing θ_s affects the spread of particles directly, without influencing the overall distance travelled.

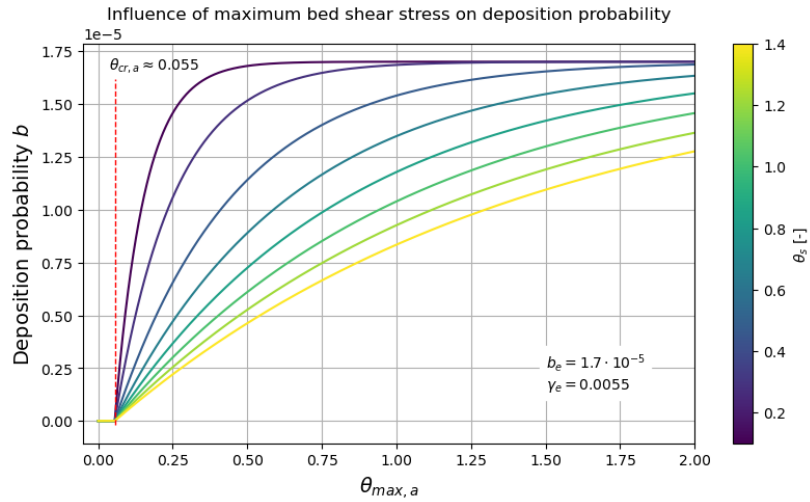


Figure 4.19 Deposition probability as it relates to the maximum bed shear stress for a range of scale parameter (θ_s) values.

4.2.3 γ_e - Long-term equilibrium proportion of free particles

When seeing the effect changing γ_e has on model results (Figure 4.20), it is clear that the model is most sensitive to this parameter in particular. With a higher proportion of free particles, the overall sediment mass moves through the system much faster. Particles are more likely to erode after deposition, and thus are able to move much more often.

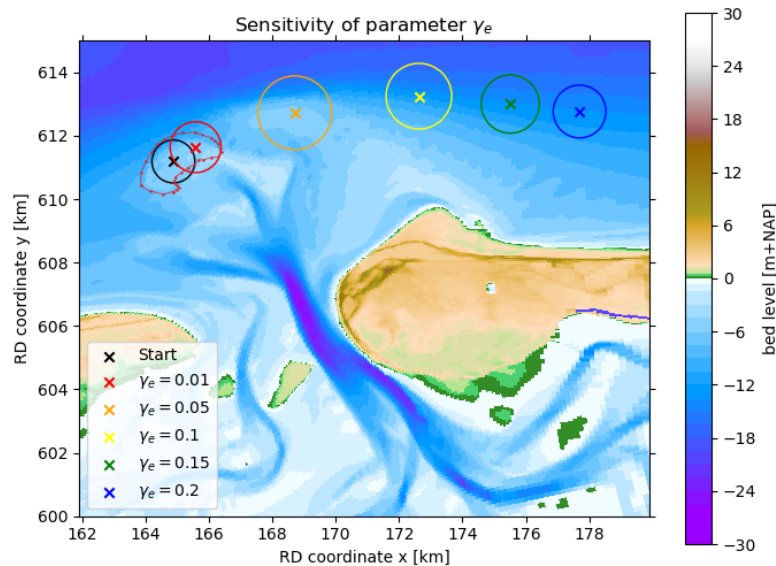


Figure 4.20 Circle plot comparing simulations of 10 days with varying values for γ_e

The coordinates of the centers and the radii are provided in Table 4.4. Here, the change in radius can be mainly attributed to a general increase in spread of particles over the ebb-tidal delta when the mass of particles moves along the edge, as opposed to specific changes in erosion probability affecting the spread. This is shown more clearly when comparing the particle density plots in Appendix B.

γ_e	x center [km]	y center [km]	Radius [m]
0.01	165.580	611.642	802
0.05	168.712	612.727	1163
0.10	172.627	613.252	1037
0.15	175.510	613.004	918
0.20	177.698	612.769	833

Table 4.4 Centers and radii of circles in Figure 4.18. Coordinates of center are given in the RD-new coordinate system.

4.2.4 Summary of sensitivity

Parameter b_e scales the deposition probability directly. It is defined as the maximum deposition probability and greatly influences how much particles can travel through the system. A lower deposition probability generally means particles spread out more as the simulation goes on. They are also able to travel slightly further, but this is caused by the erosion probability going up with an increase in b_e .

As θ_s affects the probability distribution of deposition and erosion, a change in this parameter only affects the spread of particles. Higher values for θ_s correspond with more spread.

The model responds very differently to changes in γ_e . This parameter directly affects only the erosion probability. Where deposition dictates how far a particle can travel before it gets buried again, erosion dictates how long the particle stays buried. This causes an entirely different response. Increasing the equilibrium proportion of particles that are free means particles overall move significantly more.

To summarize, higher erosion probability leads to overall faster movement of particles through the system. Lower deposition probability leads to more spread through the system. This intuitively makes sense. If particles become free again more quickly after becoming trapped, they will cover more distance over the simulation period. And if particles stay free longer, they can move further and end up depositing again at different parts of the tidal cycle.

4.3 Effects of erosion and deposition probabilities

Seven runs were defined in Table 3.5. This section shows the results from these simulations. These simulations were done under a spring-neap tidal cycle with six wave conditions. The runtime was generally 180 days to capture the model's long-term behaviour. The wave-driven bed velocity was enabled for these runs.

4.3.1 Run 1 - Original burial parameters

In the previous section, the default value of b_e as defined in Soulsby et al. (2011) was not used as it was deemed far too low. However, for a complete analysis, using $b_e = 1.7 \cdot 10^{-7}$ was also simulated. While not important previously, the initial freedom factor here had to be set to 0. If this was left at 1, the entire nourishment very quickly disappeared out of the system, leaving only a small trail of particles behind (Figure 4.21, left).

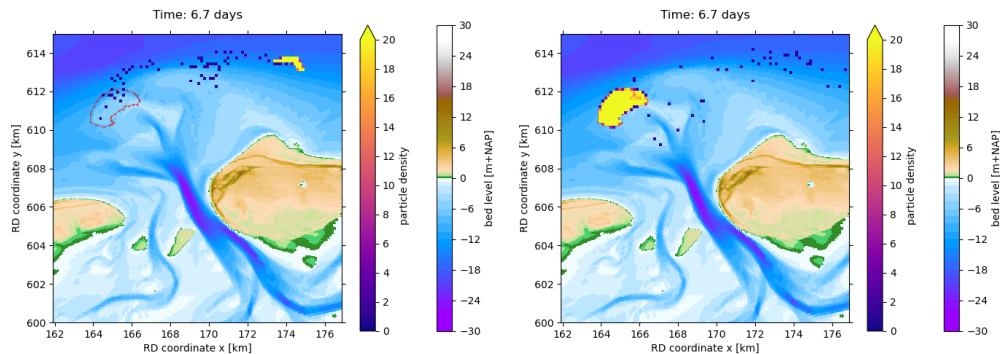


Figure 4.21 The importance of the initial freedom factor. These run used all default values from Soulsby et al. (2011), using six wave conditions. On the left, a morphological tide and an initial freedom factor $F = 1$ was used. On the right, a spring-neap tidal cycle and an initial freedom factor $F = 0$ was used.

With a maximum deposition probability at this order of magnitude, practically no deposition takes place (Figure 4.21, right). This would suggest that the nourishment has no impact on the system, with most of the sediment immediately exiting the system within days of eroding from the nourishment. Comparing to bathymetric measurements (Elias 2021, Figure 2.7) and results of morphodynamic modelling (Harlequin 2021, Figure 2.8), this is not realistic. For this reason, it is not recommended to use this burial configuration for nourishment modelling.

4.3.2 Runs 2, 3 and 4 - scaling deposition probability

Simulating now for 180 days with a spring-neap tidal cycle and six wave conditions for the parameters of run 2 results in Figure 4.22.

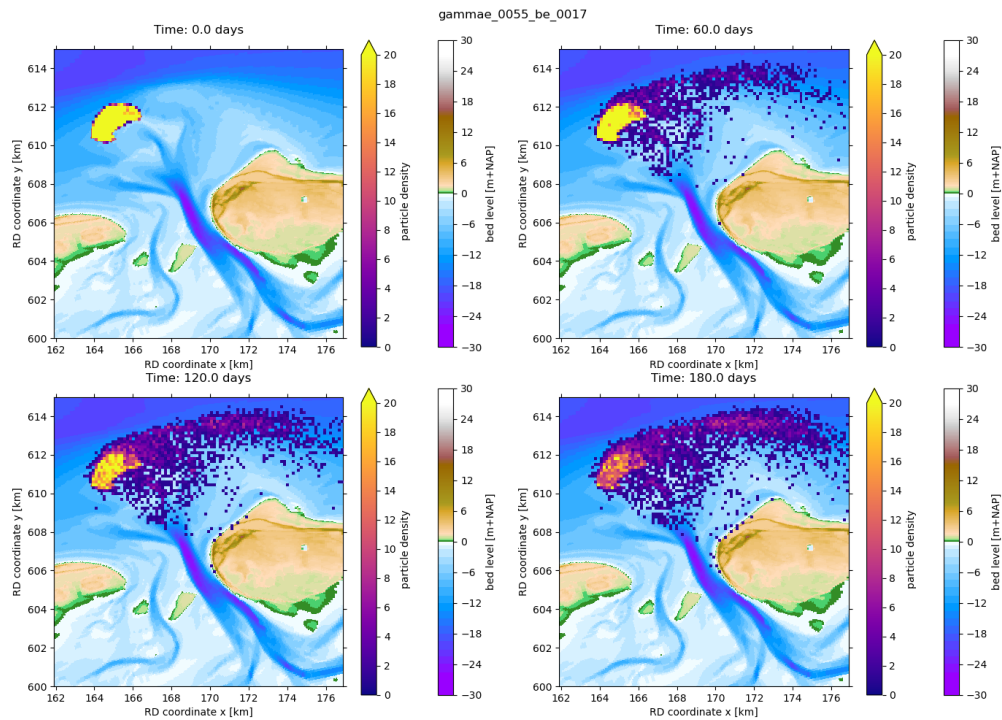


Figure 4.22 Result of 180 days of simulating dispersal of the nourishment with $b_e = 1.7 \cdot 10^{-5} s^{-1}$, $\theta_s = 0.1$ and $\gamma_e = 0.0055$.

This run shows a gradual erosion of the nourishment, with some of the sediment getting caught in the tidal circulation on the delta, while a significant amount of it is caught by sediment bypassing around the edge of the ebb-tidal delta and starts moving away from the delta relatively quickly. Only a handful of particles get near the coast on the eastern half of the ebb-tidal delta.

Using a higher deposition probability gives the result shown in Figure 4.23. This simulation shows a less significant chunk of sediment going to the sediment bypassing route, with more particles depositing on the ebb-tidal delta. Even fewer particles than before reach the west coast of Ameland.

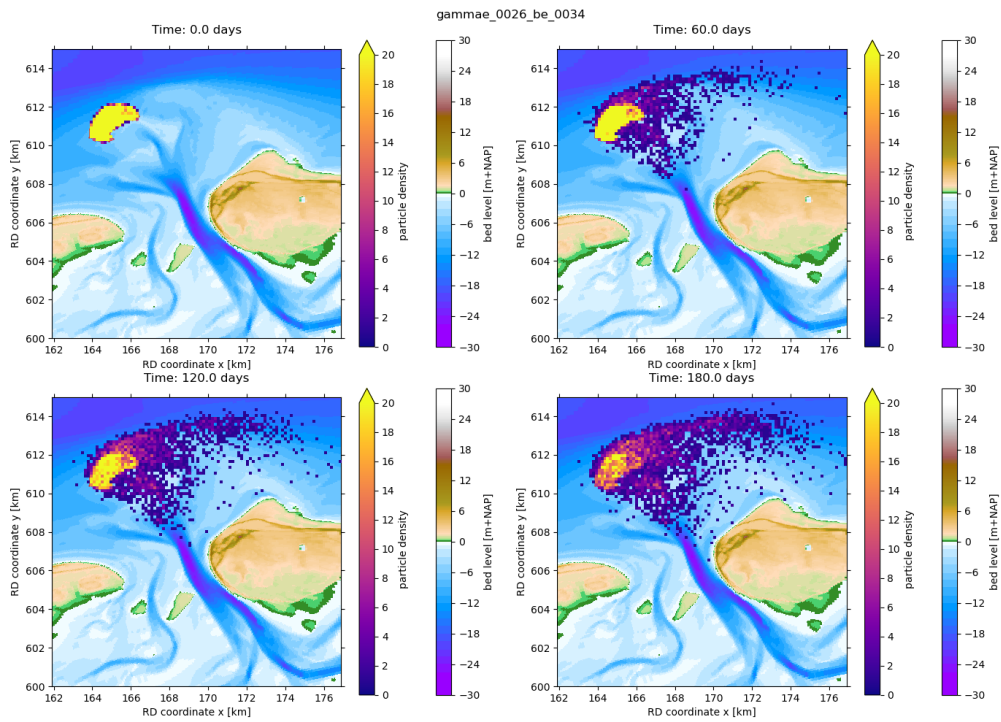


Figure 4.23 Result of 180 days of simulating dispersal of the nourishment with $b_e = 3.4 \cdot 10^{-5} s^{-1}$, $\theta_s = 0.1$ and $\gamma_e = 0.0026$.

Finally, the parameter set of run 4 (Figure 4.24) shows even less sediment going towards sediment bypassing. A significant amount stays within the area of the nourishment or directly next to it.

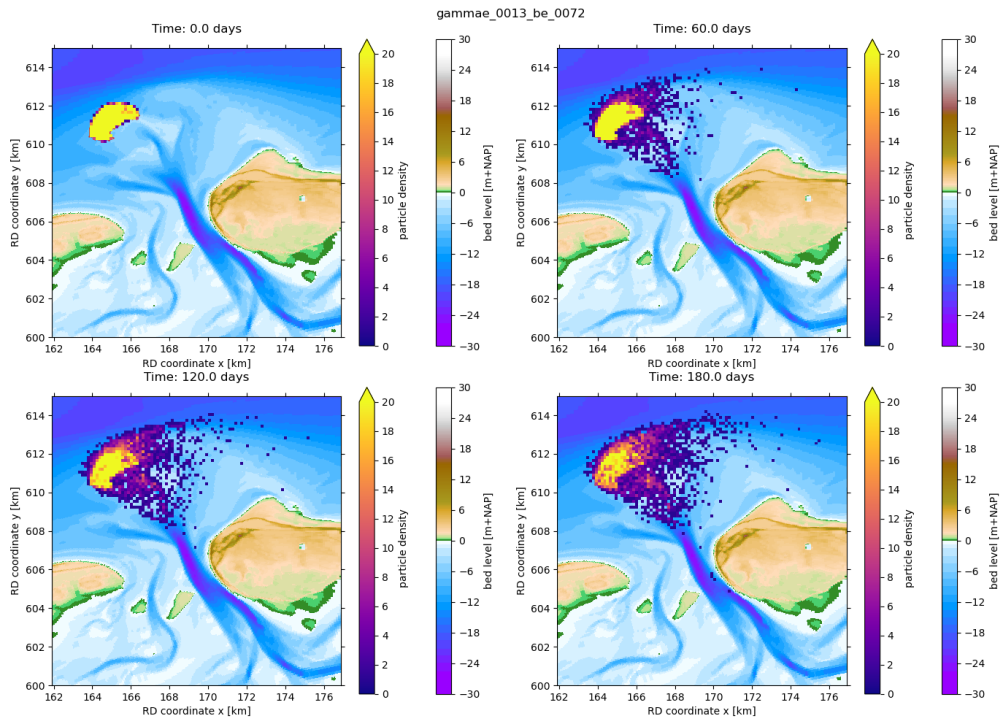


Figure 4.24 Result of 180 days of simulating dispersal of the nourishment with $b_e = 7.2 \cdot 10^{-5} s^{-1}$, $\theta_s = 0.1$ and $\gamma_e = 0.0013$.

All three simulations show similar patterns. Sediment gradually erodes from the nourishment and deposits elsewhere in the system. The ebb-shield between ebb-chutes 2 and 3 captures less sediment than the surrounding channels, similar to behaviour in other runs. Sediment generally circulates around the ebb-tidal delta, after which the particles propagate along the outer edge of the delta.

There is a significant difference between these three simulations, however. While the erosion generally reflects the gradual erosion shown in, for example, Harlequin (2021) (Figure 2.6), the deposition probability has a strong effect on the share of the nourishment lost to sediment bypassing. As deposition probability goes up, a larger amount of particles can be found on the ebb-tidal delta itself after 180 days.

To compare the distribution of particles throughout the system between the three simulations presented here, the particles at the end of the simulation were categorized based on where they land after 180 days of simulation time. Several areas were defined, as shown in Figure 4.25.

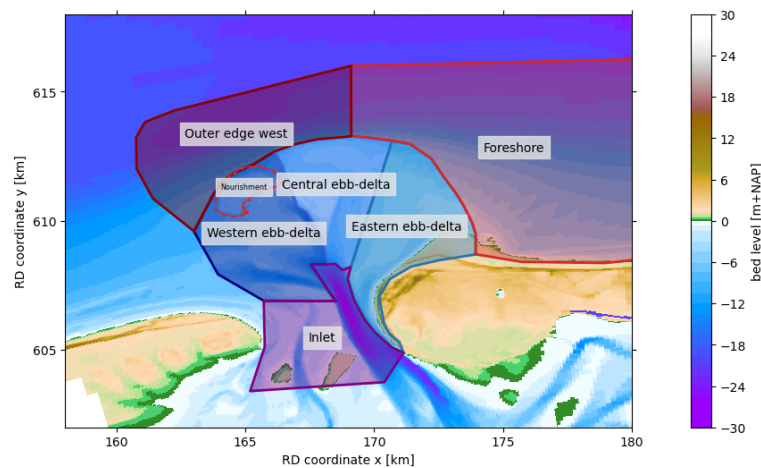


Figure 4.25 Division of Ameland ebb-tidal delta into several areas for analysis of particle distributions.

Figure 4.26 shows that the run with lower deposition probability (top) loses a much bigger share of its sediment to bypassing to the Ameland foreshore, with nearly 40% of the moved particles landing here. The higher deposition probability runs (middle and bottom) lose relatively less to the bypassing route. Lowering the deposition probability then changes the distribution of particles landing in the central- and western ebb-tidal delta areas. As deposition probability goes up, more particles land further west. However, all three distributions show very little sediment going to the Borndiep channel or the shallow Eastern section of the ebb-tidal delta. Even with the most movement Eastward, only around 3% of particles land in the eastern area of the ebb-tidal delta. With higher deposition probability, more particles end up on the outer edge of the ebb-tidal delta on the western side. This is also part of the sediment bypassing route. This is partly due to particles not being able to move as much before depositing again, thus staying on the western edge instead of transporting further east towards the bypassing section.

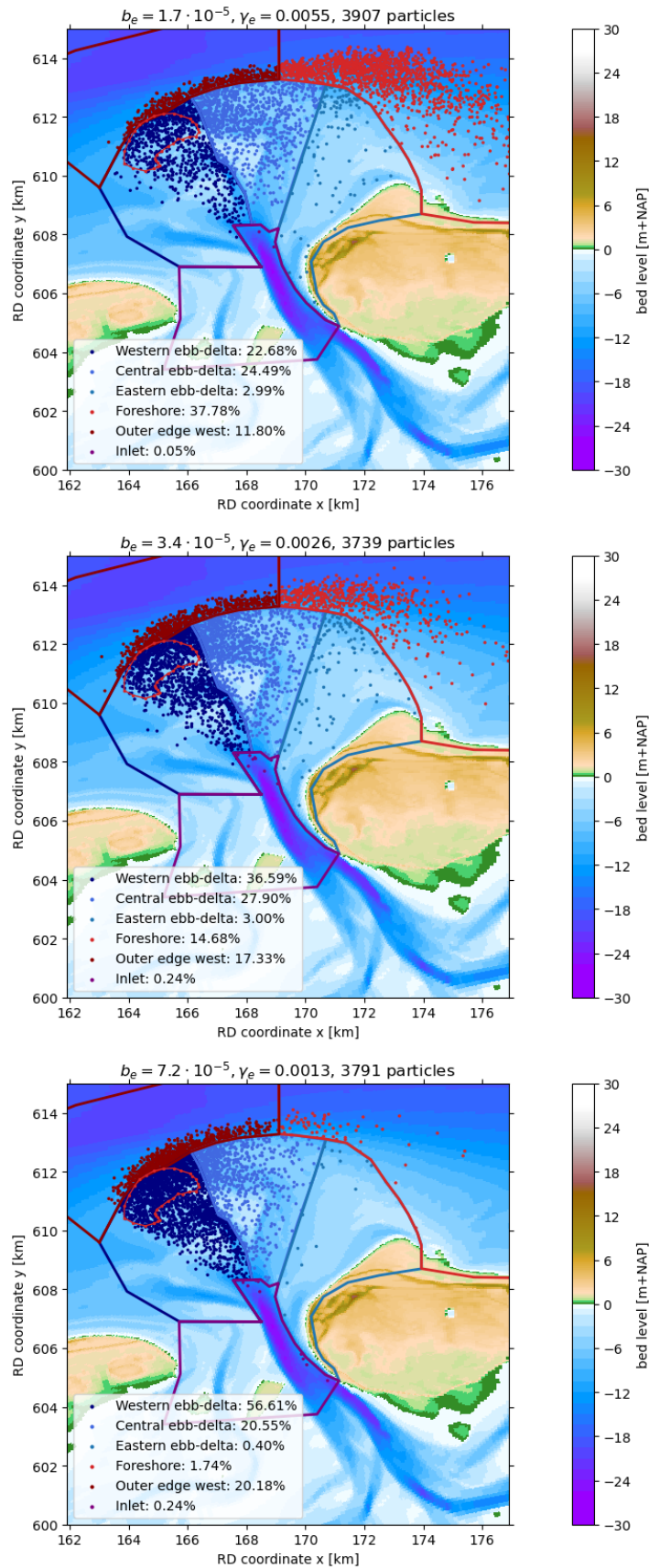


Figure 4.26 Result of 180 days of simulation with different burial parameters. Particles that have not moved within these 180 days have been filtered out. The amount of particles of the original 5000 remaining in the figure is shown in the title of each plot. The percentage of particles landing in each area is provided in the legend.

Area	$b_e = 1.7 \cdot 10^{-5}$	$b_e = 3.4 \cdot 10^{-5}$	$b_e = 7.2 \cdot 10^{-5}$
Western ebb-delta	22.68%	36.59%	56.61%
Central ebb-delta	24.40%	27.90%	20.55%
Eastern ebb-delta	2.99%	3.00%	0.40%
Foreshore	37.78%	14.68%	1.74%
Outer edge west	11.80%	17.33%	20.18%
Inlet	0.05%	0.24%	0.24%

Table 4.5 Percentage of particles landing in areas as defined in Figure 4.25 for each of the three runs with tuned erosion and deposition.

4.3.3 Run 5 - changing the scale parameter

The scale parameter, θ_s was independently increased compared to run 2 to assess the effects of this parameter at the scale of $b_e = 1.7 \cdot 10^{-5}$, as the general sensitivity tested this effect at a very different scale. Figure 4.27 does show a somewhat increased spread of the nourishment compared to Figure 4.22. Notably, the area just northeast of the nourishment has slightly lower particle density, and there is a more clear divide between particles moving into the sediment bypassing route and particles depositing on the ebb-tidal delta.

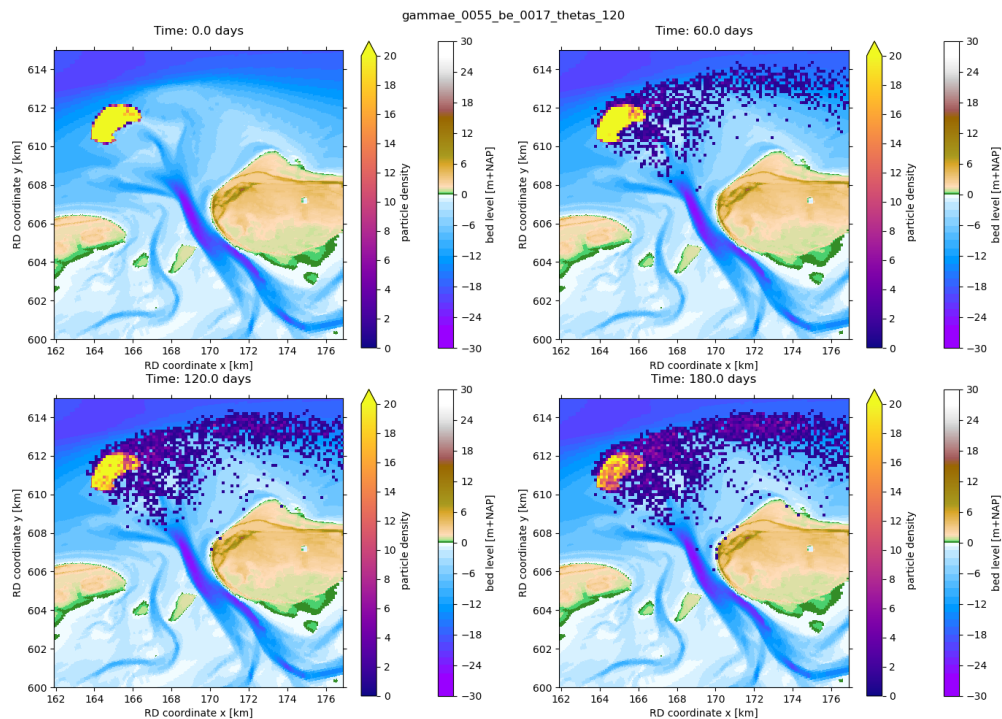


Figure 4.27 Result of 180 days of simulating dispersal of the nourishment with $b_e = 7.2 \cdot 10^{-5} s^{-1}$, $\theta_s = 1.2$ and $\gamma_e = 0.0013$.

4.3.4 Runs 6 and 7 - scaling deposition and erosion

Runs 6 and 7 had an increased value for b_e while not decreasing γ_e . This was done both to demonstrate the direct dependence of erosion probability on deposition probability and to analyse more options for nourishment modelling. Figures 4.28 and 4.29 show the results of these simulations.

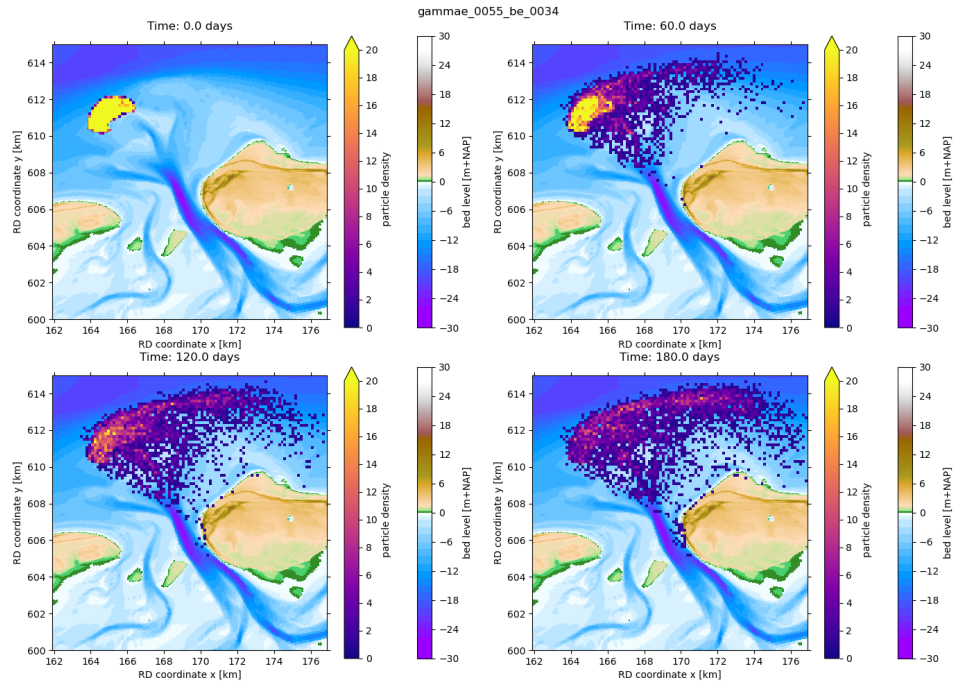


Figure 4.28 Result of 180 days of simulating dispersal of the nourishment with $b_e = 3.4 \cdot 10^{-5} s^{-1}$, $\theta_s = 0.1$ and $\gamma_e = 0.0055$.

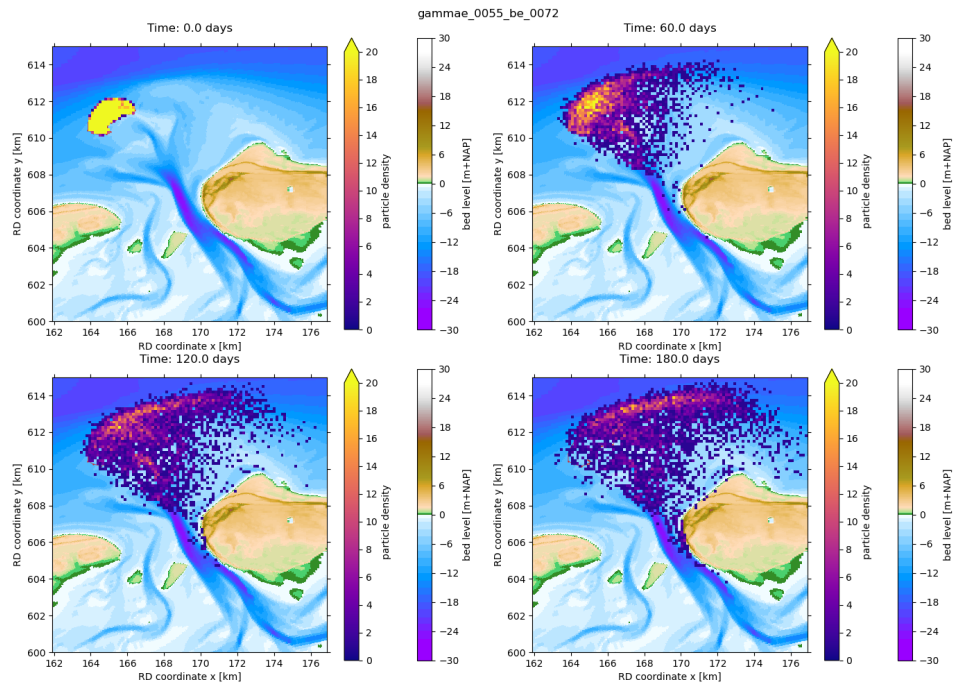


Figure 4.29 Result of 180 days of simulating dispersal of the nourishment with $b_e = 7.2 \cdot 10^{-5} s^{-1}$, $\theta_s = 0.1$ and $\gamma_e = 0.0055$.

The results after 60 days (top right in both figures) is similar the results with the adjusted erosion probability (runs 3 and 4). However, due to the increase in erosion probability, the particles start shifting further through the system. Especially in for the run with the highest erosion probability (Figure 4.29), a significant amount of sediment ends up on the outer edge of the ebb-tidal delta after 180 days. A higher erosion probability also results in more particles moving further south into the inlet and the west coast of Ameland. This can all be explained by particles being generally much more mobile in runs 6 and 7 compared to runs 3 and 4. This implies there is a sediment pathway from the southern part of the ebb-tidal delta and the inlet. However, this pathway is still insignificant, as it only concerns a relatively small amount of particles.

4.4 Summary of findings

This section provides a summary of the main findings from the modelling as shown in this chapter.

- Assessment of wave and tidal schematisations:
 - The number of wave conditions in the wave schematisation has little effect on model results. This could be due to the method of averaging wave conditions.
 - Inclusion of the wave-driven bed velocity also has limited effect. Investigation into its calculation in Delft3D-FM is required. It may not be the best mechanism for adding sediment transport by wave forcing if the residual magnitude is indeed as small as was calculated here.
 - Using a full spring-neap tidal cycle as opposed to a shorter morphological tide introduces significant changes. The spring-neap tidal cycle in this report was not calibrated, so a more in-depth investigation is required.
- Sensitivity of burial parameters:
 - b_e : directly affects deposition probability. Higher values decrease spread, but increase erosion probability slightly due to direct dependence.
 - θ_s : scales the range of deposition and erosion probability. Higher values cause more spread in particles.
 - γ_e : directly affects erosion probability only. Higher values cause sediment to move more through the system as particles are more likely to become free and can spend more time moving.
 - A value of b_e in order of magnitude of $O(10^{-5})$ can be used to simulate gradual erosion of a large amount of particles. This order of magnitude is significantly larger than the value proposed by Soulsby et al. (2011).
 - A significant increase in the scale parameter (θ_s) does not change general sediment pathways, but does affect particle density significantly.
 - Care must be taken when calibrating the erosion and deposition under the current burial configuration, as erosion scales directly to deposition.
- Dispersal of Ameland pilot nourishment:
 - Main pathways are circulation on western ebb-tidal delta and bypassing to the east, relatively far offshore.
 - Little to no interaction with the Wadden Sea basin is modelled.
 - Not much is known about the correct deposition patterns and probability. More investigation to calibrate deposition is required.
 - The percentage of nourishment sediment lost to bypassing is highly dependent on the deposition probability in SedTRAILS.

5 Discussion

This chapter connects the results from the previous chapter to the literature. The chapter is divided into four sections. First, the sensitivity to changes in both wave and tidal forcing are discussed. After this, the burial sensitivity is discussed. Next, an interpretation of the dispersal for the Ameland pilot nourishment is given. The final section of the chapter looks more broadly at nourishment modelling with SedTRAILS.

5.1 Forcing conditions

This section covers the uncertainty and limitations in the tested schematisations of wave- and tidal forcing, as well as a key limitation in the inclusion of wave-driven bed velocity.

5.1.1 Number of wave conditions

In general, SedTRAILS is not sensitive to an increased number of modelled wave conditions, even if more energetic conditions are present. This contradicts the known impact of storms on the system (e.g., [Elias and Pearson 2020](#), [Harlequin 2021](#), Figure 2.6) and the large impact that storms have on the outer edge of the ebb-tidal delta ([Elias 2021](#)). A distinction must then be made between the nourishment's response to storms and more commonly occurring conditions. For modelling dispersal under normal conditions, using fewer wave conditions produces adequate results and saves computational cost.

There is a lot of similarity between resulting grain velocity fields of the two wave condition sets as shown in Figure 4.7. This is a major reason for the small influence the inclusion of higher-energy wave conditions has. When averaging the results of all wave conditions, a weighted average based on the probability of occurrence was used.

Indeed, when modelling an energetic wave condition separately (Figure 4.8), transport patterns are significantly altered. This may be a problem with averaging of a yearly averaged wave climate. Lagrangian particle trajectories often represent gross transports through a system, with tracer variables applied to particles ([van Sebille et al. 2018](#)), whereas a yearly averaged wave climate aims to simulate the net transport through a system.

A more general problem with the wave forcing is the wave grid resolution. The computational grid used for the D-Wave module is coarser than the grid for the flow simulation, with grid cell sizes approximately four times as large. A loss in resolution will result in a loss of detail in the location of breaking waves and the propagation over the ebb-tidal delta. This cannot currently be corrected due to limitation in scope of this thesis.

5.1.2 Wave-driven bed velocity

When modelling the wave-driven bed velocity, magnitudes of only up to 4 cm/s were found. These magnitudes are surprisingly small. Orbital velocity amplitudes can be up to 1.5 m/s, with 0.1 to 0.5 m/s expected for the range of significant wave heights used here (Ruessink et al. 2012, van der Werf et al. 2022). However, works that discuss the wave-driven bed velocity parametrisation by Ruessink et al. (2012) mainly discuss the amplitude. A residual onshore velocity, which is used in SedTRAILS, would be significantly smaller than this. From previous Delft3D-4 modelling, the difference in peak onshore and offshore velocity still showed more significant magnitudes than what was calculated here, around 0. (Boechat Albernaz et al. 2019). This suggests that there may be some flaws in how the wave-driven bed velocity is calculated within Delft3D-FM.

Because of the apparent underestimation of the wave-driven bed velocity, more investigation into this option is needed. At its current magnitude, wave-driven bed velocity has only a small influence on model results after 30 days of simulation time. If the effect remains small after investigation, inclusion of this aspect of wave forcing might not be appropriate. A different method for including transport from waves is necessary in that case.

5.1.3 Offshore boundary

Changing from a morphological tide to a spring-neap tidal cycle has a significant effect on the simulation. The results shown here indicate that a changing tidal amplitude has a considerable effect on model results when compared to a morphological tide.

There are several reasons for the spring-neap tidal cycle to have such a large effect on model results. Firstly, the variation in tidal amplitude significantly alters the way waves propagate through the system. With lower water levels, waves break further offshore. Shoaling is also affected by this. While the morphological tide maintained a tidal amplitude of approximately 2 meters, the spring-neap tidal cycle has a tidal amplitude between 1.5 and 3 meters.

With changes in the tidal amplitude, there are also going to be changes in the flow velocity through and around the inlet. Around neap tide, particles move significantly less. Having periods of more and less movement over the simulation period is going to affect results compared to having a constant tidal amplitude.

One last reason the difference between the morphological and spring-neap tides is so large is the way both tidal schematisations are determined. Jiao (2014) details the process by which the morphological tide was determined. This was done based on sediment transport rates through specific transects. Meanwhile, the spring-neap tidal cycle boundary was constructed based on Schrijvershof et al. (2023). The result of this method has not been sufficiently calibrated for the Ameland tidal inlet system. This is a major limitation when comparing the two schematisations. More investigation into the influence of a spring-neap tidal cycle on model results is required, as the early comparison here clearly shows a significant change.

Using a spring-neap tidal cycle instead of a morphological tide also brings with it some practical problems. The underlying velocity field that must be generated for each wave condition is now 14 days long, instead of the 24 hours and 50 minutes for the morphological tide. Not only does this take significantly more computational time before running SedTRAILS, it also creates much bigger files that require more memory to be processed. This significantly slows down the process of using SedTRAILS. While a simulation of 5000 particles over 180 days still takes only a few hours, it requires significantly more work to get to that point (for example, see section A.1.1 in the appendices).

A longer simulation time of the underlying model does have one major advantage. When the simulation loops back to the beginning of the velocity field, there is always a small error. The velocity field at the beginning of the simulation is never exactly the same as at the end. With a much longer velocity field, this error is not present as often. While this was already minimised by setting this moment around flow reversal in the inlet, it is still notable to mention.

5.2 Burial formulation

All three parameters affect the probabilities differently and thus give very different results. In that sense, the formulation has a lot of utility for calibration. However, this method for calculating the erosion and deposition probabilities has downsides.

Perhaps most significant is the direct dependence of erosion probability on deposition probability (see section 2.4.2). When considering the processes of erosion and deposition, it would make sense for deposition to become less likely as erosion becomes more likely. However, with this burial formulation, that is not the case. In fact, deposition probability in its current state goes up as the maximum bed shear stress goes up, as Figure 4.19 shows. While deposition is not directly dependent on bed shear stress (e.g., van Rijn 2007, the default sediment transport formulation for morphodynamic Delft3D-4 and -FM simulations), the likelihood that a particle would deposit on the bed again should go down as bed shear stress goes up. With direct dependence of transition probabilities a on b , erosion does scale appropriately with increasing bed shear stress (Figure 5.1).

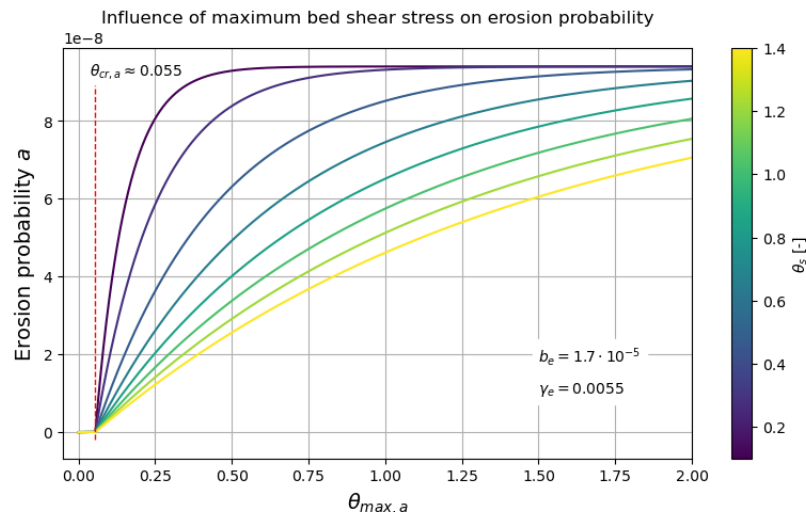


Figure 5.1 Erosion probability as it relates to the maximum bed shear stress for a range of scale parameter (θ_s) values.

In general, there is a problem when the deposition is dependent on bed shear stresses. Deposition is usually influenced by settling velocity and turbulence (e.g., van Rijn 2007). Setting a direct dependence between the erosion and deposition based on bed shear stress can thus result in unrealistic depositional patterns.

Something that should be noted as well when using this burial formulation is the simulation time step. The probabilities mentioned above are checked at each time step. In SedTRAILS, this is usually 30 seconds. However, in Soulsby et al. (2011), a time step of 20 minutes was used. This means that in SedTRAILS, deposition and erosion is checked 40 times as often as in Soulsby et al. (2011). This could significantly impact the behaviour of the model. When the probability is evaluated more often, the actual amount of free particles comes closer to the equilibrium proportion of free particles.

When changing the time step of SedTRAILS, it might be necessary to re-calibrate the burial parameters to account for this effect.

All of this results in an uncertainty when using burial. However, it is an important aspect to include in SedTRAILS. Burial provides a method for slowing down movement of sediment to mimic real major transport pathways and a suitable set of calibration parameters. The sensitivity analysis performed in this report can aid in future calibration of these parameters. The limitations of the formulation as described above do indicate a need for a different, more process-based formulation.

5.3 Modelling the Ameland pilot nourishment

As was shown at the end of Chapter 4, there are already configurations that can give qualitative insight into the dispersal of the Ameland pilot nourishment. There are two main transport pathways for the nourishment in its current location (Figure 5.2):

- Tidal recirculation, where sediment is transported south towards the inlet, only to be pushed northward again to within close proximity of the nourishment. This happens initially as sediment is moved away from the nourishment location.
- Into the sediment bypassing route. Here, the nourishment sediment is caught in the along-shore transport around the ebb-tidal delta. This concerns a significant amount of sediment and happens quickly after recirculation. Bypassing occurs through flow, as bar bypassing that is often observed at tidal inlets cannot be modelled with a static bed.

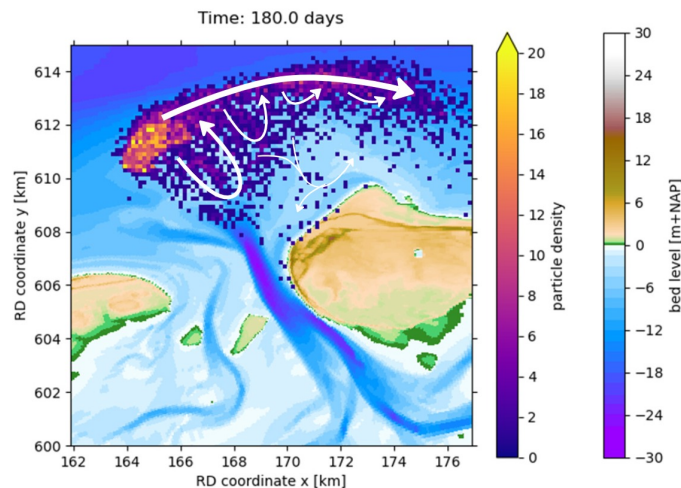


Figure 5.2 End result of SedTRAILS simulation as shown in 4.22 (run 2 in Table 3.5) The main pathways the sediment takes in this simulation are marked with white arrows.

The tidal re-circulation weakens as sediment moves further east along the bypassing route. This is likely the reason that not much sediment reaches the eastern part of the ebb-tidal delta or the west coast of Ameland. Pathways from the nourishment to this region require the sediment to reach further south at this part of the delta. As tidal currents become a less significant factor in transport in the eastern part of the delta (Elias 2021), this does not happen. Importantly, no interaction with the Wadden Sea basin is modelled. The most southward movement of particles that was modelled is towards the west coast of Ameland.

The tidal re-circulation pathways broadly match those shown by Lambregts (2021) (as shown in Figure 2.17) and Pearson et al. (2021) (as shown in Figure 2.15). Sediment from the nourishment moves eastward and circulates until it reaches the sediment bypassing route and finds the edge of the ebb-tidal delta. However, sediment in the

simulation performed in this report reaches further northward. This could be due to the moment of release within the tidal cycle. As particles erode gradually, there are many different moments during ebb or flood where motion is initiated. In the simulation by Lambregts (2021), there was only one moment of release, leading to a dominant transport direction.

The pathways found here broadly correspond to the areas of dominant forcing as identified in Elias (2021) (Figure 2.4). The outer edge, where the bulk of the nourishment is located, is mainly transported both east to the sediment bypassing route and south into the more tide-dominated zone. In this tide-dominated zone, sediment circulates more significantly with the tide, until it reaches the more wave-dominated north-eastern section of the ebb-tidal delta.

When looking more broadly at previous SedTRAILS results at the Ameland inlet by Pearson et al. (2021) and Lambregts (2021) (Figures 2.16 and 2.15), there are more similarities. Both global pathway simulations and their interpretations model the bypassing pathway at a similar position: on the outer edge of the ebb-tidal delta and far offshore from Ameland. This is different from the bar bypassing and shoal attachment that has been observed at Ameland, which occur further south and along the Bornrif platform (Elias et al. 2019, Brakenhoff et al. 2019). Figure 5.3 gives an overview of these differences in general pathways.

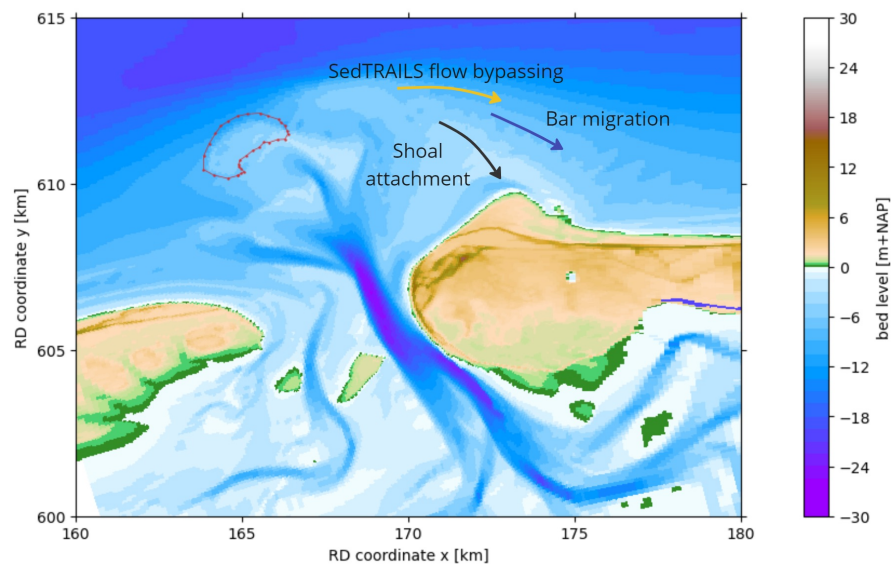


Figure 5.3 Several routes along which bypassing has been modelled and observed. The orange arrow indicates the bypassing modelled with SedTRAILS (both in results from this report and in Pearson et al. (2021), Lambregts (2021)). The blue arrow indicates a pathway for bar migration identified by Brakenhoff et al. (2019). The black arrow indicates the shoal attachment pathway over the Bornrif platform (Elias et al. 2019).

SedTRAILS is generally unable to model bar bypassing, as this process is heavily related to changes in bed levels. Non-bar bypassing along the periphery as described in Herrling and Winter (2018) does occur in the model results. However, this is further offshore than would be expected from the median sediment diameter used here (200 μm). A likely explanation for this is an underestimation of wave-driven forcing in the wave propagation direction, as was noted in section 5.1. When considering just one energetic wave condition (Figure 4.8), the sediment just east of the ebb-tidal delta is indeed much more spread out over the entire foreshore.

As stated previously, practically no sediment reaches the Borndiep inlet channel or the Wadden Sea basin. However, transport from ebb-tidal deltas into tidal basins does often occur during storm conditions (FitzGerald 1988, specifically for the Ameland inlet: Leummens (2018)). As storms are underrepresented in the current model configuration, transport of nourished sediment into the Wadden Sea is likely also underrepresented. This is confirmed by the result in Figure 4.8, where more particles end in and around the Borndiep channel and the west coast of Ameland.

When compared to the evolution of the nourishment from both the bathymetric surveys as discussed in Elias (2021) (Figure 2.7) and Delft3D-4 morphodynamic modelling in Harlequin (2021) (Figure 2.8), results with a significant amount of sediment landing in the western- and central ebb-tidal delta areas are more representative of bed level changes. The main areas that seem to be building out are directly south-east of the nourishment and in ebb-chute 2 (as seen in Figure 2.2) and the edge of the ebb-shield directly east of the nourishment. This implies the higher deposition probability runs 3 and 4 (Figure 4.26 middle and bottom) to be more representative of the morphological response of the system to the nourishment. To illustrate this, a contour plot of the particle density in run 4 (with $b_e = 7.2 \cdot 10^{-5}$, $\gamma_e = 0.0013$, see Figure 4.24) has been overlaid on the bed level change comparison by Harlequin (2021) (Figure 2.8), and can be seen in Figure 5.4. Here, areas of higher particle density (outside of the nourishment polygon) do overlap broadly with areas that show an increase in bed level change when the nourishment is present.

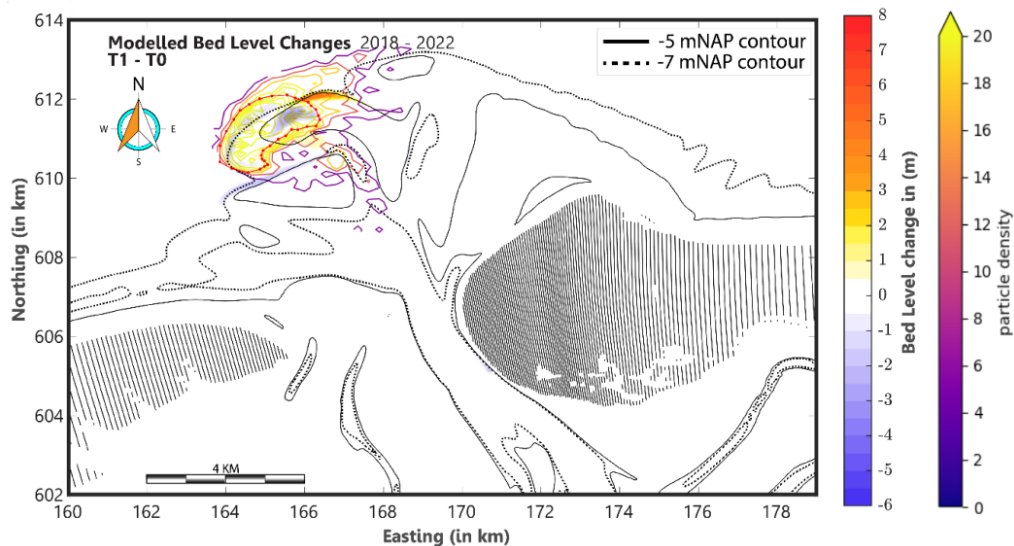


Figure 5.4 Comparison of particle density at the end of higher deposition probability simulation run 4 ($b_e = 7.2 \cdot 10^{-5}$, $\gamma_e = 0.0013$) with bed level change difference with and without nourishment in a morphodynamic Delft3D-4 simulation (Harlequin 2021).

Generally, increasing the erosion probability with the deposition probability, as done in runs 6 and 7 creates a more dynamic result, with sediment being more mobile and reaching further towards the inlet. This result is potentially more difficult to validate, as there are more significant changes over time.

There is a major limitation to this modelling. As discussed previously, burial has not been calibrated yet. While the gradual erosion of the nourishment has been replicated within SedTRAILS, there is still much uncertainty about the deposition probability.

5.4 Nourishment modelling with SedTRAILS

A general methodology was developed to model a nourishment with SedTRAILS. Once the underlying Eulerian model is finished, modelling a nourishment becomes relatively simple after calibration of burial. A large amount of sources can be set up on the area where the nourishment is placed. With a finished velocity field, testing several variants can be done very quickly. To illustrate this, two other nourishments in the Ameland tidal inlet system have also been modelled using SedTRAILS. These are the beach nourishment performed in 2019 and an alternate proposed ebb-tidal delta nourishment. The results of this can be found in Appendix C.

Testing design variants is limited to location variants, as varying for instance the height of a nourishment would require a new velocity field. Additionally, nourishment designs that significantly impact the flow patterns in a system are not going to be modelled adequately with this method unless a new Eulerian hydrodynamics field is generated to correspond to the change in bathymetry. However, modelling a new flow field with an alternate nourishment design is still relatively straightforward, as the morphodynamics do not need to be reassessed.

Using a proportion of erosion and deposition probability that is higher than that proposed in Soulsby et al. (2011), where the burial formulation originates, general insights on dispersal can already be gained with SedTRAILS. However, care must be taken with this proportion. When erosion probability is set too high, particles move around much more significantly. Generally, having erosion be on an order of magnitude of $O(10^{-7})$, with deposition being 200-800 times higher produces results that give information on the general transport and dispersal pathways. Calibration of the deposition is required to come to a more conclusive result. For these reasons, no specific set of burial parameters can be recommended. Quantification of transported sediment volumes (as described in appendix D) can provide the necessary link to available data for calibration and validation.

This report has shown a lot of results after 180 days of simulation time. However, it is unclear whether this timescale is representative of 180 days of real-time. This is due to two factors. Firstly, it is unclear if this reflects real-time erosion and deposition. The morphological timescale could be longer, similarly to how a morphological acceleration factor can be used in Eulerian morphodynamic models. Secondly, whether simulating such a timescale with SedTRAILS produces a valid result. Ebb-tidal deltas are highly dynamic systems, as shown in Elias et al. (2019). Even after 180 days in real time, channels and bars can shift positions. As mentioned before, the Delft3D-FM simulations performed for SedTRAILS are morphostatic. This is necessary to be able to reuse the same velocity field in a loop. It is currently unclear when the assumption of a static bed becomes unreasonable. When considering the development of the area immediately around the nourishment (e.g., Figure 2.7), longer simulations might be feasible, but the accuracy of the hydrodynamics will decrease the longer the SedTRAILS simulation is. More than a year of simulation time will likely be too long for the original bed to still accurately represent the hydrodynamics. Development of ebb-chutes and shoals occurs at this timescale (Elias et al. 2019).

The methodology provided here could be used to model more than just nourishments. For instance, the dispersal of individual barge loads when a nourishment is being placed could be modelled. With such a process taking a relatively short amount of time, an instantaneous release of several particles in the specific dumping area can give insight into how barge loads disperse as a nourishment is being placed.

While SedTRAILS shows promise as a tool for nourishment modelling, more work is needed to address uncertainties related to the impact of storm waves and wave-driven transport. The current implementation of burial only allows for qualitative insights into

dispersal, as the deposition is not calibrated or validated. However, these qualitative insights do give information on dispersal during calmer conditions.

6 Conclusions

Two research objectives were defined: firstly, to test and assess the impact and sensitivity of the burial formulation within SedTRAILS; secondly, to increase understanding of dispersal of the Ameland pilot nourishment. A main research question and three sub-questions were defined that assisted in reaching these objectives. A Delft3D-FM model was set up to simulate hydrodynamics at the Ameland tidal inlet. The hydrodynamics were then used to simulate particle pathways with SedTRAILS. Several schematisations of wave and tidal forcing were tested, after which sensitivity of the burial formulation was addressed in detail. With this, a preliminary evaluation of dispersal of the Ameland pilot nourishment was made. This chapter provides answers to the three sub-questions and the main research question.

1. How does dispersal of sediment change under a different schematisation in wave- and tidal forcing?

To model the Ameland ebb-tidal delta and pilot nourishment, the wave climate at Ameland was schematized into two sets of discrete wave conditions: a set of six and a set of sixteen conditions. Modelling both sets with identical settings for sediment transport and hydrodynamics revealed that an increase in wave conditions has a negligible effect on the model results. This is largely a result of the method for averaging the wave conditions. The resulting velocity fields with which particles are moved through the system are very similar for six and sixteen wave conditions. With the more energetic wave conditions getting mostly averaged out, the impact of storm conditions is minimised, while storms usually have a significant impact on the system.

The wave-driven bed velocity, intended as a method for directly including transport through wave skewness and asymmetry, had minimal impact on results. The magnitude of this wave-driven bed velocity is in the order of magnitude of 1-4 cm/s. The amplitude of such a velocity can easily reach well over 0.5 m/s for the wave climates included in the schematisations used here. Thus, the modelled wave-driven bed velocity is extremely low. However, the value for 0.5 m/s concerns the amplitude of this velocity, whereas SedTRAILS ideally uses a residual velocity. Not much information on the residual bed velocity is available, so direct comparison proved difficult. Investigation into the validity of the method and the magnitude that was found is recommended.

Both a morphological tide, as defined for Ameland in [Jiao \(2014\)](#), and a spring-neap tidal cycle determined with the method from [Schrijvershof et al. \(2023\)](#) were used to test the response from SedTRAILS. The spring-neap tidal cycle produced very different results to the morphological tide. This suggests that the dynamics that arise with spring- and neap tide could be important to the transport pathways at the Ameland tidal inlet. As the spring-neap tidal cycle was not adequately validated, nothing conclusive can be said yet. However, the significant difference indicates the need for further investigation.

2. How is dispersal of sediment particles affected by changes in sediment burial probabilities?

To address the first objective, many different configurations of the burial formulation in SedTRAILS were tested. The burial formulation in SedTRAILS relies on a probability that a particle, when trapped, erodes from the bed and a probability that a particle, when free, deposits on the bed. The erosion and deposition probabilities, named a and b respectively, have a significant effect on the particle pathways and thus how SedTRAILS models the dispersal of a nourishment. Three parameters are used to calibrate the burial:

- b_e : directly affects deposition probability. Higher values decrease spread, but increase erosion probability slightly due to direct dependence.

- θ_s : scales the range of deposition and erosion probability. Higher values cause more spread in particles.
- γ_e : directly affects erosion probability only. Higher values cause sediment to move more through the system as particles are more likely to become free and can spend more time moving.

Generally, when deposition probability goes up, particles spend less time travelling around the system and will more quickly deposit again. This causes spread of particles to go down. Erosion probability going up causes particles to start moving again more quickly after depositing. This causes particles to generally reach much further into the system within a given simulation time.

Some issues arise with the current burial implementation. The erosion probability is directly dependent on the deposition probability. This causes issues when tuning the three aforementioned parameters. It also leads deposition probability to scale up with maximum bed shear stress. These problems together make it difficult to calibrate this aspect of SedTRAILS.

3. What dispersal of the Ameland pilot nourishment is modelled when burial is included in the transport formulation?

To model the Ameland pilot nourishment with SedTRAILS, 5000 points were chosen at the nourishment location. Particles were released from these locations to simulate the dispersal of nourished sediment through the tidal inlet system.

From insights in the burial formulation gained from the previous research question, a definitive set of parameters could not be identified. The dispersal and deposition of sediment has not been calibrated. For qualitative analysis of dispersal, the following parameters provide a gradual erosion of many particles released at the start of the simulation, with deposition showing the general pathways of sediment:

- $b_e = 1.7 \cdot 10^{-5}$ [1/s] - The scale of erosion and deposition that this value brings captures the gradual erosion of sediment and spread throughout the system. However, this is more an indication of order of magnitude than an actual value, as there is much uncertainty on how deposition has to be calibrated. This value is significantly higher than the original value as defined by Soulsby et al. (2011).
- $\theta_s = 0.1$ [-] - The standard value from Soulsby et al. (2011), where the transport formulation originates.
- $\gamma_e = 0.0055$ [-] - This parameter has to be tuned together with the value of b_e , but the magnitude of erosion probability that this value provides simulates gradual erosion of the nourishment as has been observed. While this value is significantly lower than the one defined in Soulsby et al. (2011), it still scales up erosion compared to the erosion probability defined by Soulsby et al. (2011). This is a result of parameter b_e being scaled up significantly.

These values provide a gradual erosion of the nourishment and a qualitative sense of the pathways particles take in the system, as shown in Figure 6.1.

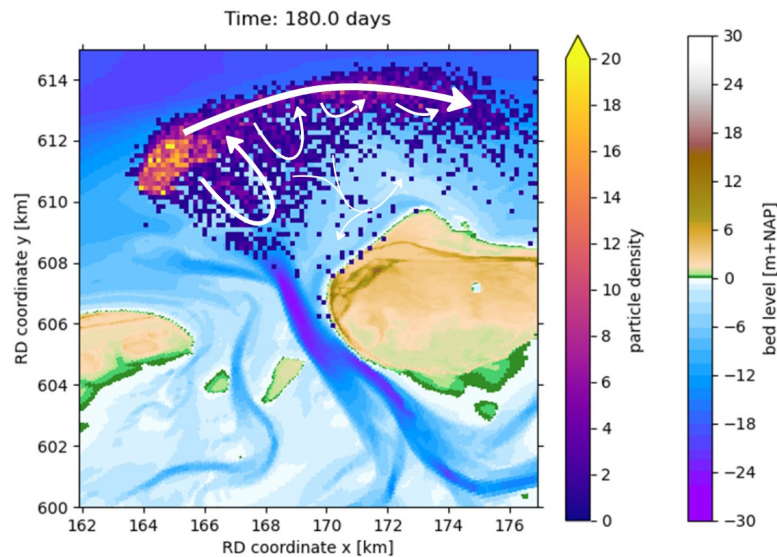


Figure 6.1 Result of 180 days of simulation of the Ameland pilot nourishment with SedTRAILS

Two main pathways for sediment were modelled:

- Tidal recirculation, where sediment is transported south towards the inlet, only to be pushed northward again to within close proximity of the nourishment. This happens initially as sediment is moved away from the nourishment location.
- Into the sediment bypassing route. Here, the nourishment sediment is caught in along-shore transport around the ebb-tidal delta. This concerns a significant amount of sediment (up to 40%) and happens quickly after recirculation. Bypassing occurs through flow, as bar bypassing that is often observed at tidal inlets (FitzGerald 1988, Elias et al. 2019) cannot be modelled with a static bed.

The main pathways have broad qualitative overlap with previous model studies by Harlequin (2021), Lambregts (2021) and Pearson et al. (2021). The amount of sediment lost to bypassing is importantly influenced by the burial configuration, with higher deposition probability leading to fewer particles moving east beyond the ebb-tidal delta. In all model runs, little to no interaction with the Wadden Sea basin is modelled.

These results are limited by the underlying Delft3D-FM model. For the Ameland inlet, the model still has some uncertainties in wave-driven transport. These mistakes are repeated by SedTRAILS. Storm conditions normally have a significant influence on morphology and transport in the system. This aspect is underrepresented in the wave schematizations used and the method by which the wave schematisations were combined.

The underestimation of wave-driven transport and the impact of storm conditions partly contribute to very little sediment depositing on the eastern section of the ebb-tidal delta and very little interaction with the tidal basin respectively.

How can SedTRAILS be used to analyse dispersal of sand nourishments in hydrodynamically complex environments?

Modelling nourishments in SedTRAILS can be achieved by placing a large amount of particles on the original nourishment location. By utilising the model's burial formulation, a gradual erosion of the nourishment can be replicated. It's possible to calibrate this erosion based on volume changes in measurements. However, deposition has not yet been calibrated or validated. Finding validation data for this is difficult. There is not much data available that isolates the influence of the nourishment.

SedTRAILS does provide a useful tool for assessing many different nourishment designs within one system. By utilising an underlying velocity field and releasing particles from different locations, many different nourishment locations can be tested on the same velocity field. This does come with a limitation. The velocity field will have to be re-made with the nourishment design present. Still, this approach is significantly faster than other modelling approaches, such as using a morphodynamic Delft3D model. The modelling results from SedTRAILS can be used to complement morphodynamic models of (to be) nourished systems by giving early indications of dispersal.

The early results obtained in this thesis show that SedTRAILS has the potential to become a useful tool for coastal managers looking to design and evaluate nourishments like the pilot nourishment in systems as complex as the Ameland tidal inlet. Addressing the uncertainties in wave schematisation, tidal forcing and the burial formulation can help improve the evaluation of existing nourishments (such as the Ameland pilot nourishment) and the feasibility and effectiveness of future nourishments.

7 Recommendations

This chapter provides recommendations on future research when modelling the Ameland pilot nourishment and nourishments generally with SedTRAILS.

7.1 Recommendations for model set-up

After testing several schematisations for wave- and tidal forcing, as well as the wave-driven bed velocity, some problems remained. This section covers steps to address these problems.

7.1.1 Forcing conditions

A SedTRAILS simulation is only as good as its underlying Eulerian flow model. The Delft3D-FM model that was used to model the Ameland tidal inlet has several known issues relating to the wave forcing and morphodynamics in the system. Wave-driven transports are often underestimated, especially in the more wave-dominated zones of the ebb-tidal delta ([Harlequin 2021](#)). SedTRAILS is bound to reflect those issues, as it directly uses the underlying model results to calculate transport. For that reason, more work on the Ameland model is required before the pilot nourishment can be properly modelled with SedTRAILS.

Of this, the wave climate is an important known factor. Especially around the area of the nourishment, storm waves have a significant impact on the morphology of the system ([Elias 2021](#), [Harlequin 2021](#)). This is underrepresented both in the FM model and SedTRAILS, as these low-probability conditions contribute very little to the overall velocity field.

From comparing simulations, it became apparent that using a spring-neap tidal cycle over a previously defined morphological tide produced significantly different results. Transports were overall less significant. This brought with it several complications in running the model. To increase usability of the model, recalibrating the morphological tide for SedTRAILS could be valuable. This can be used to substitute the spring-neap tidal cycle for easier use of SedTRAILS. Such a morphological tide would have to be calibrated based more on similarity in pathways and spread of particles between a spring-neap tidal cycle and the shorter tidal window, instead of the net sediment transport rates the tide from [Jiao \(2014\)](#) was calibrated on. However, doing such a calibration is not possible until SedTRAILS is further calibrated and validated. Additionally, the changes in tidal amplitude may be too important to the method of transport calculation for a shorter tidal window to be adequately representative of a spring-neap tidal cycle. Additionally, the spring-neap tidal cycle was not calibrated for this report. For these reasons, it is important to first investigate the spring-neap tidal cycle in more depth through proper calibration and validation of the transport in the system. After that, the morphological and spring-neap tides can be properly compared.

To remedy the uncertainty in modelling the Ameland ebb-tidal delta, other locations can be studied. Every year, many other nourishments are placed in the Netherlands. Systems such as the Oosterschelde or Westerschelde could prove useful for validation. These tide-dominated estuaries have also had nourishment works carried out over the past decade (e.g., Roggenplaat nourishment, [van der Werf et al. \(2019\)](#)), with several bathymetric surveys and model studies available (e.g., [de Vet et al. 2020](#)).

7.1.2 SedTRAILS settings

The method for averaging the wave conditions led to underestimation of impact of energetic conditions, as these were much less likely. There are other ways of combining and comparing the schematisations, however.

Possibly, the power relation between the hydrodynamic and sediment transport vectors needs to be assessed more in-depth to account for larger values more appropriately. However, with the transport formulation of SedTRAILS, this is not so straightforward. In equation 2.1, u_{gr} is linearly dependent on u_c , with bed shear stresses mainly influencing factors P and R directly. As the value of burial factor F flips between 1 and 0 based on transition probabilities, the exact power relation becomes even more complex. For that reason, it is likely that manually weighing storm conditions with a higher probability of occurrence will give better results than investigating the power relation between flow and grain velocities.

Another methodology that should be tested is to run all wave conditions separately and to combine the particle densities as a probability field as opposed to discrete particle positions (as was done for the result shown in Figure 4.5). The use of probability fields is already used in Lagrangian ocean analysis, similarly to how particle density is used in this report (van Sebille et al. 2018). This could resolve the issue of representing gross and net transports through the system, giving storm conditions more visible influence on the result.

A major limitation of the burial formulation is the direct dependence of erosion probability a on deposition probability b . Additionally, it is solely based on the difference between maximum bed shear stress and critical bed shear stress. A different burial formulation that removes the direct dependence and includes more processes relevant to deposition would improve results.

In this report, only instantaneous release of particles at the start of the simulation was investigated. However, a continuous release of particles might be capable of capturing dispersal adequately as well. Continuous release has not yet been tested in combination with burial. As a continuous release of particles would substitute the gradual erosion of particles facilitated by a low erosion probability, using a continuous release of particles would require re-calibration of the burial parameters.

7.2 SedTRAILS calibration and validation

While a significant amount of knowledge on the burial formulation was gained in the sensitivity analysis, the defined set of burial parameters cannot be considered definitive. Figure 4.26 illustrates the need for further calibration and validation, as there is still much uncertainty on the depositional pattern of sediment. To validate SedTRAILS results, transport needs to be quantified so it can be directly compared to validation data. This section provides recommendations for both quantification and the identification of validation data.

7.2.1 Quantification

To validate the model, the transport of sediment modelled with SedTRAILS will need to be quantified in terms of sediment volumes. One way to do that would be to assign a volume of sand to a particle. Volume per particle can be calculated based on observed volume changes of the nourishment. Harlequin (2021) showed a specified amount of volume within the nourishment polygon that was also used in the source setup of SedTRAILS simulations in this report. Counting the amount of particles still within this polygon and comparing it to the volume changes leads to an amount of m^3 of sand. To then compare it to observations and other models, bed level changes can be calculated as follows:

$$\Delta z = \frac{V_{particle} \cdot n_{particles,cell}}{A_{cell}} \quad (7.1)$$

Where:

- Δz : Bed level change [m]
- $V_{particle}$: Volume per particle [m^3]
- $n_{particles,cell}$: Amount of particles within a specific area in the system (as seen in the particle density maps in this report) [-]
- A_{cell} : Area within which $n_{particles,cell}$ is defined [m^2]

A preliminary quantification with subsequent bed level changes is provided in Appendix D as reference.

7.2.2 Validation data

Validation data for these simulations can be difficult to attain. It is difficult to determine the influence of solely the nourishment on the bathymetry, especially in a system as dynamic as the Ameland ebb-tidal delta. One method for this is similar to what was done in Harlequin (2021). There, the system was modelled both with and without the nourishment. From that, bed level changes can be directly compared to assess how the nourishment has impacted the morphodynamics of the system. These results already lined up broadly with what was found in the SedTRAILS modelling, but a more in-depth look at this type of result could prove interesting. One limitation of the Harlequin (2021) result is the use of a morphological tide. Additionally, the result uses a larger timescale than was deemed viable for the static bed simulation with SedTRAILS. Ideally, both simulations use the exact same forcing and boundary conditions while operating on similar timescales. As Delft3D-FM is much more widely used and, importantly, validated, than SedTRAILS, the comparison is useful.

It would make sense to compare SedTRAILS results to tracer studies. After all, SedTRAILS simulates particles as they move through a system, similar to how tracer sediment can be tracked within a system. However, when quantifying transport in SedTRAILS based on a volume per particle (Appendix D), individual grains stop being representative of the transport that is being modelled. For that reason, it is likely that this comparison will not provide the type of validation data that is needed. Tracer studies will serve as useful comparison for more general dispersal pathways, but they will not serve as easily comparable data to validate model results.

Validation from laboratory testing to directly compare SedTRAILS results to real conditions could be the missing factor. In a lab setting, there is complete control over the conditions. With these controlled conditions, validation is more reliable. However, lab experiments, especially on a larger scale, could prove expensive. A possible experi-

ment would be to use easily identifiable (e.g., coloured) sediment grains. This sediment can be placed in an initial position within a larger set-up. Forcing from flow and waves can be tested separately and in combination to test and compare to configurations for the velocity field in a SedTRAILS simulation. The start and end positions of different sand particles can then be identified through different colours. This can provide either something similar to the particle density plots seen in this report or the system-wide trajectories in [Pearson et al. \(2021\)](#) and [Lambregts \(2021\)](#), depending on initial set-up of particles. Comparing these results to changes in bed levels in the laboratory set-up can also aid in finding the volume per particle for quantification of transport.

References

- Aldama-Campino, A., K. Döös, J. Kjellsson, and B. Jönsson (2020). *TRACMASS: Formal release of version 7.0*. Version v7.0-beta. DOI: [10.5281/zenodo.4337926](https://doi.org/10.5281/zenodo.4337926). URL: <https://doi.org/10.5281/zenodo.4337926>.
- Bisschop, F. (2023). “Modelling sediment and propagule pathways to improve mangrove rehabilitation: A case study of the pilot project in Demak, Indonesia”. MSc Thesis. Delft University of Technology.
- Boechat Albernaz, M., G. Ruessink, H. R. A. Jagers, and M. G. Kleinhans (2019). “Effects of Wave Orbital Velocity Parameterization on Nearshore Sediment Transport and Decadal Morphodynamics”. In: *Journal of Marine Science and Engineering* 7.6. ISSN: 2077-1312. DOI: [10.3390/jmse7060188](https://doi.org/10.3390/jmse7060188). URL: <https://www.mdpi.com/2077-1312/7/6/188>.
- Booij, N., R. C. Ris, and L. H. Holthuijsen (1999). “A third-generation wave model for coastal regions: 1. Model description and validation”. In: *Journal of Geophysical Research*. DOI: <https://doi.org/10.1029/98JC02622>.
- Bosboom, J. and M. J. F. Stive (2022). *Coastal Dynamics*. [Online; accessed 2024-05-23]. Delft University of Technology.
- Brakenhoff, L., G. Ruessink, and M. van der Vegt (2019). “Characteristics of saw-tooth bars on the ebb-tidal deltas of the Wadden Islands”. In: *Ocean Dynamics* 69, pp. 1273–1285. DOI: <https://doi.org/10.1007/s10236-019-01315-w>.
- Brand, E., G. Ramaekers, and Q. Lodder (2022). “Dutch experience with sand nourishments for dynamic coastline conservation – An operational overview”. In: *Ocean & Coastal Management* 217, p. 106008. ISSN: 0964-5691. DOI: <https://doi.org/10.1016/j.ocecoaman.2021.106008>. URL: <https://www.sciencedirect.com/science/article/pii/S0964569121004919>.
- Dagestad, K.-F., J. Röhrs, Ø. Breivik, and B. Ådlandsvik (2018). “OpenDrift v1.0: a generic framework for trajectory modelling”. In: *Geoscientific Model Development* 11.4, pp. 1405–1420. DOI: [10.5194/gmd-11-1405-2018](https://doi.org/10.5194/gmd-11-1405-2018). URL: <https://gmd.copernicus.org/articles/11/1405/2018/>.
- Davis, R. A. and M. O. Hayes (1984). “What is a Wave-Dominated Coast?” In: *Hydrodynamics and Sedimentation in Wave-Dominated Coastal Environments*. Ed. by B. Greenwood and R.A. Davis. Vol. 39. Developments in Sedimentology. Elsevier, pp. 313–329. DOI: [https://doi.org/10.1016/S0070-4571\(08\)70152-3](https://doi.org/10.1016/S0070-4571(08)70152-3). URL: <https://www.sciencedirect.com/science/article/pii/S0070457108701523>.
- de Vet, P. L. M., B. C. van Prooijen, I. Colosimo, N. Steiner, T. Ysebaert, P. M. J. Herman, and Z. B. Wang (2020). “Variations in storm-induced bed level dynamics across intertidal flats”. In: *Scientific Reports*, p. 12877. DOI: <https://doi.org/10.1038/s41598-020-69444-7>.
- Deltares (2023). *D-Flow Flexible Mesh User Manual*. Available at <https://oss.deltares.nl/web/delft3dfm/manuals>. Accessed: 2024-05-02.
- Ebbens, E. (2019). *Tussenrapportage pilotsuppletie Buitendelda Amelander Zeegat*. Rijkswaterstaat. URL: https://www.helpdeskwater.nl/publish/pages/162296/tussenrapportage_pilot_amelander_zeegat.pdf.
- Elias, E. P. L. (2017). *Understanding the present-day morphodynamics of Ameland inlet*. URL: <https://www.deltares.nl/en/expertise/publicaties/understanding-the-present-day-morphodynamics-of-ameland-inlet>.

- Elias, E. P. L. (2021). *Morfologische analyse buitendelta Ameland en de rol van de pilot-suppletie*. Deltares. URL: <https://www.deltares.nl/expertise/publicaties/morfologische-analyse-buitendelta-ameland-en-de-rol-van-de-pilotsuppletie>.
- Elias, E. P. L. and S. G. Pearson (2020). *SedTRAILS - Sediment TRANsport visualization & Lagrangian Simulator; A novel method to visualize and analyse sediment transport pathways*. Deltares.
- Elias, E. P. L., S. G. Pearson, A. J.F. van der Spek, and S. Pluis (2022). "Understanding meso-scale processes at a mixed-energy tidal inlet: Ameland Inlet, the Netherlands – Implications for coastal maintenance". In: *Ocean & Coastal Management* 222, p. 106125. ISSN: 0964-5691. DOI: <https://doi.org/10.1016/j.ocecoaman.2022.106125>. URL: <https://www.sciencedirect.com/science/article/pii/S0964569122001004>.
- Elias, E. P. L., F. E. Roelvink, S. G. Pearson, and B. J. A. Huisman (2021). *Investigation of Sediment Pathways in the Put van Hansweert: morphological effects of dumping in a deep pit of the Western Scheldt*. Deltares. URL: <https://www.deltares.nl/en/expertise/publicaties/investigation-of-sediment-pathways-in-the-put-van-hansweert-morphological-effects-of-dumping-in-a-deep-pit-of-the-western-scheldt>.
- Elias, E. P. L., A. J.F. Van der Spek, S. G. Pearson, and J. Cleveringa (2019). "Understanding sediment bypassing processes through analysis of high-frequency observations of Ameland Inlet, the Netherlands". In: *Marine Geology* 415, p. 105956. ISSN: 0025-3227. DOI: <https://doi.org/10.1016/j.margeo.2019.06.001>. URL: <https://www.sciencedirect.com/science/article/pii/S0025322718304997>.
- FitzGerald, D. M. (1988). "Shoreline Erosional-Depositional Processes Associated with Tidal Inlets". In: *Hydrodynamics and Sediment Dynamics of Tidal Inlets*. Ed. by D. G. Aubrey and Lee W. New York, NY: Springer New York, pp. 186–225. ISBN: 978-1-4757-4057-8.
- Fitzgerald, D. M., N. C. Kraus, and E. B. Hands (2000). "Natural Mechanisms of Sediment Bypassing at Tidal Inlets". In: *ERDC/CHL CHETN-IV-30*. URL: https://www.researchgate.net/publication/255571013_Natural_Mechanisms_of_Sediment_Bypassing_at_Tidal_Inlets.
- Gornitz, V. (1991). "Global coastal hazards from future sea level rise". In: *Palaeogeography, Palaeoclimatology, Palaeoecology* 89.4, pp. 379–398. ISSN: 0031-0182. DOI: [https://doi.org/10.1016/0031-0182\(91\)90173-O](https://doi.org/10.1016/0031-0182(91)90173-O). URL: <https://www.sciencedirect.com/science/article/pii/003101829190173O>.
- Harlequin, D. (2021). "Morphodynamic Modelling of the Ameland Ebb-Tidal Delta: An assessment of the 2018-2019 pilot nourishment". MSc Thesis. Delft University of Technology.
- Herrling, G. and C. Winter (2018). "Tidal inlet sediment bypassing at mixed-energy barrier islands". In: *Coastal Engineering* 140, pp. 342–354. ISSN: 0378-3839. DOI: <https://doi.org/10.1016/j.coastaleng.2018.08.008>. URL: <https://www.sciencedirect.com/science/article/pii/S0378383917305896>.
- Huisman, B. J. A., J. W. M. Huisman, S. M. Arens, C. T. M. Vertegaal, L. van der Valk, S. C. van Donk, H. S. I. Vreugdenhil, and M. D. Taal (2021). *Evaluatie van 10 jaar Zandmotor: Bevindingen uit het Monitoring- en Evaluatie Programma (MEP) voor de periode 2011 tot 2021*. URL: <https://23g-sharedhosting-zandmotor.s3.eu-west-1.amazonaws.com/app/uploads/2021/06/21114926/Evaluatie-van-10-jaar-Zandmotor.pdf>.
- Jiao, J. (2014). "Morphodynamics of Ameland Inlet: Medium-term Delft3D Modelling". MSc Thesis. Delft University of Technology.

- Lambregts, P. (2021). "Sediment bypassing at Ameland inlet". MSc Thesis. Delft University of Technology.
- Lesser, G.R., J.A. Roelvink, J.A.T.M. van Kester, and G.S. Stelling (2004). "Development and validation of a three-dimensional morphological model". In: *Coastal Engineering* 51.8. Coastal Morphodynamic Modeling, pp. 883–915. ISSN: 0378-3839. DOI: <https://doi.org/10.1016/j.coastaleng.2004.07.014>. URL: <https://www.sciencedirect.com/science/article/pii/S0378383904000870>.
- Leummens, M. (2018). "Hydrodynamics and sand transport on the lower shoreface of the Ameland tidal inlet". MSc Thesis. University of Twente.
- MacDonald, N. J. and M. H. Davies (2006). "Particle-based sediment transport modelling". In: *Coastal Engineering*. DOI: https://doi.org/10.1142/9789812709554_0262.
- Madec, G. et al. (n.d.). *NEMO ocean engine*. URL: <http://hdl.handle.net/2122/13309>.
- Meijers, C. (2021). "Sediment Transport Pathways in Burrard Inlet". MSc Thesis. Delft University of Technology.
- Pearson, S. G., E. P. L. Elias, M. van Ormondt, F. E. Roelvink, P. M. Lambregts, Z. B. Wang, and B. van Prooijen (2021). "Lagrangian sediment transport modelling as a tool for investigating coastal connectivity". In: *Coastal Dynamics Conference 2021*. Delft University of Technology.
- Pearson, S. G., B. C. van Prooijen, E. P. L. Elias, S. Vitousek, and Z. B. Wang (2020). "Sediment Connectivity: A Framework for Analyzing Coastal Sediment Transport Pathways". In: *Journal of Geophysical Research: Earth Surface* 125.10. e2020JF005595. DOI: <https://doi.org/10.1029/2020JF005595>. eprint: <https://agupubs.onlinelibrary.wiley.com/doi/pdf/10.1029/2020JF005595>. URL: <https://agupubs.onlinelibrary.wiley.com/doi/abs/10.1029/2020JF005595>.
- Pearson, S. G., A. Reniers, and B. van Prooijen (2023). "REVEALING THE HIDDEN STRUCTURE OF COASTAL SEDIMENT TRANSPORT PATHWAYS USING LAGRANGIAN COHERENT STRUCTURES". In: *Coastal Sediments 2023: The Proceedings of the Coastal Sediments 2023*. World Scientific, pp. 1212–1221.
- van Rhijn, M. W. (2021). "Sediment transport during the execution of the pilot nourishment Ameland Inlet". MSc Thesis. Delft University of Technology.
- Rijkswaterstaat (n.d.). *Onderzoeksprogramma Beheer en Onderhoud kust*. <https://www.helpdeskwater.nl/onderwerpen/waterveiligheid/kust/onderzoeksprogramma-beheer-onderhoud-kust/>. Accessed: 2024-04-18.
- Rijkswaterstaat (1990). *Kustverdediging na 1990: Beleidskeuze voor de kustlijn*. URL: <http://resolver.tudelft.nl/uuid:a4c7d579-d528-4f26-9364-1346817230ba>.
- Roelvink, D., A. Reniers, A. van Dongeren, J. van Thiel de Vries, R. McCall, and J. Lescinski (2009). "Modelling storm impacts on beaches, dunes and barrier islands". In: *Coastal Engineering* 56.11, pp. 1133–1152. ISSN: 0378-3839. DOI: <https://doi.org/10.1016/j.coastaleng.2009.08.006>. URL: <https://www.sciencedirect.com/science/article/pii/S0378383909001252>.
- Ruessink, B.G., G. Ramaekers, and L.C. van Rijn (2012). "On the parameterization of the free-stream non-linear wave orbital motion in nearshore morphodynamic models". In: *Coastal Engineering* 65, pp. 56–63. ISSN: 0378-3839. DOI: <https://doi.org/10.1016/j.coastaleng.2012.03.006>. URL: <https://www.sciencedirect.com/science/article/pii/S0378383912000488>.
- Schrijvershof, R. A., D. S. van Maren, P. J. J. F. Torfs, and A. J. F. Hoitink (2023). "A Synthetic Spring-Neap Tidal Cycle for Long-Term Morphodynamic Models". In: *Jour-*

Journal of Geophysical Research: Earth Surface 128.3. e2022JF006799. DOI: <https://doi.org/10.1029/2022JF006799>. eprint: <https://agupubs.onlinelibrary.wiley.com/doi/pdf/10.1029/2022JF006799>. URL: <https://agupubs.onlinelibrary.wiley.com/doi/abs/10.1029/2022JF006799>.

Shadloo, M. S., G. Oger, and D. Le Touzé (2016). “Smoothed particle hydrodynamics method for fluid flows, towards industrial applications: Motivations, current state, and challenges”. In: *Computers & Fluids* 136, pp. 11–34. ISSN: 0045-7930. DOI: <https://doi.org/10.1016/j.compfluid.2016.05.029>. URL: <https://www.sciencedirect.com/science/article/pii/S0045793016301773>.

Sommer, P. S. (2024). *psypplot: Interactive data visualization with Python*. DOI: 10.5281/zenodo.593798. URL: <https://codebase.helmholtz.cloud/psypplot/psypplot>.

Soulsby, R. L., C. T. Mead, B. R. Wild, and M. J. Wood (2011). “Lagrangian Model for Simulating the Dispersal of Sand-Sized Particles in Coastal Waters”. In: *Journal of Waterway, Port, Coastal, and Ocean Engineering* 137.3, pp. 123–131. DOI: 10.1061/(ASCE)WW.1943-5460.0000074. eprint: <https://ascelibrary.org/doi/pdf/10.1061/%28ASCE%29WW.1943-5460.0000074>. URL: <https://ascelibrary.org/doi/abs/10.1061/%28ASCE%29WW.1943-5460.0000074>.

Soulsby, R.L., L. Hamm, G. Klopman, D. Myrhaug, R.R. Simons, and G.P. Thomas (1993). “Wave-current interaction within and outside the bottom boundary layer”. In: *Coastal Engineering* 21.1. Special Issue Coastal Morphodynamics: Processes and Modelling, pp. 41–69. ISSN: 0378-3839. DOI: [https://doi.org/10.1016/0378-3839\(93\)90045-A](https://doi.org/10.1016/0378-3839(93)90045-A). URL: <https://www.sciencedirect.com/science/article/pii/037838399390045A>.

Stive, M. J.F., M. A. de Schipper, A. P. Luijendijk, S. G. J. Aarninkhof, C. van Gelder-Maas, J. S. M. van Thiel de Vries, S. de Vries, M. Henriquez, S. Marx, and R. Ranasinghe (2013). “A New Alternative to Saving Our Beaches from Sea-Level Rise: The Sand Engine”. In: *Journal of Coastal Research* 29.5, pp. 1001–1008. DOI: 10.2112/JCOASTRES-D-13-00070.1. URL: <https://doi.org/10.2112/JCOASTRES-D-13-00070.1>.

Storlazzi, C. D., M. van Ormondt, Y.-L. Chen, and E. P. L. Elias (2017). “Modeling Fine-Scale Coral Larval Dispersal and Interisland Connectivity to Help Designate Mutually-Supporting Coral Reef Marine Protected Areas: Insights from Maui Nui, Hawaii”. In: *Frontiers in Marine Science* 4. ISSN: 2296-7745. DOI: 10.3389/fmars.2017.00381. URL: <https://www.frontiersin.org/articles/10.3389/fmars.2017.00381>.

Swart, H.E. de and J.T.F. Zimmerman (2009). “Morphodynamics of Tidal Inlet Systems”. In: *Annual Review of Fluid Mechanics* 41. Volume 41, 2009, pp. 203–229. ISSN: 1545-4479. DOI: <https://doi.org/10.1146/annurev.fluid.010908.165159>. URL: <https://www.annualreviews.org/content/journals/10.1146/annurev.fluid.010908.165159>.

Thillaigovindarasu, N. R. (2023). “Mangrove-Sediment Connectivity in the Presence of Structures Used to Aid Restoration: A Demak Case Study”. MSc Thesis. Delft University of Technology.

van der Werf, J. J., R. A. Schrijvershof, L. B. Brakenhoff, and B. T. Grasmeijer (2022). “Observations of near-bed orbital velocities and small-scale bedforms on the Dutch lower shoreface”. In: *Ocean & Coastal Management* 218, p. 106012. ISSN: 0964-5691. DOI: <https://doi.org/10.1016/j.ocecoaman.2021.106012>. URL: <https://www.sciencedirect.com/science/article/pii/S0964569121004956>.

van der Werf, J.J., P.L.M. de Vet, M.P. Boersema, T.J. Bouma, A.J. Nolte, R.A. Schrijvershof, L.M. Soissons, J. Stronkhorst, E. van Zanten, and T. Ysebaert (2019). “An integral approach to design the Roggenplaat intertidal shoal nourishment”. In: *Ocean*

& *Coastal Management* 172, pp. 30–40. ISSN: 0964-5691. DOI: <https://doi.org/10.1016/j.ocecoaman.2019.01.023>. URL: <https://www.sciencedirect.com/science/article/pii/S0964569118306574>.

van Rijn, L. C. (2007). *Principles of Sediment Transport in Rivers, Estuaries and Coastal Seas*. Aqua Publications.

van Sebille, E. et al. (2018). “Lagrangian ocean analysis: Fundamentals and practices”. In: *Ocean Modelling* 121, pp. 49–75. ISSN: 1463-5003. DOI: <https://doi.org/10.1016/j.ocemod.2017.11.008>. URL: <https://www.sciencedirect.com/science/article/pii/S1463500317301853>.

Wageningen University (n.d.). *TRAILS: TRacking Ameland Inlet Living Lab Sediment*. <https://www.wur.nl/en/project/trails-tracking-ameland-inlet-living-lab-sediment.htm>. Accessed: 2024-04-18.

A Processing methods and scripts

This appendix is a way to communicate specific methods within Matlab and Python, for use as reference by those that work on modelling (dispersal) with SedTRAILS in the future.

A.1 Pre-processing scripts

This section details the specific methods for pre-processing data before a SedTRAILS simulation. This mainly concerns the transition from Delft3D-FM output to SedTRAILS input.

A.1.1 Partition merging (Python)

Simulating an entire spring-neap tidal cycle for six different wave conditions is computationally expensive compared to a morphological tide. A way to speed this up is to partition the model and run parallel computations. This is an existing function within Delft3D-FM. However, at the end, SedTRAILS output needs to be combined into a single file to work with the rest of the code. The following script uses Python 3 modules `xarray` and `dask` to combine the outputs of 16 partitions, utilising `numpy.where` to remove duplicate points.

```
import xarray as xr
import dask
import numpy as np

def merge_partition_output(output_folder):
    """
    Script that merges FM SedTRAILS output of partitioned run into one netcdf file.
    Important to change:
        output_folder - location of dflowfm output folder
    """

    # Find folder where all partitioned sedtrails output files are located

    # Create multi-file dataset, drop unnecessary variables
    ds = xr.open_mfdataset(output_folder + f"*sedtrails.nc",
                          chunks={'time':522, 'net_xcc':100, 'net_ycc':100},
                          combine='nested', concat_dim='nNodes',
                          drop_variables=['FlowElemDomain', 'FlowElemGlobalNr', 'timestep'],
                          parallel=True)

    print('Done loading')
    # Remove duplicate points
    idx = np.sort(np.unique([ds.net_xcc.values, ds.net_ycc.values], axis=1, return_index=True)
                 [1])
    ds = ds.isel({'nNodes':idx})
    print('Done slicing')
    # Save merged sedtrails output file to netcdf in same folder
    ds.to_netcdf(output_folder + "rif4_merged_sedtrails.nc")
    print('Saved!')
```

Within SedTRAILS, the file can then be used. For longer simulations (e.g., 14 days, 11 hours, 50 minutes), this script can take quite a while to run. If possible, run overnight in a loop for all your wave conditions, as it takes at least an hour per condition in this current configuration.

A.1.2 Source set-up (Python)

The sources are 5000 random points within the pre-defined nourishment polygon. To do this, the `geopandas.sample_points()` function was used. The script to generate them (with random seed 5000 for consistency) is provided below:

```

import numpy as np
import matplotlib.pyplot as plt
import geopandas as gpd
import shapely as sh

# Load nourishment polygon
nourishment = np.loadtxt('C:\\MSc thesis\\SedTRAILS\\setup\\Nourishment Location.pol',
    skiprows=8)
nourishment_pol = sh.polygons(nourishment)
# Convert polygon to geoseries
gseries = gpd.GeoSeries(data=nourishment_pol)
# Sample 5000 points in polygon and convert coordinates to numpy array
points = gseries.sample_points(5000, rng=5000)
coords = points.get_coordinates()
coords = coords.to_numpy()

# plot polygon and source locations
plt.plot(nourishment[:,0],nourishment[:,1],color='tab:red', marker='o',linewidth=0.5,
    markersize=0.7)
plt.scatter(coords[:,0],coords[:,1])

# Save source locations
np.savetxt(f'sources{len(coords)}_locs.txt',coords)

```

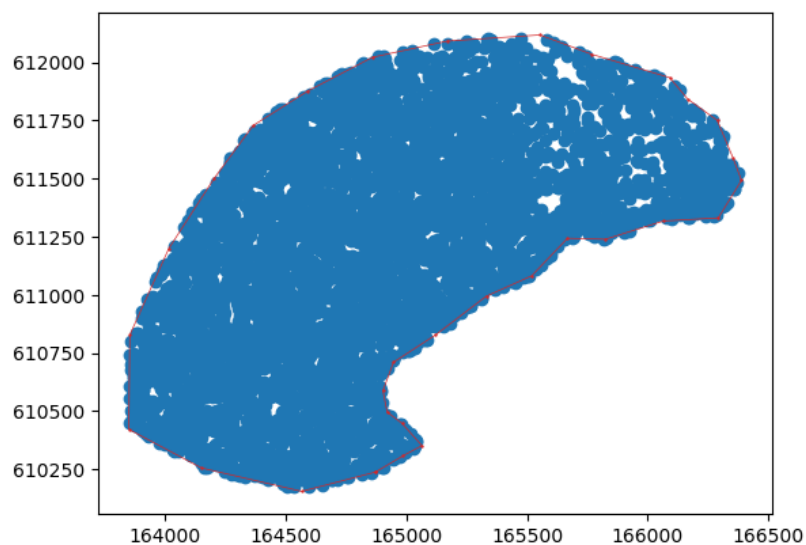


Figure A.1 Plot output from script A.1.2

A.1.3 Combining wave conditions (MATLAB)

Combining the results is done within the SedTRAILS step01 script. Matlab is made to cycle through all six different Delft3D-FM output folders and add up the weights.

```

waveprobs = [0.2741,0.2397,0.1193,0.2134,0.1183,0.0352];
wavenames = ["wc1","wc2","wc3","wc4","wc5","wc6"];

for nn = 1:length(waveprobs)
    if nn==1
        % first wave condition: initialise the weighted input structure
        weightedSoulsbyInput = results;
        weightedSoulsbyInput.Name = 'soulsby_input_weighted';
        weightedSoulsbyInput.Uc_x = weightedSoulsbyInput.Uc_x .* waveprobs(nn);
        weightedSoulsbyInput.Uc_y = weightedSoulsbyInput.Uc_y .* waveprobs(nn);
        weightedSoulsbyInput.mean_bss_mag = weightedSoulsbyInput.mean_bss_mag .* waveprobs(
            nn);
        weightedSoulsbyInput.max_bss_mag = weightedSoulsbyInput.max_bss_mag .* waveprobs(nn);
    };
    weightedSoulsbyInput.waterdepth = weightedSoulsbyInput.waterdepth .* waveprobs(nn);
else

```

```

        % add the weighted input of each wave condition
        weightedSoulsbyInput.Uc_x = weightedSoulsbyInput.Uc_x + results.Uc_x .* waveprobs(
            nn);
        weightedSoulsbyInput.Uc_y = weightedSoulsbyInput.Uc_y + results.Uc_y .* waveprobs(
            nn);
        weightedSoulsbyInput.mean_bss_mag = weightedSoulsbyInput.mean_bss_mag + results.
            mean_bss_mag .* waveprobs(nn);
        weightedSoulsbyInput.max_bss_mag = weightedSoulsbyInput.max_bss_mag + results.
            max_bss_mag .* waveprobs(nn);
        weightedSoulsbyInput.waterdepth = weightedSoulsbyInput.waterdepth + results.
            waterdepth .* waveprobs(nn);
    end
end

```

The `weightedSoulsbyInput` data structure is then used as input for the Soulsby et al. (2011) grain velocity calculations.

A.2 Post-processing scripts

This report includes many visualisations and processing of results from SedTRAILS.

A.2.1 Loading SedTRAILS output in Python

SedTRAILS outputs in `.mat` file format. For use with MATLAB, this works fine. However, the data structure is slightly less intuitive when using Python. The below script takes the `.mat` file as input and outputs a `pandas` dataframe with every particle position in the 'x' and 'y' columns, with time in the 'time' column. Particle source names are listed as category for potential sorting by source.

```

import numpy as np
import pandas as pd
import h5py

# Load .mat file from filepath
f = h5py.File(filepath, 'r')

# Extract only trajectories
n_sources = 5000

data = f.get('parameters/parameter')
data = data[2:2+n_sources]

n_parts = f[data[0][0]]['x'].shape[0]
n_time = f[data[0][0]]['x'].shape[1]

# Write trajectories to numpy arrays:
x = np.zeros((n_sources, n_parts, n_time))
y = np.zeros((n_sources, n_parts, n_time))
t = np.zeros((n_sources, n_parts, n_time))

for i in range(n_sources):
    x[i] = np.array(f[data[i][0]]['x'])
    y[i] = np.array(f[data[i][0]]['y'])
    t[i] = np.array(f[data[i][0]]['time']).T

# Create pandas dataframe from numpy arrays
lst = []
for i in range(n_sources):
    for j in range(n_parts):
        df = pd.DataFrame(data={'x':x[i,j], 'y':y[i,j], 'time':t[i,j], 'source':f'source {i
+1:04d}', 'particle':j+1})
        lst.append(df)

sedtrails = pd.concat(lst)
sedtrails = sedtrails.replace(np.inf, np.nan)
sedtrails.dropna(axis=0, inplace=True)
sedtrails['source'] = sedtrails['source'].astype("category")
sedtrails['particle'] = sedtrails['particle'].astype("category")

```

This dataframe can then be easily used for analysis and visualisation.

A.2.2 Unstructured grid plotting (Python)

To plot unstructured grids, the module psyplot (Sommer 2024) has been used. It allows for plotting data on unstructured grids following the UGRID conventions. As FM map file output follows this convention, it made plotting of FM output with Python module matplotlib possible.

It should be noted that only full "_map.nc" output files from FM are compatible with this method, as the "_sedtrails.nc" file structure does not include the unstructured grid and interpolates all face values to the node points. In its current version, psyplot is not able to plot variables defined on nodes.

Firstly, to plot the bathymetry, the colormap GMT Globe was used. As this is not available as a standard colormap in matplotlib, it was created as well. After this, psyplot can be initiated.

```
import numpy as np

import matplotlib.pyplot as plt
from matplotlib.colors import LinearSegmentedColormap, Normalize
import matplotlib.cm as cm

import psyplot.project as psy

# make matplotlib colormap for GMT_globe
rgb = np.loadtxt('GMT_globe.rgb', delimiter=' ', skiprows=2)
GMT_globe = LinearSegmentedColormap.from_list('GMT_globe', colors=rgb, N=256)
bath_norm = Normalize(vmin=-30, vmax=30)

# other plot setup
psy.rcParams['plotter.plot2d.cbar'] = {'r'}
zoom_x_min = 161900
zoom_x_max = 176900
zoom_y_min = 600000
zoom_y_max = 615000

# Open dataset using psyplot (properly assigns coordinates)
fm = psy.open_dataset(fp_fm, engine='scipy') # fp_fm: filepath to _map.nc output file

# plot bathymetry
fig, ax = plt.subplots(1, 1)

bathymetry1 = fm.psy.plot.plot2d(name='mesh2d_flowelem_b1', cmap=GMT_globe, ax=ax, time=0,
                                bounds=bath_norm,
                                clabel='bed level [m+NAP]',
                                xticks
                                =[162000, 164000, 166000, 168000, 170000, 172000, 174000, 176000],
                                xticklabels=['162', '164', '166', '168', '170', '172', '174', '
                                176'],
                                yticks
                                =[600000, 602000, 604000, 606000, 608000, 610000, 612000, 614000],
                                yticklabels=['600', '602', '604', '606', '608', '610', '612', '
                                614'],
                                xlabel='RD coordinate x [km]',
                                ylabel='RD coordinate y [km]',
                                cticks={'N': 11, 'method': 'rounded', 'vmin': -30, 'vmax': 30},
                                xlim=[zoom_x_min, zoom_x_max], ylim=[zoom_y_min, zoom_y_max]
                                )

ax.set_aspect('equal') # set aspect ratio of plot
```

This script produces the following plot:

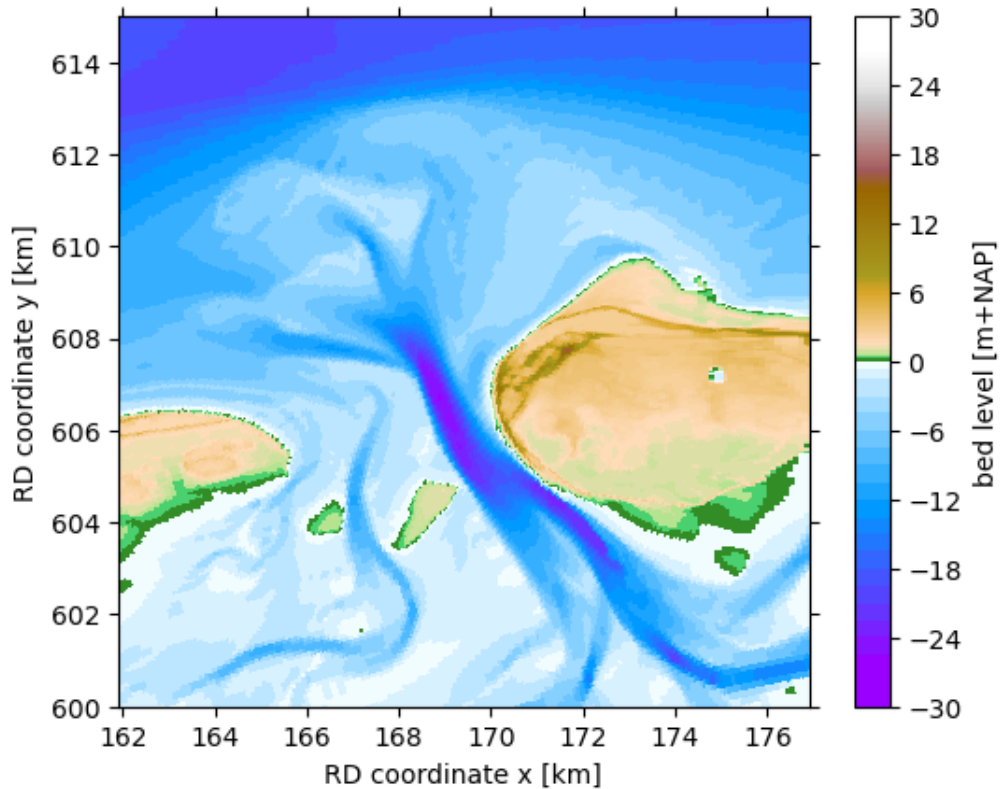


Figure A.2 Result of running the script above: an empty plot of the Ameland inlet's bathymetry from the unstructured grid output of Delft3D-FM.

A.2.3 Particle density plotting - two ways (Python)

For finding the particle density, two different methods are available. Initially, the module "datashader" was used. This allows for quick plotting of huge datasets because it aggregates points into pixel data by default.

```
from datashader.mpl_ext import dsshow
# Slice sedtrails dataframe on time step to be plotted (t_plot)
df = sedtrails.loc[(sedtrails['time'] == t[0][0][t_plot])]

# Add datashader to current plot
hist = dsshow(df, ds.Point('x', 'y'), ds.count(), cmap='plasma', ax=ax,
             fignum=1, aspect='equal',
             plot_width=100, plot_height=100,
             x_range=[zoom_x_min, zoom_x_max], y_range=[zoom_y_min, zoom_y_max],
             vmin=0, vmax=20
             )

# In combination with pyplot, datashader result needs to be set on top of pyplot
explicitly:
hist.set_zorder(len(ax.get_children())-4)

# Colorbar for the particle density
plt.colorbar(mappable=hist, cmap='plasma', ax=ax, label='particle density', location='right',
            ticks=np.linspace(0, 20, 11), extend='max')
```

The above script can be used together with the script in the previous section to produce a plot with the bathymetry as background and the 2d histogram on top.

The main downside of datashader is that the data is difficult to manipulate afterwards. If any calculation based on, for instance, the density, is required, a lot of "cheating" would need to be done to get the results to display correctly. For that reason, the `numpy . 2`

`dhistogram()` function can also be used. To use `numpy` instead, replace the above script with the following:

```
# Slice sedtrails dataframe on time step to be plotted (t_plot)
df = sedtrails.loc[(sedtrails['time'] == t[0][0][t_plot])]

# Make 2d histogram of particle density
hist_2d = np.histogram2d(df.x,df.y,range=[[x_min,x_max],[y_min,y_max]],bins=[100,100])
density = np.where(hist_2d[0]==0,np.nan,hist_2d[0]).T # if 0, shows up as transparent on a plot

# Plot the histogram on the current axis
hist = ax.pcolormesh(hist_2d[1],hist_2d[2],density,cmap='plasma',vmin=0,vmax=20)
```

Another advantage of this method is that the `zorder` of plot elements does not need to be changed to work with `psycopg`.

A.2.4 Alternative wave combination method (Python)

Figure 3.9 showcased a method for combining wave conditions through post-processing. The below script was used to accomplish this.

```
import numpy as np
import pandas as pd
import h5py

# Probability of occurrence of 6 wave conditions
wave_probs = np.array([0.2741,0.2397,0.1193,0.2134,0.1183,0.0352])

for wave in range(len(wave_probs)):
    print(f'Start wavecon {wave+1}')
    f = h5py.File(filepath, 'r') # set filepath to SedTRAILS output folder of wave condition run

    # Extract only trajectories
    n_sources = 5000

    test = f.get('parameters/parameter')
    test = test[2:2+n_sources]

    n_parts = f[test[0][0]]['x'].shape[0]
    n_time = f[test[0][0]]['x'].shape[1]
    # Write trajectories to numpy arrays:
    x = np.zeros((n_sources,n_parts,n_time))
    y = np.zeros((n_sources,n_parts,n_time))
    t = np.zeros((n_sources,n_parts,n_time))

    for i in range(n_sources):
        x[i] = np.array(f[test[i][0]]['x'])
        y[i] = np.array(f[test[i][0]]['y'])
        t[i] = np.array(f[test[i][0]]['time']).T
    lst = []
    if wave == 0:
        for i in range(n_sources):
            for j in range(n_parts):
                df = pd.DataFrame(data={'x':x[i,j], 'y':y[i,j], 'time':t[i,j], 'source':f'source {i+1:04d}', 'particle':j+1})
                lst.append(df)
            sedtrails = pd.concat(lst)
            sedtrails = sedtrails.replace(np.inf,np.nan)
            sedtrails['source'] = sedtrails['source'].astype("category")
            sedtrails['particle'] = sedtrails['particle'].astype("category")
            sedtrails['x'] = sedtrails['x'] * wave_probs[wave]
            sedtrails['y'] = sedtrails['y'] * wave_probs[wave]
    elif wave > 0:
        for i in range(n_sources):
            for j in range(n_parts):
                df = pd.DataFrame(data={'x':x[i,j], 'y':y[i,j], 'time':t[i,j], 'source':f'source {i+1:04d}', 'particle':j+1})
                lst.append(df)
            new_sed = pd.concat(lst)
```

```
new_sed = new_sed.replace(np.inf, np.nan)
sedtrails['x'] = sedtrails['x'] + new_sed['x'] * wave_probs[wave]
sedtrails['y'] = sedtrails['y'] + new_sed['y'] * wave_probs[wave]
```

This creates a `pandas` dataframe that can be used in the same way as in the previous scripts.

B Sensitivity runs

This appendix includes a lot of the graphs used to determine the statements made in the sensitivity analysis in Chapter 4. All of these simulated 10 days with the six wave conditions given in Chapter 3. If not specifically mentioned, the burial parameters were set as follows:

- $b_e = 1.7 \cdot 10^{-3}$ [1/s]
- $\gamma_e = 0.1$ [-]
- $\theta_s = 0.1$ [-]

B.1 b_e : Maximum free-to-trapped transition probability

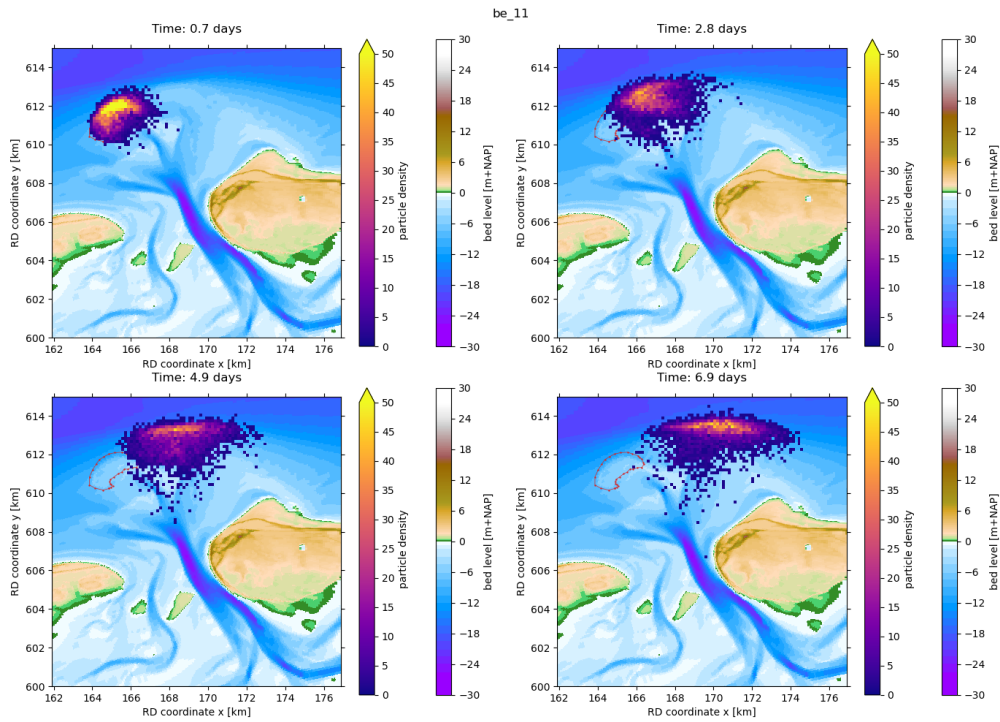


Figure B.1 $b_e = 1.1 \cdot 10^{-3}$

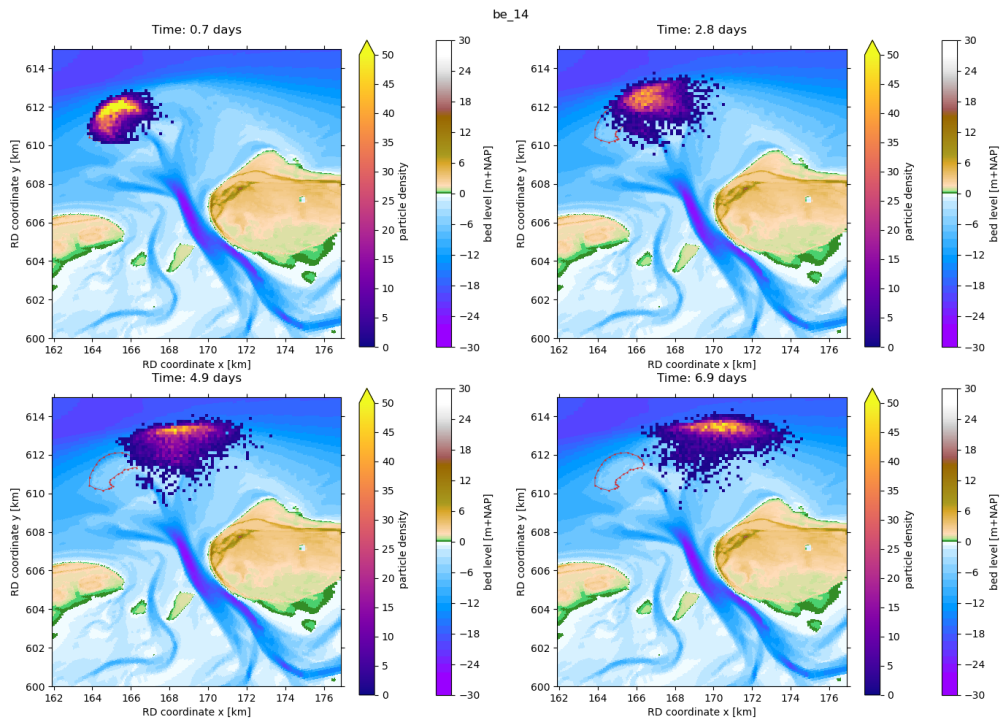


Figure B.2 $b_e = 1.4 \cdot 10^{-3}$

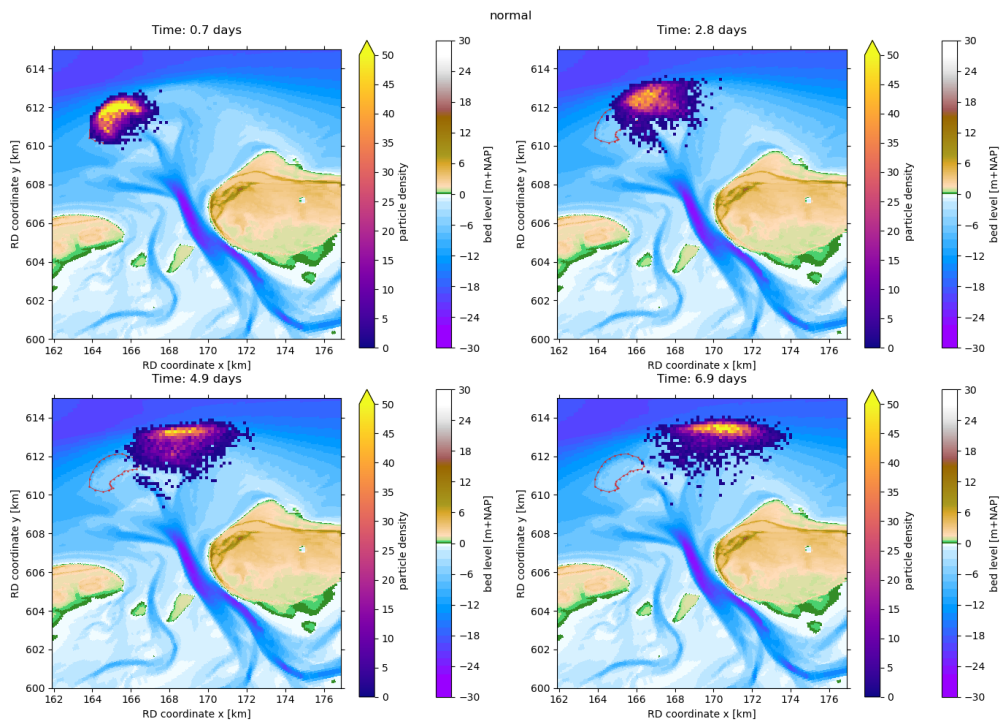


Figure B.3 $b_e = 1.7 \cdot 10^{-3}$

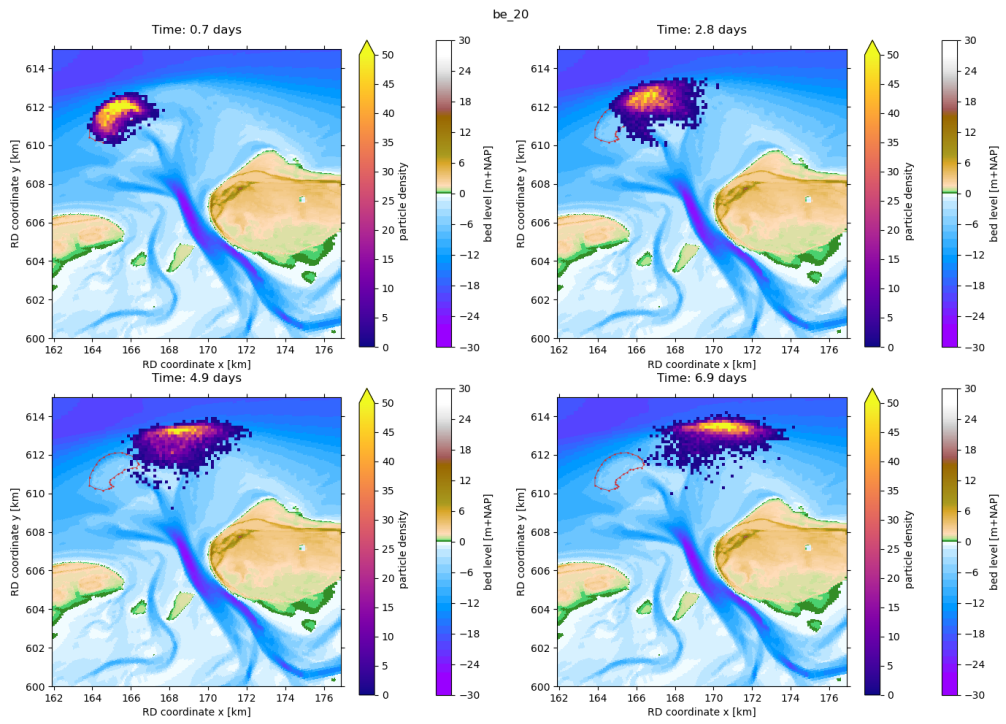


Figure B.4 $b_e = 2.0 \cdot 10^{-3}$

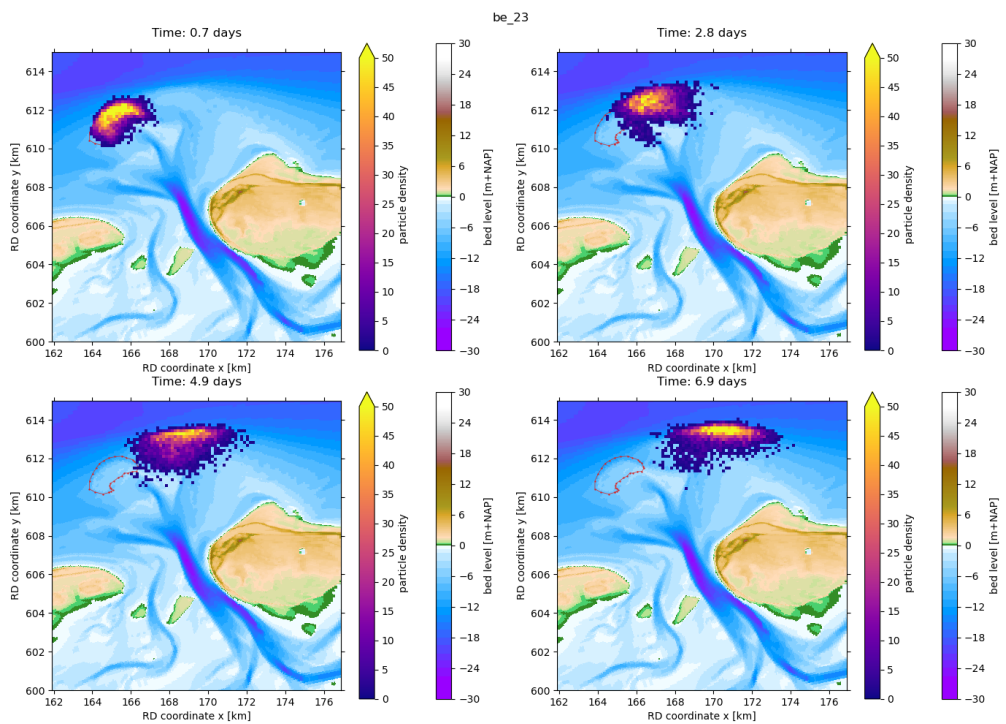


Figure B.5 $b_e = 2.3 \cdot 10^{-3}$

B.2 θ_s : Transition scale value

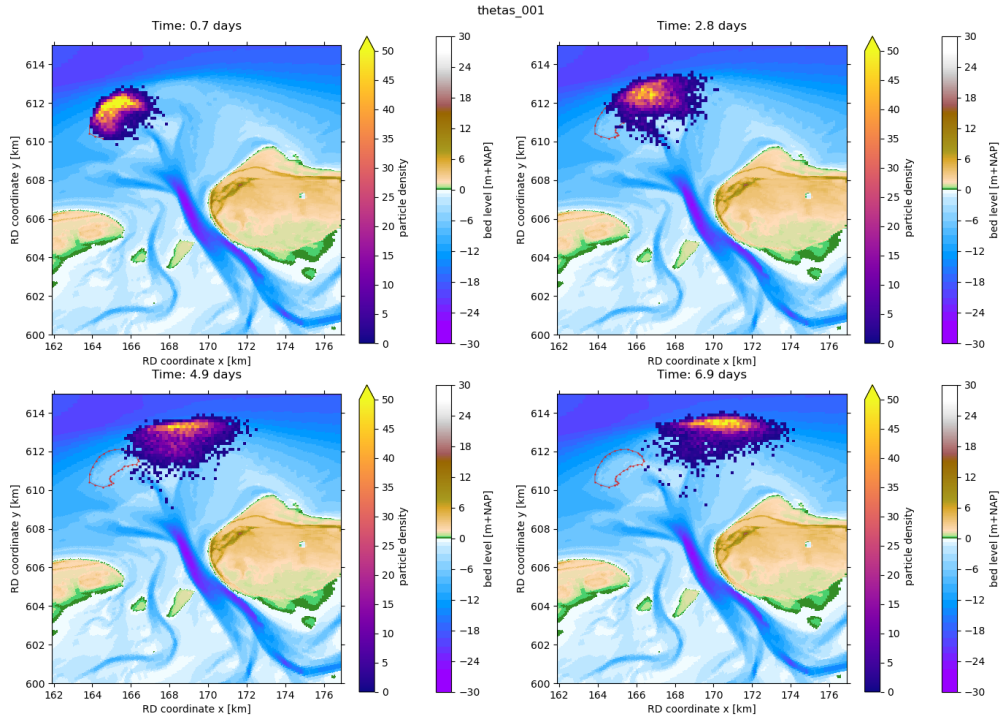


Figure B.6 $\theta_s = 0.01$

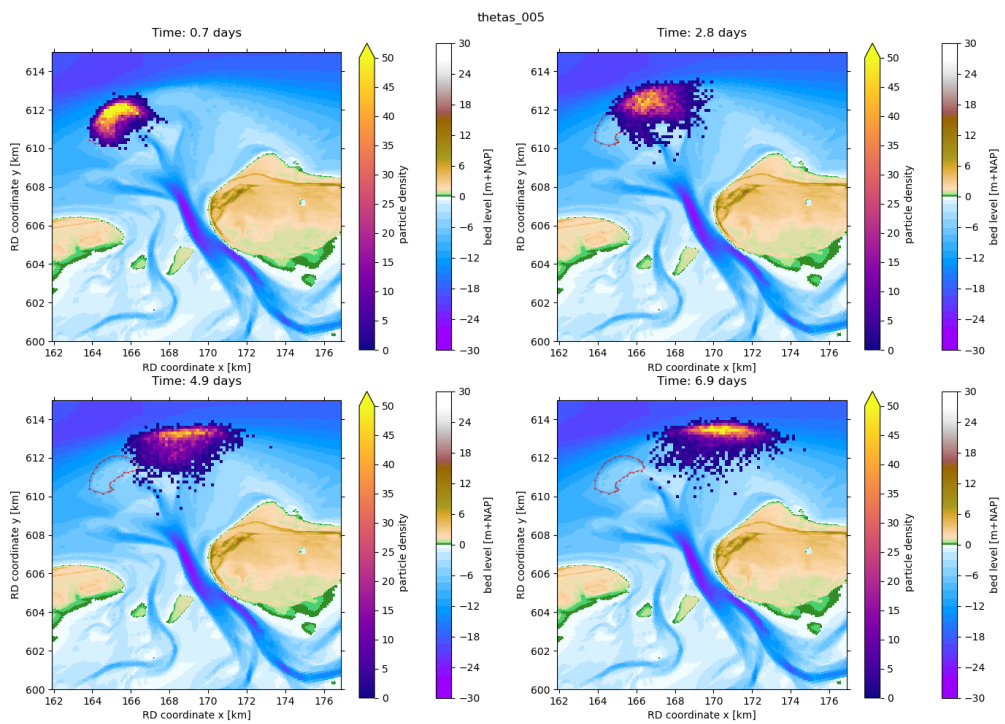


Figure B.7 $\theta_s = 0.05$

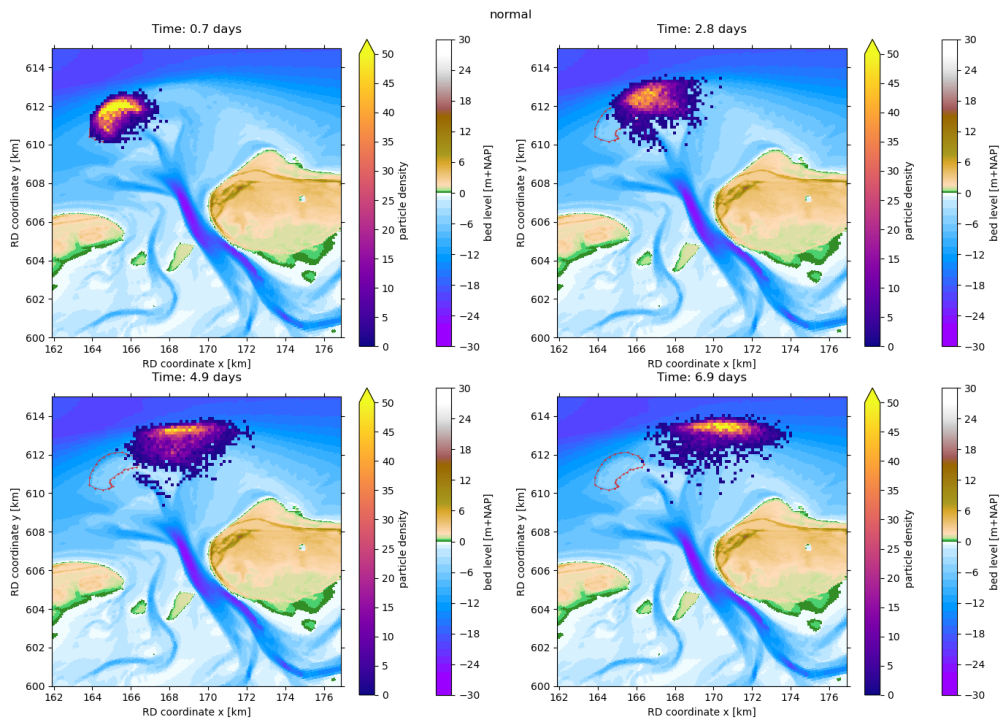


Figure B.8 $\theta_s = 0.1$

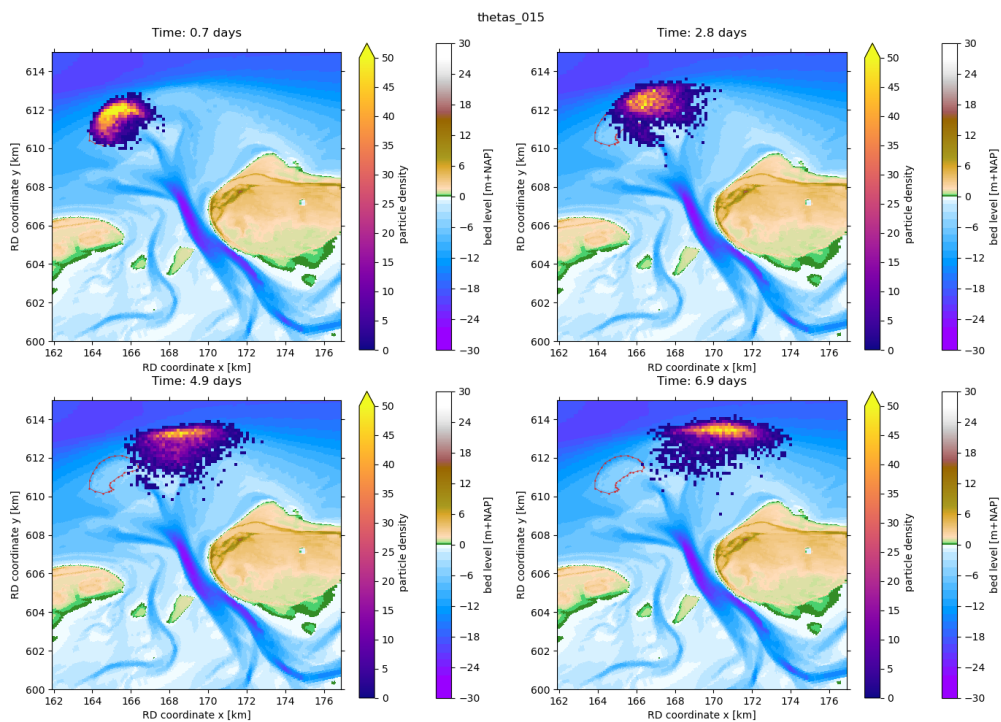


Figure B.9 $\theta_s = 0.15$

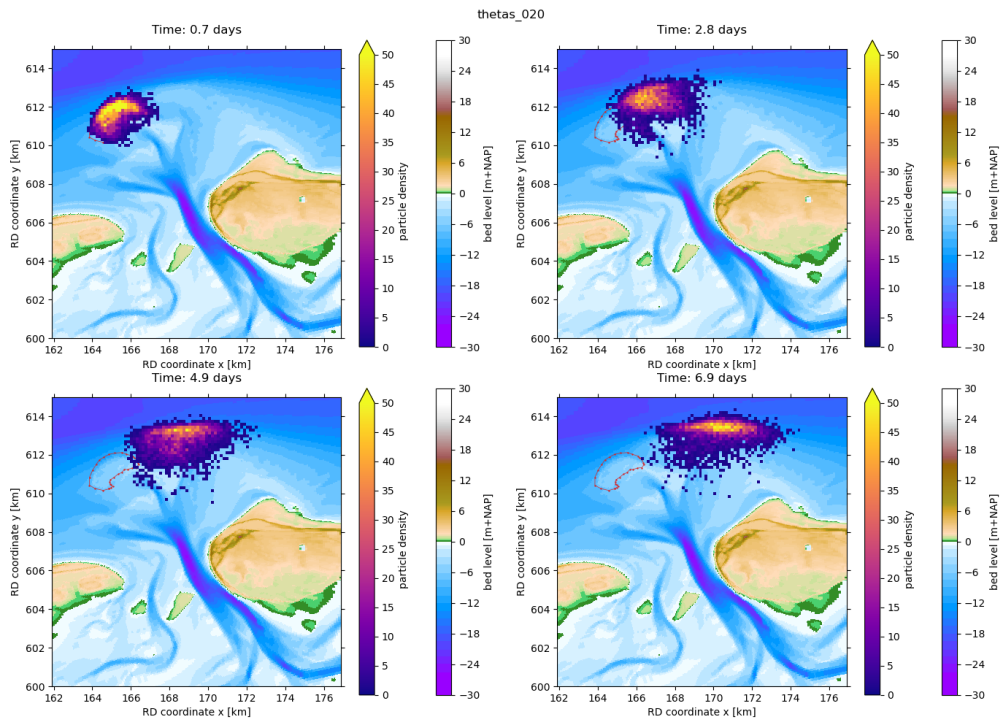


Figure B.10 $\theta_s = 0.2$

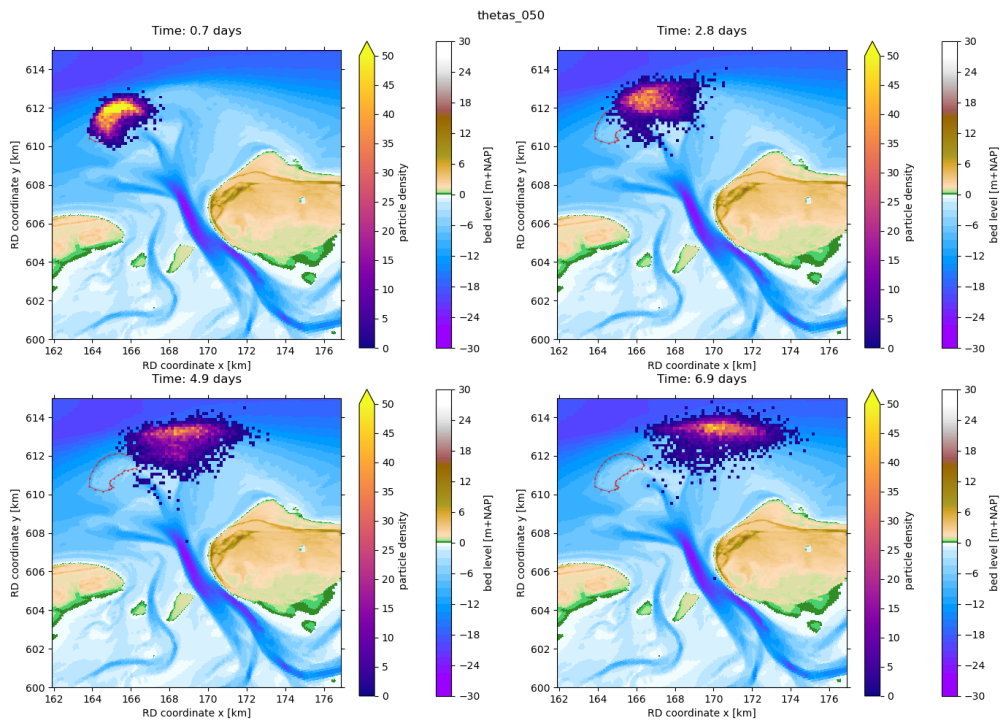


Figure B.11 $\theta_s = 0.5$

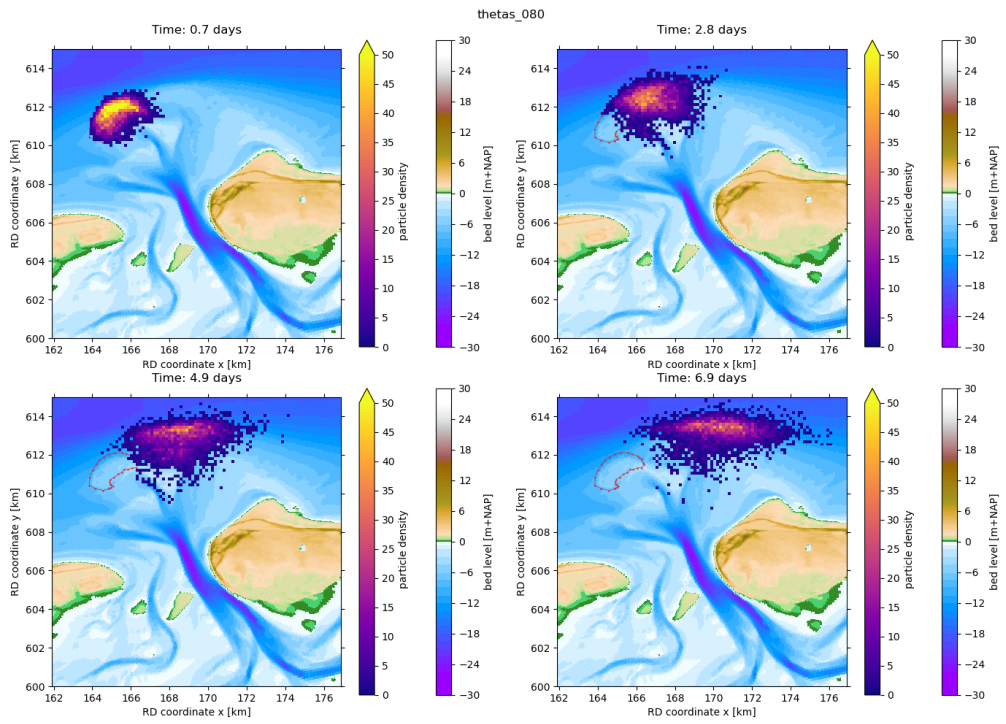


Figure B.12 $\theta_s = 0.8$

B.3 γ_e : Long-term equilibrium proportion of free particles

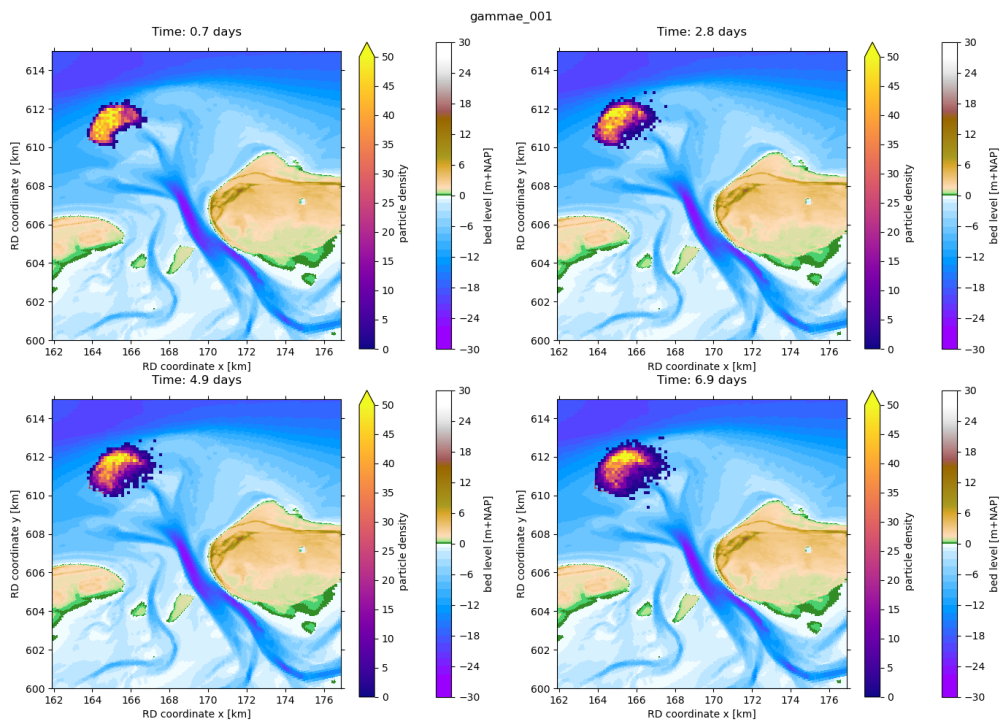


Figure B.13 $\gamma_e = 0.01$

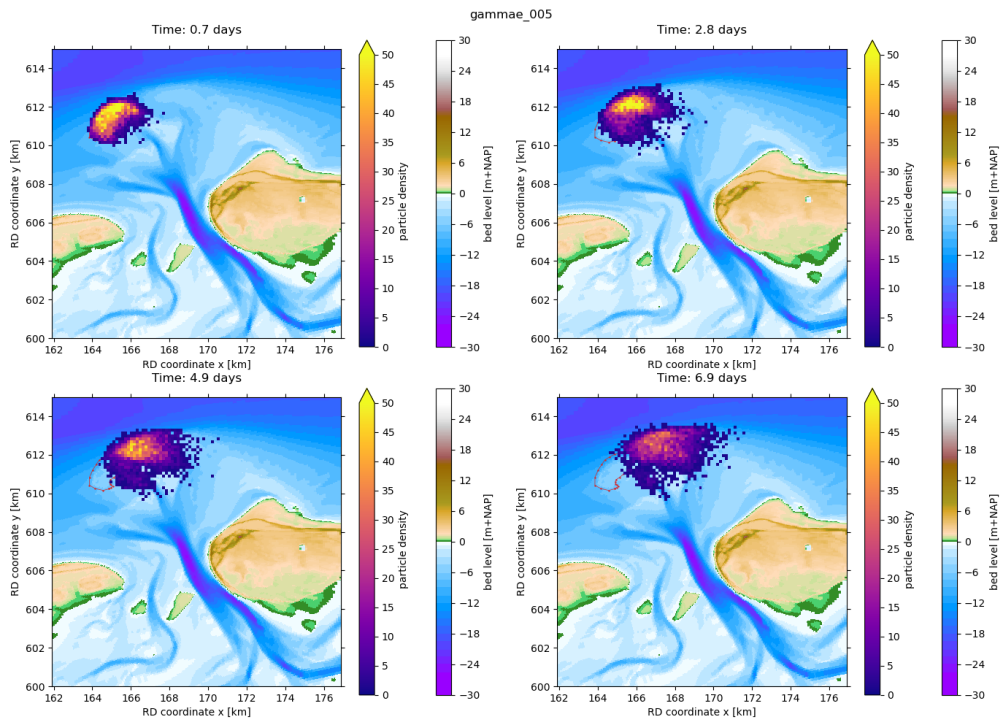


Figure B.14 $\gamma_e = 0.05$

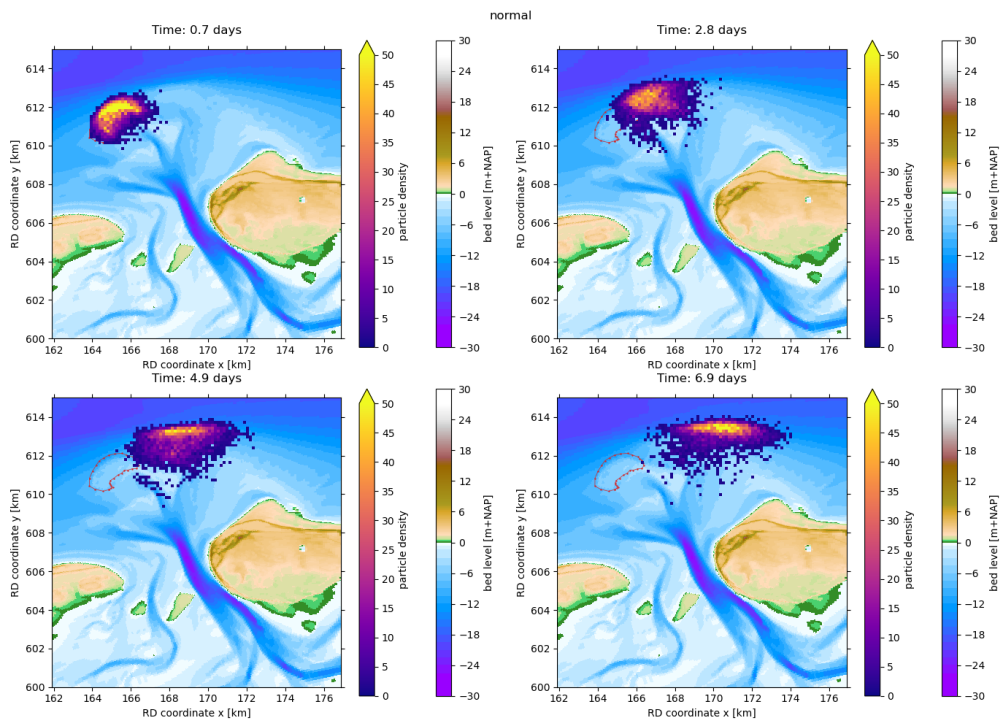


Figure B.15 $\gamma_e = 0.1$

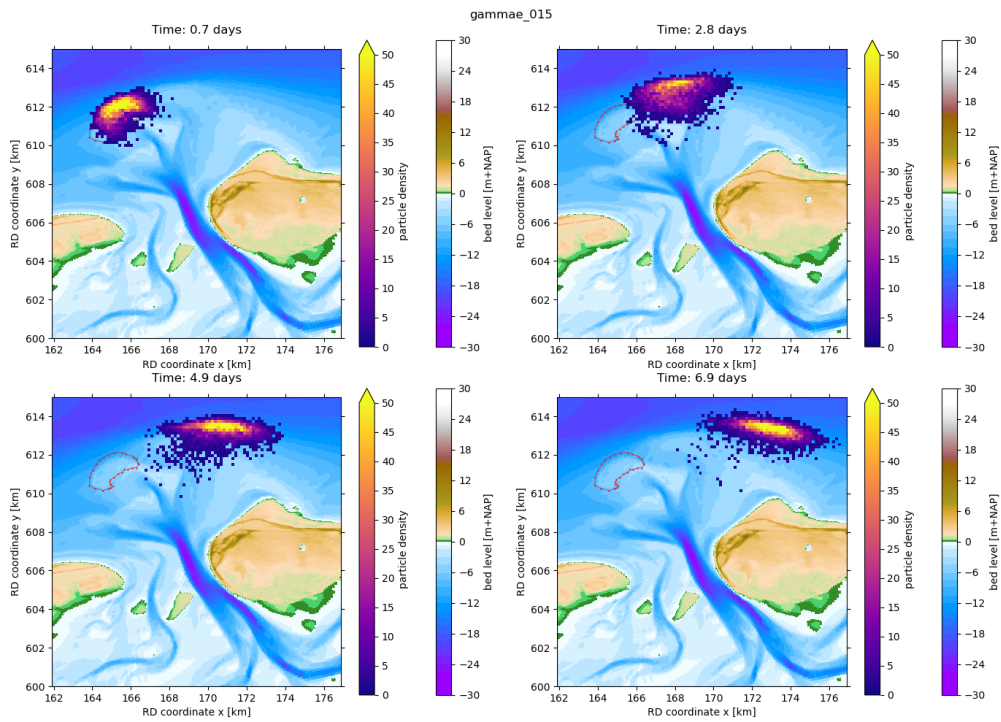


Figure B.16 $\gamma_e = 0.15$

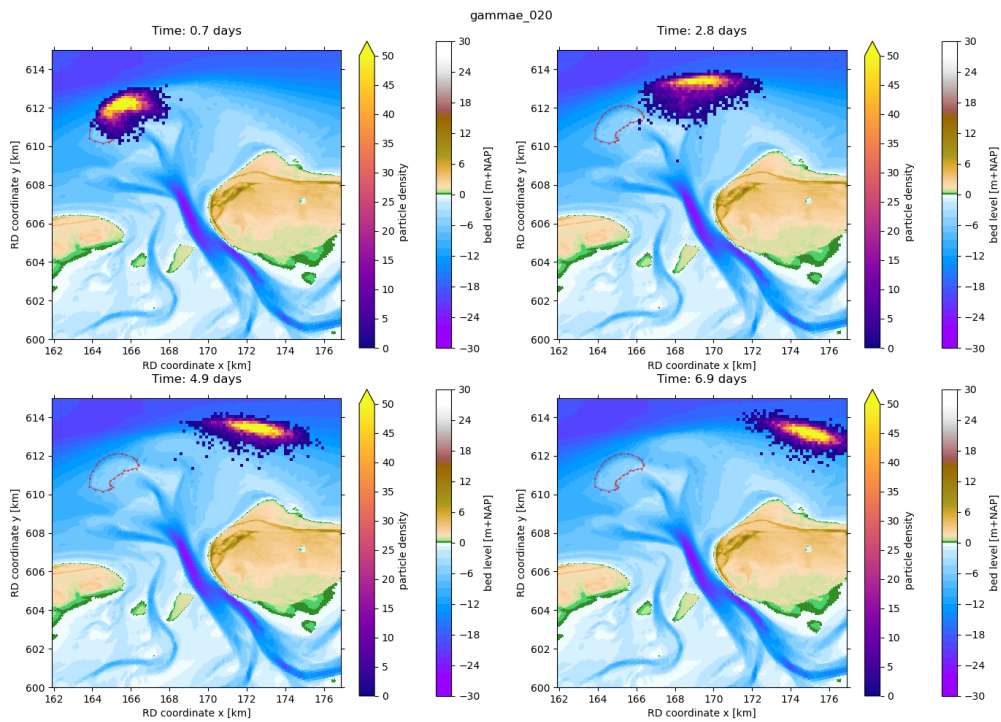


Figure B.17 $\gamma_e = 0.2$

C Other modelled nourishments at Ameland

This appendix provides some other modelled nourishments at the Ameland tidal inlet. This was done to demonstrate the possibility to study many different variants quickly using SedTRAILS. Once the underlying model has been completed, it is relatively simple to model a different nourishment. Note that for these new runs, the underlying bathymetry for Delft3D-FM was not changed. Thus, these runs still include the bathymetry with the pilot nourishment in it. All runs shown in this chapter were performed with six wave conditions, a spring-neap tidal cycle and the following burial parameters:

- $b_e = 1.7 \cdot 10^{-5}$ [1/s]
- $\theta_s = 0.1$ [-]
- $\gamma_e = 0.0055$ [-]

C.1 Alternate pilot nourishment location

The location for the variant tested in this section is based on "Nourishment v3" as shown in Harlequin (2021). Figure C.1 shows the particle source locations. These were again generated by randomly selecting 5000 points in the nourishment polygon.

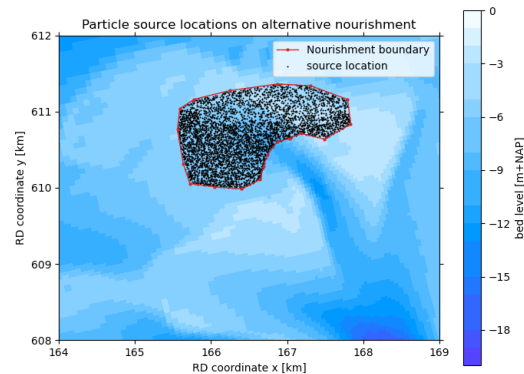


Figure C.1 5000 source locations for alternative location of pilot nourishment.

The result of a simulation of 180 days can be found in Figure C.2.

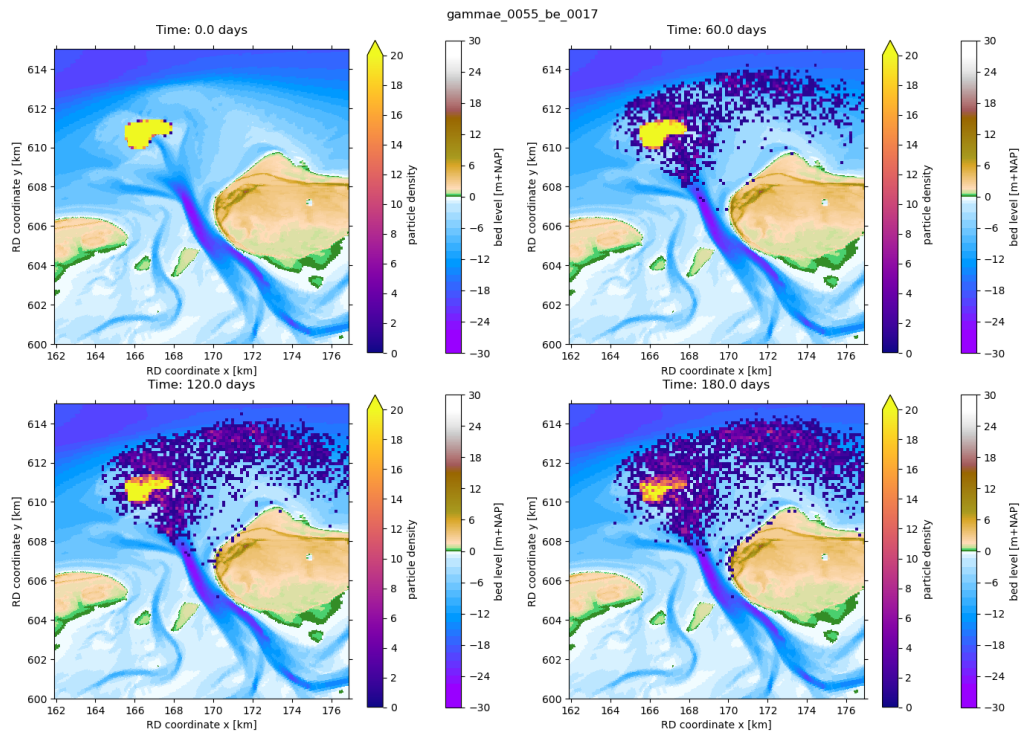


Figure C.2 Result of 180 day SedTRAILS simulation of alternative location for pilot nourishment.

This version of the nourishment has more spread over the ebb-tidal delta, but a significant amount of it still gets transported away along the sediment bypassing route. Because of the increased spread along the ebb-tidal delta, however, more sediment reaches or at least gets close to the coast.

C.2 2019 beach nourishment

In 2019, a beach nourishment was performed on the northwestern coast of Ameland. This nourishment disappeared quite quickly. It is in fact second in a line of three consecutive beach nourishments over the past 6 years. It was modelled here to see if SedTRAILS could give insight on its dispersal. The source set-up is shown in Figure C.3.

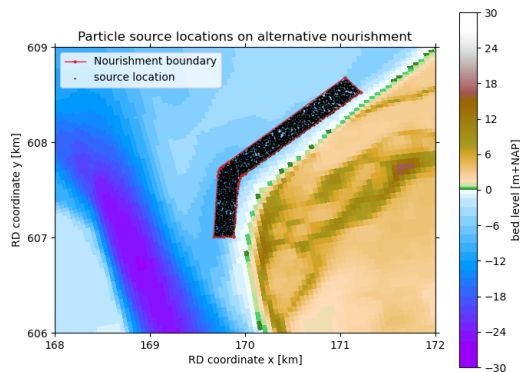


Figure C.3 5000 source locations for 2019 beach nourishment.

The result of a simulation of 180 days can be found in C.4.

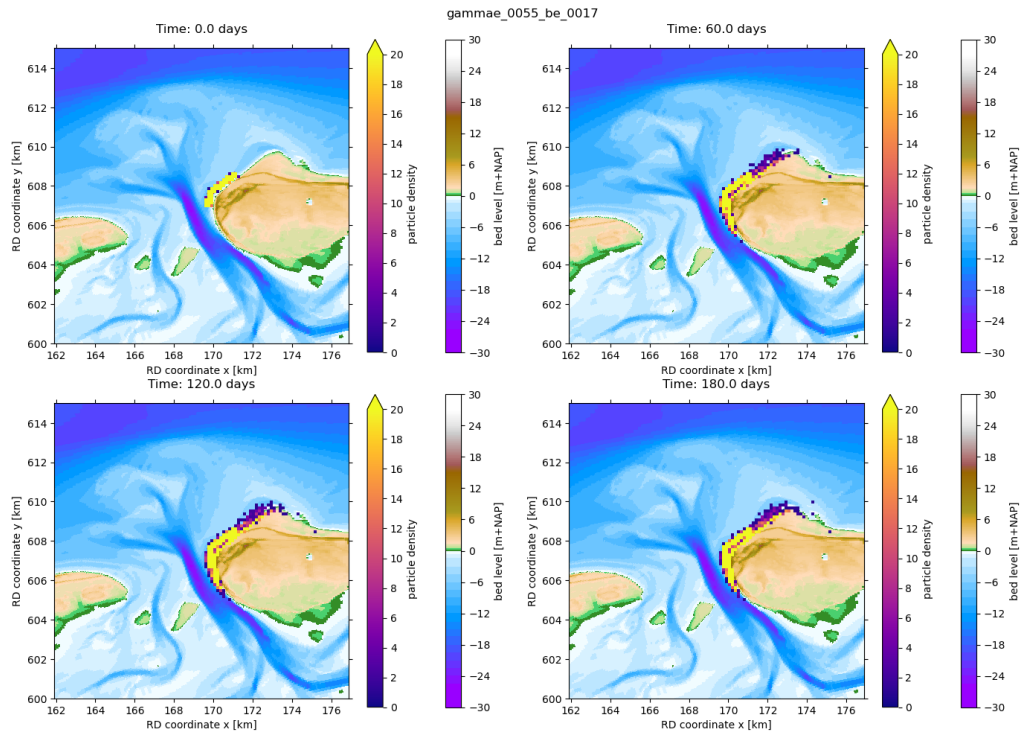


Figure C.4 Result of 180 day SedTRAILS simulation of beach nourishment at west coast of Ameland.

A significant amount of sediment in this simulation stays at the Ameland coast. This is likely due to several issues in the burial formulation having a much bigger effect here, right next to the main tidal inlet channel, than on the ebb-tidal delta. SedTRAILS also does not take bed slope effects into account. In reality, the strong bed level gradient at this section of coast would cause a lot of sediment to fall into the main tidal channel to then be transported away.

D Preliminary quantification

D.1 Particle counting

To calibrate the model, the amount of particles still within the nourishment polygon must first be known. For that, the script below was used. This utilises the `pandas` dataframe structure of SedTRAILS output as seen in Appendix A.

```
import numpy as np
import pandas as pd
import shapely as sh

# Load nourishment polygon
nourishment = np.loadtxt(nourishment_fp, skiprows=8) #filepath to .pol file of nourishment
nourishment_pol = sh.polygons(nourishment)

# Count particles within nourishment polygon for each output time step
count = np.zeros(n_time)
for i in range(n_time):
    df = sedtrails.loc[(sedtrails['time'] == t[0][0][i])]
    if len(df) > 0:
        points = list(zip(df.x.values, df.y.values)) # gets tuples of each point within the
        dataframe at chosen time step
        count[i] = sum(1 for point in points if nourishment_pol.contains(sh.Point(point)))
    # does the actual counting
```

Figure D.1 shows this counting performed on runs 2, 3 and 4.

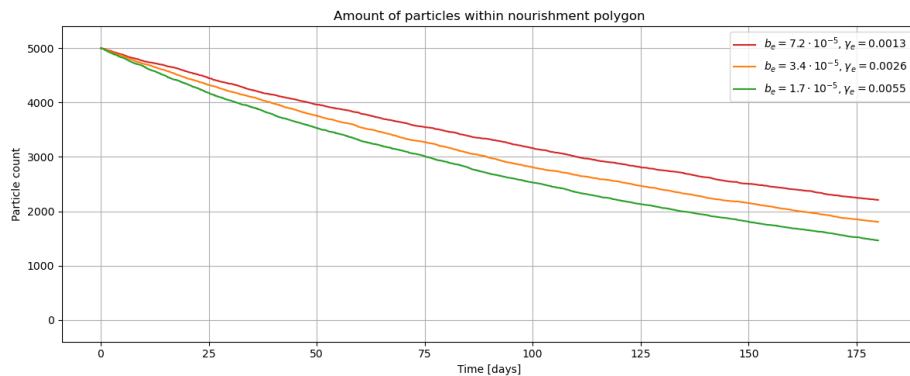


Figure D.1 Amount of particles within the nourishment polygon for the three final runs.

D.2 Bed level changes

The volume per particle depends on the timescale of the simulation. For 180 days, the nourishment has lost approximately $500\,000\text{ m}^3$ (Harlequin 2021). All three runs shown in Figure D.1 have lost different amounts of particles. For that reason, the volume per particle will differ. They are as follows:

- Run 2: 141.40 m^3 per particle
- Run 3: 156.45 m^3 per particle
- Run 4: 179.15 m^3 per particle

With the same volume and a lower amount of particles having left the nourishment, that means for the higher deposition run, one particle represents more volume.

The volume per particle can be turned into bed level changes using the following formula:

$$\Delta z = \frac{V_{particle} \cdot n_{particles,cell}}{A_{cell}} \quad (D.1)$$

With $V_{particle}$ and $n_{particles,cell}$ (particle density) having been determined, only A_{cell} remains. A_{cell} is dependent on the size of the 2D histogram that is being made for the particle density plot. Using the limits of the simulation and setting an amount of bins in the x and y directions, the area for all cells is calculated. In this case, 300 bins were used in the x-direction and 240 bins in the y-direction. This gives a cell area $A_{cell} = 21937.53m^2$.

Turning this into bed level change then becomes an easy calculation based on the particle density plots seen throughout this report and the two constants determined here. The result of this is shown in Figure D.2.

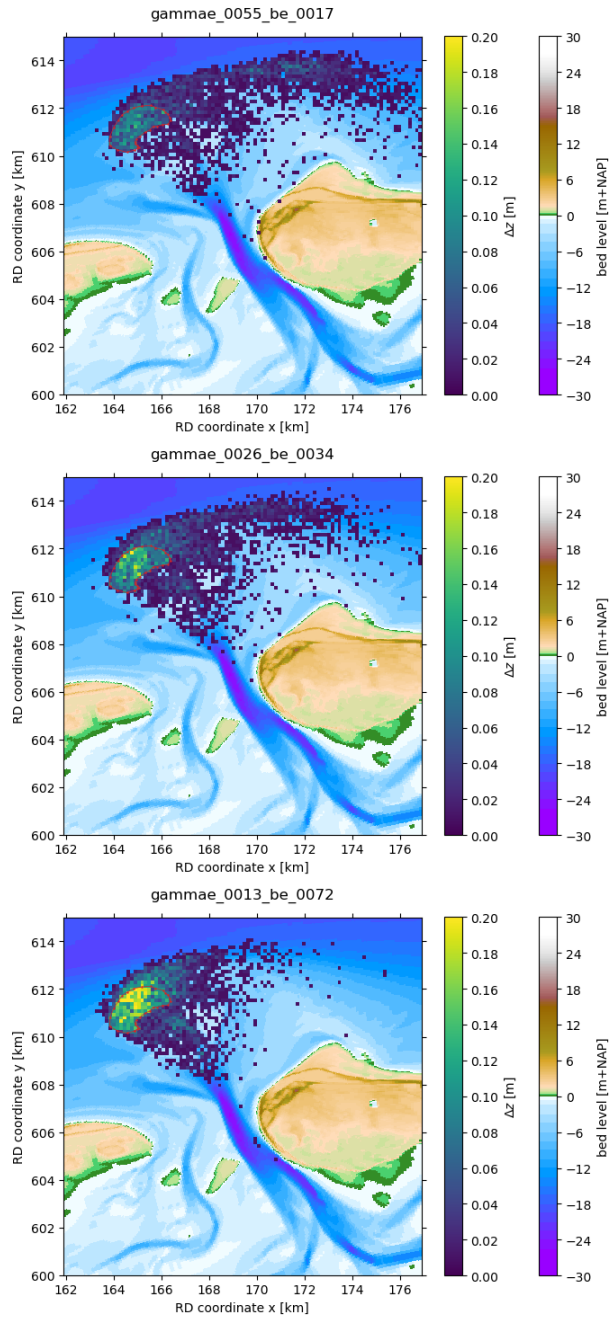


Figure D.2 Bed level changes after 180 days for runs 2, 3 and 4.

The bed level changes from these volumes are somewhat insignificant. Of course, only around 10% of the nourishment has been modelled here.

Deltares is an independent institute for applied research in the field of water and subsurface. Throughout the world, we work on smart solutions for people, environment and society.

Deltares

www.deltares.nl